From Source to Sink: Measuring and Modeling Processes Affecting Methane Emissions and Loss

Thesis by
Newton H. Nguyen

In Partial Fulfillment of the Requirements for the
Degree of
Doctor of Philosophy

CALIFORNIA INSTITUTE OF TECHNOLOGY
Pasadena, California

2024
Defended July 21, 2023

Newton H. Nguyen
ORCID: 0000-0002-9118-8672

ACKNOWLEDGEMENTS

Growing up, I was told that "people like you can't do science." Being a blind scientist in climate science, which is a field heavily reliant on visualizations, has presented numerous and seemingly insurmountable challenges. However, these challenges have put me in contact with so many amazing and kind individuals.

I want to thank those who have especially helped me along the way. My advisor, Christian Frankenberg, always believed in me. He pushed me to become a more technically rigorous and independent scientist, encouraging me to find something I am passionate about. Christian, thank you for your insight, constant encouragement, and kindness. I feel grateful to have been your student.

I have also had the pleasure of being lab mates with many kind and thoughtful individuals in the Frankenberg Group. Rui, Yi, Troy, Phillip, Liyin, and Siraput, thank you for teaching me about remote sensing and for your friendship.

Tapio Schneider was one of my project advisors during my first year. Tapio, thank you for believing in me, your insightful comments and perspectives, and for treating me as if I were one of your own.

I have also received a lot of support from mentors outside of Caltech. Dan Feldman, who was my supervisor at Lawrence Berkeley, guided me through the marathon of graduate school. He also guided me in the 2022 California International Marathon. Dan, thank you for getting the jello shot for me at mile 25. I needed it.

Sometimes, you meet people whom you want to be when you grow up. Alex Turner, thank you for your mentorship, insightful thoughts and perspectives, laughs over beers, and for hosting me at UC Berkeley and the University of Washington. I am so lucky to have met you.

During the last year of grad school, I worked remotely from Stanford. Alison Hoyt adopted me into her group and made sure I felt like I belonged. Alison, Jack, Julie, Clarice, Jenny, and Scott, thank you for taking me in. I am deeply grateful for sharing an office with you and for your friendship.

The enthusiasm of Julie Lee's personality alone made me want to go to Caltech. Julie, thank you for listening to me all these years; thank you for leaving my favorite chocolates in the qualifying exam room before Quals; and thank you for introducing me to the love of my life. I really appreciate you!

Nora Oshima and Bronagh Glaser, thank you for keeping this department together and for all of your help these past years. I really enjoyed our conversations in the hallway and the coffee room.

My family has been supportive during the challenging time of graduate school. I want to thank my sisters, Emerald and Sylviann, for always being there for me when we were growing up. I also want to thank my parents, Duke and Hue, for raising me. They set their expectations really high by naming me Newton.

The stories from *The Lord of the Rings* have brought me escape and solace during such a globally and academically tumultuous time. I want to thank J. R. R. Tolkien for telling the world about Middle Earth and its beloved Hobbits, where "the power of friendship and fellowship can overcome even the greatest of evils."

My graduate school experience has been defined by my friendships, new and old. Sometimes, others see the potential and humanity in you before you see it in yourself. Those people are friends who you should truely cherish. Tiffany, Alan, Isaac, and NIck, thank you for being there fore me after all these years. I am so grateful that we are still friends after our time at Berkeley. You saw me at my lowest lows and highest highs. For that, thank you and Go Bears!

Will, Renee, Charles, and Guannan, I love spending time with all of you. You are such amazing friends, talented individuals, and have wicked senses of humor. I look back on the memory of us putting together IKEA furniture in my empty apartment so fondly. Thank you for doing that and for being my friends.

Will and Renee, thank you for all of our fun lunches, attending Caltech Triathlon Club spin classes and workout sessions together, and for being there for me.

Andrei, Fernando, Rebecca, Amy, Tevis, Rae, Adrian, Celia, and Vince, I loved our times together and will always fondly remember you all when I think of these years of my life. I can't believe that we met during student orientation and have become so close. Our dinner parties and trips, like Big Bear, travels throughout LA, SF, and Oakland, have been so much fun. I can't wait to continue our friendships. You all changed me for the better and helped me believe in myself.

Adrian, Andrei, and Fernando, thank you especially for always being there for me during the pandemic, for helping me whenever I was in a pinch, and for your friendship. I never thought I would find new best friends.

Adrian, I am especially grateful for you. You were always there for me. From our

morning runs during the pandemic to our late-night bar crawls, thank you for being my best friend.

Erica, I am so lucky to have met you. Thank you for all of your support, bringing me coffee in the mornings when I am curled up in bed, believing in me, and your love. You have brought so much joy to my life. I cannot believe that we lived in three cities together, traveled to Southeast Asia in September, and are now working at Stanford together. I will always cherish the times that we spent at working on our laptops at Central Market in Austin, chowing down on delicious Japanese food at Takuya in Pasadena, and hikes with our puppy in San Fransisco. You are the light of my life. I love you.

ABSTRACT

Methane is a key target for climate change mitigation efforts. With a radiative forcing 85 times stronger than CO_2 over a 20-year period and an atmospheric lifespan of only a decade, mitigating methane emissions will slow climate change in the near-term. However, quantifying methane emissions from specific sectors accurately poses a significant challenge. This is because top-down estimations of methane emissions demand precise observations and constraints on a range of physical and chemical processes. In this thesis, I seek to enhance the accuracy of methane emissions calculations by resolving these processes in detail and advocating for an expansion of the methane monitoring network.

The primary mechanism for atmospheric methane destruction is its oxidation by the Hydroxyl radical (OH). Chemical feedbacks due to temporal variations in OH availability can substantially influence the methane lifetime and, consequently, emissions trends over recent decades. In Chapter 2, I quantify the impact of this predominant chemical loss mechanism on methane emissions calculations.

Methane loss to the stratosphere represents the second most significant methane destruction mechanism, although the processes involved remain highly uncertain. Accurately quantifying methane loss via stratospheric-tropospheric exchange is crucial for improving the accuracy of methane emissions calculations. In Chapter 3, I utilize chemical tracers to determine how stratospheric-tropospheric exchange influences global methane emissions trends.

Current understanding of greenhouse gas fluxes from a top-down perspective typically relies on atmospheric inversions, which depend on spatial and temporal gradients in observed greenhouse gas concentrations. However, maintaining highly accurate ground-based measurements poses logistical and financial challenges, while satellites currently do not provide the requisite accuracy and spatial resolution for long-term monitoring. In Chapter 4, I explore the potential of frequency combs in measuring environmental impacts on greenhouse gas sensing and as tools to expand the observation network.

In summary, this thesis contributes to a more profound understanding of the two primary methane sinks and how their variations affect methane emissions trends over recent decades. It also lays the groundwork for the next-generation greenhouse gas observation network using laser frequency combs by quantifying environmental

impacts on greenhouse gas spectroscopy directly in the field. Future advances should focus on a more accurate understanding of methane sink processes, improved spectroscopy, and expanded measurement networks. This will require advances in both modeling and measurements.

Ultimately, rapid and efficient mitigation of methane emissions remains the most feasible approach to curb anthropogenic climate change. To do this however, accurate assessments of methane trends and emissions necessitate bringing methane measurements and modeling of methane destruction processes closer to the real world.

PUBLISHED CONTENT AND CONTRIBUTIONS

Cole, Ryan K. et al. (2023). "Precision Doppler Shift Measurements with a Frequency Comb Calibrated Laser Heterodyne Radiometer". In: *Optics Letters*. URL: https://arxiv.org/abs/2307.07441.
N.N helped conceive the study, performed analysis on the meteorological data, devellopedthe software and spectral code, and assisted in writing the study.

Nguyen, Newton H. et al. (2020). "Effects of Chemical Feedbacks on Decadal Methane Emissions Estimates". In: *Geophysical Research Letters* 47.3, e2019GL085706. ISSN: 1944-8007. DOI: 10.1029/2019GL085706.
N.N led, designed, executed, and wrote the study. This work was adapted for Chapter 2.

Collins, William D. et al. (2018). "Large regional shortwave forcing by anthropogenic methane informed by Jovian observations". In: *Science Advances* 4.9. Publisher: American Association for the Advancement of Science, eaas9593. DOI: 10.1126/sciadv.aas9593.
N.N gathered and analyzed the meteorological data, assisted in develloping the software, and assisted in writing the study.

TABLE OF CONTENTS

LIST OF ILLUSTRATIONS

Number *Page*

LIST OF TABLES

Chapter 1

INTRODUCTION

1.1 Motivation

Methane emissions mitigation has emerged as a pivotal approach to curb anthropogenic climate change in the forthcoming decades. As a major contributor to radiative forcing, methane, which is responsible for a third of radiative forcing, harbors a global warming potential 85 times more potent than carbon dioxide over a 20-year span (W. Collins et al., 2022; Shindell, Fuglestvedt, and W. J. Collins, 2017). Nonetheless, its atmospheric lifespan is relatively brief, lasting about a decade, significantly less than the centuries-long lifespan of carbon dioxide. Therefore, accurately attributing the sources of methane emissions and discerning the driving factors influencing atmospheric methane trends are paramount for the effective execution of climate change mitigation strategies.

1.2 Methane Sources and Sinks

Both anthropogenic and natural sources contribute to methane emissions. Anthropogenic emissions arise from sectors such as oil and gas, rice farming, cattle rearing, waste treatment, and landfills. Conversely, natural sources are linked to wetlands, permafrost thaw, and wildfires. However, substantial uncertainties concerning emissions from these sectors persist. Noteworthy studies such as those by A. J. Turner et al. (2015), employing GEOS-Chem inversions constrained by GOSAT, indicated that oil and gas emissions in the United States have been underestimated. In addition, through the utilization of ground-based sensors, Alvarez et al. (2018) further quantified this underestimation to be upwards of 40%. Meanwhile, other studies argue that oil and gas emissions have remained relatively stable over recent decades.

Predicting and quantifying methane emissions from natural sources present considerable challenges, given their spatially diffuse, temporally episodic, and spatio-temporally heterogeneous nature (Goodrich et al., 2011; Morin et al., 2017; Peltola et al., 2018). For instance, methane emissions from wetlands encompass numerous processes such as bubbling in the water column, anoxic sediment, soil diffusion, and even tree emissions. These factors, coupled with the monitoring challenges in remote tropical wetlands and permafrost regions, lead to significant uncertainty in quantifying natural methane emissions (Saunois et al., 2020).

Understanding how methane emissions from natural sources will respond to climate change is a complex task. Methanogenesis, the primary methane production process carried out by microbes, is influenced by factors such as soil moisture, nutrient availability, and temperature (France et al., 2022; Feng et al., 2022; Ma et al., 2021; Schaefer et al., 2016). Methanotrophy, the microbial consumption of methane in the soil, is another factor to consider. Despite its importance, our understanding of methanotrophy is limited. Therefore, focusing on the modeling of microbial methane production and consumption processes is key to determining the extent of anthropogenic methane mitigation needed to stabilize methane concentrations (Thompson, 2021).

Methane's atmospheric lifespan is approximately a decade, and it is primarily destroyed through the oxidation processes involving hydroxyl (OH) radicals and chlorine (Cl) radicals, stratospheric escape, and soil-surface methanotrophy. The OH oxidation process accounts for nearly 90% of methane destruction. Yet measuring OH concentrations directly is a challenge due to its short lifespan, spatio-temporal heterogeneity, and reactivity with many atmospheric species that can both increase and decrease its abundance (Nicely et al., 2018; Patra, Houweling, et al., 2011; Naik et al., 2013; Wolfe et al., 2019). It is also important to note that OH oxidation, when combined with NO and NO_2, leads to the formation of tropospheric ozone, a major air pollutant. As a result, methane emission mitigation not only helps in climate change mitigation but also enhances air quality (Fiore et al., 2008). To comprehend the factors influencing methane trends, quantifying global OH trends along with other methane sinks is essential. I will quantify the impacts of these sinks in Chapters 2 and 3. The current imbalance between methane sources and sinks has led to a tripling of methane concentrations, surging from 600 parts per billion (ppb) in 1850 to more than 1900 ppb in 2023.

1.3 Proxying Methane Processes

Methane proxies play a critical role in constraining global methane trends. The primary observables include $^{12}CH_4$, $^{13}CH_4$, and MCF. The dominant methane isotope, $^{12}CH_4$, is observed from various vantage points, such as space, air, and the Earth's surface. $^{13}CH_4$, the secondary methane isotope, serves as a proxy for methane sources, as different sources exhibit unique $^{13}CH_4$ signatures. Methyl Chloroform (MCF) proxies for variations in the hydroxyl radical. $^{13}CH_4$ and MCF observations are primarily surface-based.

In recent years, global $^{13}CH_4$ ratios have experienced a decline. This shift towards lighter methane indicates either a surge in emissions from biogenic methane sources, such as agricultural or microbial activities (Schaefer et al., 2016; Nisbet et al., 2016), or a reduction in emissions from isotopically heavier sources like biomass burning (Worden et al., 2017). Microbial sources generally exhibit lighter signatures around -60 per mil, while biomass burning displays the heaviest signature of -29 per mil. Fossil fuel sources fall in-between at about -45 per mil. However, these figures assume that the isotopic signature of specific sources remain spatially consistent and constant over time, which might not always hold true.

Methyl Chloroform (MCF), an industrial solvent whose use has been declining since its ban under the Montreal Protocol, is deployed to proxy variations in the OH radical. As MCF has no other destruction pathways in the troposphere, changes in its loss frequency can be attributed to changes in OH concentrations (Montzka et al., 2011; Patra, Krol, et al., 2021). Therefore, joint inversions of MCF, $^{12}CH_4$, and $^{13}CH_4$ have been instrumental in understanding methane trends (McNorton et al., 2016; Alexander J. Turner, Christian Frankenberg, Wennberg, et al., 2017).

1.4 The Methane Stabilization Mystery

Over the past few decades, methane levels have risen from 1650 ppb in 1983 to 1910 ppb in 2022. Interestingly, this constant rise in methane was briefly interrupted between 2000 and 2007, leading to a stabilization period. The causes for the onset and termination of this stabilization remain elusive.

Numerous studies have leveraged methane isotopic signatures and trends to attribute the end of the stabilization period to increases in emissions from biogenic sources or fossil fuels. This is because observations of $^{13}CH_4$ have steadily been inclining towards lighter methane, which is more indicative of biogenic emissions.

However, other studies have emphasized the role of changes in the primary methane sink, oxidation by the OH radical, in attributing the onset and termination of the stabilization period. Joint inversions of methane concentrations, along with observations of Methyl Chloroform (MCF), which proxy the variability of OH concentrations, suggest that OH variations played a role during this stabilization period. Nevertheless, a causal mechanism for changes in OH concentrations has yet to be discovered.

The ongoing debate surrounding the stabilization period underscores the complexity of the global methane cycle. The stabilization requires only a change of 3.5%

in OH concentrations or a 20 Tg/yr change in methane emissions (Alexander J. Turner, Christian Frankenberg, and Kort, 2019), a small change considering the greater than 550 Tg/yr emission rate. A comprehensive global observation system, capable of monitoring both natural and anthropogenic emissions, alongside an improved understanding and precise measurements of OH sinks, is required to fully characterize methane emissions and trends. I will discuss this further in Chapter 2.

1.5 Sensing Methane

The infrared absorption features of methane facilitate the quantification of its spatial distribution and temporal trends. Various methods, such as orbital satellite platforms, spectrometers on aircraft, and ground-based in situ sensors, are employed to monitor methane levels. Accurately mapping methane concentrations is crucial as top-down emission calculations rely on methane gradiants to quantify and attribute specific sources.

Satellites offer significant advantages as they can continuously map at global and regional scales using a single instrument (Jacob et al., 2016). Instruments like Sciamachy have been utilized to detect high-emission regions, such as the Four Corners and the Amazon C. Frankenberg et al., 2005. The Japanese Greenhouse Gas Observing Satellite (GOSat) has played a pivotal role in quantifying US oil and gas emission (A. J. Turner et al., 2015). Meanwhile, the European Tropospheric Monitoring Instrument (Tropomi) has identified super-emitters in Turkmenistan (Varon et al., 2019). The global, continuous observations facilitated by these satellites have shed light on global methane emissions.

However, satellites do have limitations in terms of accuracy, revisit time, and cost. Future satellites like GHGSat aim to enhance coverage by continuously monitoring specific regions using multiple satellites in a geosynchronous orbit configuration. Simultaneously, the Franco-German Merlin satellite seeks to measure methane concentrations with an accuracy better than 1% (Delahaye et al., 2016).

Aircraft provide a valuable resource to monitor specific methane sources and regions. For instance, NASA's AVERIS, an aircraft-mounted spectrometer, has been instrumental in identifying methane plumes and quantifying emissions (Christian Frankenberg et al., 2016; Duren et al., 2019). recently used AVERIS to measure methane emissions in California, revealing that the majority of emissions stem from the top 30% of sources.

Ground-based measurements, though offering less coverage than satellites, boast

higher accuracy and accessibility. Most ground-based instruments utilize infrared spectroscopy to measure methane concentrations. While some of these instruments measure at the point scale, such as cavity ring-down spectroscopy, others are capable of longer path measurements, like Fourier transform spectroscopy and dual-comb spectroscopy.

The current global greenhouse gas measurement network relies on laboratory analyses for obtaining highly accurate methane concentration readings (Sweeney et al., 2015). However, the logistical difficulty and expense associated with sample collection, flask shipping, and laboratory measurements limit these measurements to a few select sites.

Despite these advancements, tropical regions remain under-observed and underrepresented due to frequent cloud cover and logistical challenges. Notably, the tropical atmosphere is where the majority of uncertainty in methane emissions are located, in addition to where the majority of methane destruction occurs, given the abundance of the OH radical. Consequently, innovative approaches are necessary to enhance coverage in these pivotal areas. The development of the next-generation observation network, which I will discuss in Chapter 4, holds the promise of revolutionizing methane monitoring by offering accurate, continuous, and automated measurements.

1.6 Methane Spectroscopy and Retrievals

The interaction between light and methane molecules is complex due to methane's tetrahedral configuration. Methane consists of a carbon atom bonded to four hydrogen atoms, which generate temporary dipole moments from the stretching and rotation of C-H bonds when infrared radiation is absorbed. This phenomenon is key in the greenhouse effect.

Accurate modelling of methane spectroscopy is crucial for precisely retrieving methane concentrations throughout the atmosphere. Methane spectroscopy's complexity arises from these temporarily induced dipole moments, which is why the field is ever-evolving. Moreover, it is vital to accurately model environmental effects on methane spectra, such as pressure and temperature influences on molecular absorption lines. Near the surface, pressure broadening, characterized by a Gaussian line-shape, is more dominant, while Doppler broadening, induced by temperature effects and depicted by a Lorentzian line-shape, prevails at higher altitudes. The Voigt Line-shape accounts for both pressure and temperature effects by convolving

the Lorentzian and Gaussian line-shapes. Errors in modeling these line-shapes will result in errors in retrieving greenhouse gas concentrations. In Chapter 4, I delve into the impact of environmental effects on the accuracy of methane and CO_2 retrievals.

1.7 Thesis Outline

Precise monitoring and evaluation of methane emissions necessitate both observational and modelling breakthroughs. In Chapter 2, I delve into the complexity of the CH_4-CO-OH system by quantifying the effect of OH radical variations on methane emissions and demonstrating how surges in CO emissions, such as those from wildfires, lead to increases in methane emissions.

Stratospheric methane loss, which accounts for 3-16% of global methane loss, stands as the second largest sink of atmospheric methane. In Chapter 3, I employ stratospheric water vapor observations, along with surface observations of methane, CO, and MCF to ascertain the effect of fluctuations in stratospheric-tropospheric exchange time on methane emissions and OH concentrations. Here, MCF serves as a proxy for OH and is assumed to undergo constant or no stratospheric loss, influencing inferred OH concentrations. I also link methane emissions, OH concentrations, and lower stratospheric H_2O concentrations to ENSO, linking large-scale atmospheric dynamics to atmospheric chemistry.

Looking to the future, I discuss the instruments that will form the next-generation greenhouse gas observational network. We leverage the time-keeping stability of the laser frequency comb, initially developed for pico-second time-keeping, to measure greenhouse gas concentrations with high accuracy. This facilitates the accurate examination of environmental influences, such as pressure and temperature, on molecular spectroscopy directly in the field, since laser frequency combs are free from the spectrally distorting effect of the instrument line-shape. This feature will promote automated, accurate, and traceable greenhouse gas measurements in remote areas and help expand the greenhouse gas observational network.

Overall, this thesis advances understanding of the main methane sink processes, namely oxidation by the OH radical and stratospheric loss. It also paves the way for increased accuracy in methane remote sensing by quantifying how environmental conditions affect greenhouse gas and radiation interactions, measured directly in the field. By improving our understanding of the factors influencing global methane trends and enhancing methane remote sensing, my aim is to provide a comprehensive approach to accurately quantify methane emissions, thereby contributing to our

collective effort in mitigating climate change.

BIBLIOGRAPHY

Alvarez, Ramón A. et al. (June 21, 2018). "Assessment of methane emissions from the U.S. oil and gas supply chain". In: *Science*, eaar7204. ISSN: 0036-8075, 1095-9203. DOI: 10.1126/science.aar7204. URL: https://www.sciencemag.org/lookup/doi/10.1126/science.aar7204 (visited on 07/21/2023).

Collins, W. et al. (July 4, 2022). "Monitoring methane emissions from oil and gas operations‡". In: *Optics Express* 30.14. Publisher: Optica Publishing Group, pp. 24326–24351. ISSN: 1094-4087. DOI: 10.1364/OE.464421. URL: https://opg.optica.org/oe/abstract.cfm?uri=oe-30-14-24326 (visited on 05/14/2023).

Delahaye, T. et al. (2016). "Precise methane absorption measurements in the 1.64 m spectral region for the MERLIN mission". In: *Journal of Geophysical Research: Atmospheres* 121.12, pp. 7360–7370. ISSN: 2169-8996. DOI: 10.1002/2016JD025024. (Visited on 01/06/2022).

Duren, Riley M. et al. (Nov. 2019). "California's methane super-emitters". In: *Nature* 575.7781. Number: 7781 Publisher: Nature Publishing Group, pp. 180–184. ISSN: 1476-4687. DOI: 10.1038/s41586-019-1720-3. URL: https://www.nature.com/articles/s41586-019-1720-3 (visited on 07/12/2023).

Feng, Liang et al. (June 17, 2022). "Methane emissions responsible for record-breaking atmospheric methane growth rates in 2020 and 2021". In: *Atmospheric Chemistry and Physics Discussions*. Publisher: Copernicus GmbH, pp. 1–23. DOI: 10.5194/acp-2022-425. URL: https://acp.copernicus.org/preprints/acp-2022-425/ (visited on 10/15/2022).

Fiore, Arlene M. et al. (Apr. 30, 2008). "Characterizing the tropospheric ozone response to methane emission controls and the benefits to climate and air quality". In: *Journal of Geophysical Research* 113 (D8). ISSN: 0148-0227. DOI: 10.1029/2007JD009162. URL: http://doi.wiley.com/10.1029/2007JD009162 (visited on 06/12/2018).

France J. L., James L. et al. (Jan. 24, 2022). "13C methane source signatures from tropical wetland and rice field emissions". In: *Philosophical Transactions of the Royal Society A: Mathematical, Physical and Engineering Sciences* 380.2215. Publisher: Royal Society, p. 20200449. DOI: 10.1098/rsta.2020.0449. URL: https://royalsocietypublishing.org/doi/10.1098/rsta.2020.0449 (visited on 10/13/2022).

Frankenberg, C. et al. (May 13, 2005). "Assessing Methane Emissions from Global Space-Borne Observations". In: *Science* 308.5724, pp. 1010–1014. ISSN: 0036-8075, 1095-9203. DOI: 10.1126/science.1106644. URL: https://www.science.org/doi/10.1126/science.1106644 (visited on 07/21/2023).

Frankenberg, Christian et al. (Aug. 30, 2016). "Airborne methane remote measurements reveal heavy-tail flux distribution in Four Corners region". In: *Proceedings of the National Academy of Sciences of the United States of America* 113.35, pp. 9734–9739. ISSN: 1091-6490. DOI: 10.1073/pnas.1605617113.

Goodrich, Jordan P. et al. (2011). "High-frequency measurements of methane ebullition over a growing season at a temperate peatland site". In: *Geophysical Research Letters* 38.7. ISSN: 1944-8007. DOI: 10.1029/2011GL046915.

Jacob, Daniel J. et al. (Nov. 18, 2016). "Satellite observations of atmospheric methane and their value for quantifying methane emissions". In: *Atmospheric Chemistry and Physics* 16.22, pp. 14371–14396. ISSN: 1680-7324. DOI: 10.5194/acp-16-14371-2016. URL: https://www.atmos-chem-phys.net/16/14371/2016/ (visited on 04/03/2020).

Ma, Shuang et al. (Sept. 2021). "Satellite Constraints on the Latitudinal Distribution and Temperature Sensitivity of Wetland Methane Emissions". In: *AGU Advances* 2.3. ISSN: 2576-604X, 2576-604X. DOI: 10.1029/2021AV000408. URL: https://onlinelibrary.wiley.com/doi/10.1029/2021AV000408 (visited on 10/15/2022).

McNorton, Joe et al. (June 30, 2016). "Role of OH variability in the stalling of the global atmospheric CH_4 growth rate from 1999 to 2006". In: *Atmospheric Chemistry and Physics* 16.12, pp. 7943–7956. ISSN: 1680-7316. DOI: https://doi.org/10.5194/acp-16-7943-2016. URL: https://www.atmos-chem-phys.net/16/7943/2016/ (visited on 11/25/2019).

Montzka, S. A. et al. (Jan. 7, 2011). "Small Interannual Variability of Global Atmospheric Hydroxyl". In: *Science* 331.6013, pp. 67–69. ISSN: 0036-8075, 1095-9203. DOI: 10.1126/science.1197640. URL: https://science.sciencemag.org/content/331/6013/67 (visited on 06/19/2019).

Morin, T. H. et al. (May 1, 2017). "Combining eddy-covariance and chamber measurements to determine the methane budget from a small, heterogeneous urban floodplain wetland park". In: *Agricultural and Forest Meteorology* 237-238, pp. 160–170. ISSN: 0168-1923. DOI: 10.1016/j.agrformet.2017.01.022. URL: https://www.sciencedirect.com/science/article/pii/S0168192317300321 (visited on 01/24/2023).

Naik, V. et al. (May 27, 2013). "Preindustrial to present-day changes in tropospheric hydroxyl radical and methane lifetime from the Atmospheric Chemistry and Climate Model Intercomparison Project (ACCMIP)". In: *Atmospheric Chemistry and Physics* 13.10, pp. 5277–5298. ISSN: 1680-7324. DOI: 10.5194/acp-13-5277-2013. URL: https://www.atmos-chem-phys.net/13/5277/2013/ (visited on 11/26/2019).

Nicely, Julie M. et al. (2018). "Changes in Global Tropospheric OH Expected as a Result of Climate Change Over the Last Several Decades". In: *Journal of Geophysical Research: Atmospheres* 123.18, pp. 10, 774–10, 795. ISSN: 2169-8996.

DOI: 10.1029/2018JD028388. URL: https://agupubs.onlinelibrary.wiley.com/doi/abs/10.1029/2018JD028388 (visited on 06/19/2019).

Nisbet, E. G. et al. (Sept. 1, 2016). "Rising atmospheric methane: 2007–2014 growth and isotopic shift". In: *Global Biogeochemical Cycles* 30.9, pp. 1356–1370. ISSN: 1944-9224. DOI: 10.1002/2016GB005406. URL: https://agupubs.onlinelibrary.wiley.com/doi/10.1002/2016GB005406 (visited on 11/27/2019).

Patra, P. K., M. C. Krol, et al. (2021). "Methyl Chloroform continues to constrain the hydroxyl (OH) variability in the troposphere". In: *Journal of Geophysical Research: Atmospheres* (), e2020JD033862. ISSN: 2169-8996. DOI: 10.1029/2020JD033862. (Visited on 01/12/2021).

Patra Prabir K., P. K., S. Houweling, et al. (Dec. 19, 2011). "TransCom model simulations of CH₄ and related species: linking transport, surface flux and chemical loss with CH₄ variability in the troposphere and lower stratosphere". In: *Atmospheric Chemistry and Physics* 11.24, pp. 12813–12837. ISSN: 1680-7324. DOI: 10.5194/acp-11-12813-2011. URL: https://acp.copernicus.org/articles/11/12813/2011/ (visited on 02/18/2021).

Peltola, Olli et al. (Feb. 15, 2018). "Technical note: Comparison of methane ebullition modelling approaches used in terrestrial wetland models". In: *Biogeosciences* 15.3, pp. 937–951. ISSN: 1726-4189. DOI: 10.5194/bg-15-937-2018. URL: https://bg.copernicus.org/articles/15/937/2018/ (visited on 10/15/2022).

Saunois, Marielle et al. (July 15, 2020). "The Global Methane Budget 2000–2017". In: *Earth System Science Data* 12.3. Publisher: Copernicus GmbH, pp. 1561–1623. ISSN: 1866-3508. DOI: 10.5194/essd-12-1561-2020. URL: https://essd.copernicus.org/articles/12/1561/2020/ (visited on 10/15/2022).

Schaefer, Hinrich et al. (Mar. 10, 2016). "A 21st century shift from fossil-fuel to biogenic methane emissions indicated by 13CH4". In: *Science*, aad2705. ISSN: 0036-8075, 1095-9203. DOI: 10.1126/science.aad2705. URL: http://science.sciencemag.org/content/early/2016/03/09/science.aad2705 (visited on 09/11/2018).

Shindell, D. T., J. S. Fuglestvedt, and W. J. Collins (Aug. 22, 2017). "The social cost of methane: theory and applications". In: *Faraday Discussions* 200.0, pp. 429–451. ISSN: 1364-5498. DOI: 10.1039/C7FD00009J. URL: https://pubs.rsc.org/en/content/articlelanding/2017/fd/c7fd00009j (visited on 08/15/2019).

Sweeney, Colm et al. (2015). "Seasonal climatology of CO2 across North America from aircraft measurements in the NOAA/ESRL Global Greenhouse Gas Reference Network". In: *Journal of Geophysical Research: Atmospheres* 120.10, pp. 5155–5190. DOI: 10.1002/2014JD022591.

Thompson, Rona L. (Sept. 2021). "Climate Feedback From Wetland Emissions of Methane May Necessitate Greater Anthropogenic Reductions". In: *AGU Advances* 2.3. ISSN: 2576-604X, 2576-604X. DOI: 10.1029/2021AV000533. URL: https://onlinelibrary.wiley.com/doi/10.1029/2021AV000533 (visited on 10/15/2022).

Turner, A. J. et al. (June 30, 2015). "Estimating global and North American methane emissions with high spatial resolution using GOSAT satellite data". In: *Atmospheric Chemistry and Physics* 15.12. Publisher: Copernicus GmbH, pp. 7049–7069. ISSN: 1680-7316. DOI: 10.5194/acp-15-7049-2015. URL: https://acp.copernicus.org/articles/15/7049/2015/ (visited on 07/10/2023).

Turner, Alexander J., Christian Frankenberg, and Eric A. Kort (Feb. 19, 2019). "Interpreting contemporary trends in atmospheric methane". In: *Proceedings of the National Academy of Sciences* 116.8, pp. 2805–2813. ISSN: 0027-8424, 1091-6490. DOI: 10.1073/pnas.1814297116. URL: https://www.pnas.org/content/116/8/2805 (visited on 06/19/2019).

Turner, Alexander J., Christian Frankenberg, Paul O. Wennberg, et al. (Apr. 12, 2017). "Ambiguity in the causes for decadal trends in atmospheric methane and hydroxyl". In: *Proceedings of the National Academy of Sciences*, p. 201616020. ISSN: 0027-8424, 1091-6490. DOI: 10.1073/pnas.1616020114. URL: http://www.pnas.org/content/early/2017/04/11/1616020114 (visited on 08/14/2018).

Varon, D. J. et al. (Nov. 28, 2019). "Satellite Discovery of Anomalously Large Methane Point Sources From Oil/Gas Production". In: *Geophysical Research Letters* 46.22, pp. 13507–13516. ISSN: 0094-8276, 1944-8007. DOI: 10.1029/2019GL083798. URL: https://onlinelibrary.wiley.com/doi/10.1029/2019GL083798 (visited on 07/21/2023).

Wolfe, Glenn M. et al. (June 4, 2019). "Mapping hydroxyl variability throughout the global remote troposphere via synthesis of airborne and satellite formaldehyde observations". In: *Proceedings of the National Academy of Sciences* 116.23, pp. 11171–11180. ISSN: 0027-8424, 1091-6490. DOI: 10.1073/pnas.1821661116. URL: https://www.pnas.org/content/116/23/11171 (visited on 11/19/2019).

Worden, John R. et al. (Dec. 20, 2017). "Reduced biomass burning emissions reconcile conflicting estimates of the post-2006 atmospheric methane budget". In: *Nature Communications* 8.1, p. 2227. ISSN: 2041-1723. DOI: 10.1038/s41467-017-02246-0. URL: https://www.nature.com/articles/s41467-017-02246-0 (visited on 01/18/2018).

Chapter 2

EFFECTS OF COUPLED CHEMISTRY ON METHANE EMISSIONS

2.1 Abstract

Methane's 9-year lifetime makes it an attractive target for near-term radiative forcing mitigation. However, the coupled chemistry of carbon monoxide (CO), methane and the hydroxyl radical (OH) can modulate the methane lifetime, which is often ignored in methane flux inversions; and the impacts of neglecting those feedbacks have not been quantified. Using a coupled chemistry box model, we show that neglecting these effects can lead to a 50% bias in calculating methane source perturbations over multiple decades. The impact of inter-annual variations in CO abundances on OH can create ~10 Tg/yr methane pseudo-sources. Moreover, CO emissions (via biomass burning) during strong El Niño events can have comparable effects on methane abundances as direct emissions. Finally, we quantify the biases of including (or excluding) coupled chemistry in the context of recent methane and CO trends. Given these non-negligible errors, decadal methane emissions inversions should incorporate chemical feedbacks for more robust methane trend analyses.

2.2 Background

Methane is the second most important anthropogenic greenhouse gas. Globally averaged concentrations have risen from ~750 ppb during the pre-industrial to 1850 ppb in 2018, contributing to ~25% of overall radiative forcing (IPCC, 2013), with even higher contributions when considering all indirect impacts (Shindell et al., 2005). This increase includes a brief pause from 2000 to 2007 with a subsequent resumption in growth. The cause of the onset and termination of this stabilization remains debated (see Turner, Frankenberg, and Kort, 2019, and references therein for a review of recent trends). Due to nonlinear feedbacks affecting the main methane sink, which is oxidation by the Hydroxyl Radical (OH), perturbations of methane and other species controlling OH loss may affect the methane lifetime (Prather, 1994; Prather, 1996), especially in the context of recent methane and CO trends. This is often overlooked in methane inversion studies, as static OH fields are often employed, which may impact flux inversions at longer time-scales (Prather and Christopher D. Holmes, 2017). Our main objective here is to investigate how assumptions on the

oxidant chemistry affect methane emissions estimates.

Variations in methane fluxes have been inferred with constraints from methane concentrations and $\Delta^{13}C$ growth rates to study the 2000-2007 stabilization. However, by ignoring coupled chemistry, there are no changes in methane loss; thus any changes in methane abundances can only be attributed to methane source changes (e.g., Nisbet et al., 2016; Schaefer et al., 2016; Schwietzke et al., 2016; Thompson et al., 2018; J. R. Worden et al., 2017).

Other studies have focused on a possible change in the main methane sink (e.g., Gaubert et al., 2017; McNorton et al., 2016; Rigby et al., 2017; Turner, Frankenberg, Wennberg, et al., 2017). Gaubert et al. (2017) focused on the impact of CO on the methane lifetime. They found that a decline in CO concentrations, resulting from decreases in CO emissions in the 2000s (H. M. Worden et al., 2013), would result in increased OH concentrations during the stabilization period and, consequently, a decline in the methane lifetime. This change in the methane lifetime would require an even stronger increase in methane emissions to explain recent trends.

Rigby et al. (2017) and Turner, Frankenberg, Wennberg, et al. (2017) concluded it was likely that OH concentrations declined during the stabilization period. However, both studies ignored interactive chemistry but used observations of methyl chloroform (MCF) to constrain globally averaged OH concentrations. Yet Prather and Christopher D. Holmes (2017) pointed out two main problems: 1) using MCF to constrain OH is highly uncertain due to uncertainties in MCF emissions and loss, and 2) both studies did not explicitly account for chemical feedbacks (terms beyond the first order terms in Eq. 2.1). Given these uncertainties, alongside the contradicting hypotheses discussed here, the question remains: *"how do simplifying assumptions on coupled chemistry affect methane emissions estimates?"*

Studies employ simplifying assumptions in order to decrease computational cost, and the biases inherent in those assumptions are not well characterized, possibly contributing to contradicting hypotheses around the stabilization period. For instance, box model results have been criticized for not realistically modeling the impacts of atmospheric transport (Naus et al., 2019). On the other hand, sophisticated atmospheric transport models with 3D chemistry are used to invert methane fluxes, but they typically use static OH fields to model methane oxidation. In that context, we believe that the simplicity of a box model is an ideal way to isolate the impact of neglecting coupled chemistry on methane flux inversions from other error sources. To do this, we can conceptualize the complexity of the coupled drivers

affecting the decay of a methane perturbation $\delta[CH_4]$ into a linear expansion of chemical mechanisms, similar to Taylor series expansions:

$$\frac{d\delta[CH_4]}{dt} = \sum_i \left(\frac{\partial(d[CH_4]/dt)}{\partial[X_i]} \right) \delta[X_i]. \tag{2.1}$$

In Eq. 2.1, each X_i represents the concentration of species i (e.g. methane, CO, OH, NO_x), which might interact with the methane lifetime. Conceptually, a perturbation in i will either directly affect the methane lifetime (as is the case for [OH]) or indirectly affect methane loss by changing oxidant levels (e.g., higher CO will lead to a decrease in OH, whereas NO_x emissions will typically lead to increased OH abundance and methane loss). The coupled chemistry comes into play as methane oxidation impacts the steady state concentration of OH itself directly and indirectly, as the oxidation leads to CO, which interacts with OH at shorter timescales. Here, we focus on the coupled chemistry of methane, CO, and OH by using a 2-hemispheres box model with coupled methane, CO, and OH chemistry (Prather, 1994; Prather, 1996). We will quantify the impacts of critical assumptions in methane flux inversions (Table 2.4).

2.3 Hemispherically Averaged Concentrations

We use observations of methane (NOAA), CO (NOAA), and MCF (NOAA, GAGE/AGAGE) concentrations, where hemispheric averaging was done following Turner, Frankenberg, Wennberg, et al. (2017). In short, hemispheric averaging was done by bootstrapping from deseasonalized surface observations. We sampled from the observational record in each hemisphere with replacement, where number of times sampled is equal to the number of observational records available in that hemisphere for that species. We also rejected sites that had less than 5 yr of data and required that older observations had higher uncertainties than more recent observations, with a minimum uncertainty of 2 ppb. The randomly drawn observations were blocked-averaged into 1 yr windows. This process was repeated 50 times, so the mean and varience can be computed from these 50 timeseries.

CO is not well-mixed in the atmosphere, exhibiting large spatial gradients. In addition, each species experiences its own oxidative capacities (Naus et al., 2019; Lawrence and Jockel, 2001). Therefore, in order to model CO oxidation by OH, we selected stations in the tropics (23.5° S to 23.5° N). This is because most oxidation of CO occurs in the tropics, where OH concentrations are highest. We refer the reader to Table 2.2 and 2.3 for station locations and details. The hemispherically

averaged concentrations were calculated with the same bootstrapping procedure outlined above.

2.4 Constructing the Forward Model

OH oxidizes methane to form CO, which is also oxidized by OH, resulting in a coupled chemical system (Table 2.1). The equations in Table 2.1 are solved for each hemispheric box. The exchange between the hemispheric boxes are a function of the inter-hemispheric exchange time (1 yr) and inter-hemispheric concentration gradients.

We also employ simplifying assumptions to our model to abstract the complexity of OH production, recycling, and loss. OH is also the primary oxidant for a number of other compounds in the atmosphere (e.g., ethane and other non-methane hydrocarbons) (Jos Lelieveld et al., 2016), so we follow Prather (1994) and Prather (1996) and abstract this complexity with an arbitrary molecule, X, acting as an additional OH sink. In TAble 2.4 and 2.1, S_{OH} represents the production rate of OH, which is primarily driven by UV radiation in the presence of ozone and water vapor, in addition to chemical recycling by other species, especially NO_x (J. Lelieveld et al., 2002; Jos Lelieveld et al., 2016; Nicely et al., 2018). We do not explicitly account for these effects here and instead abstract this complexity with a term, S_{OH}, in our model, which then yields the OH concentration given the sources and sinks of OH. It should also be noted that here, non-interactive chemistry means that the methane oxidation rate is static, meaning that the globally averaged methane lifetime as well as the perturbation decay rates are fixed to ~9 yr. On the other hand, interactive chemistry allows for [OH] to respond to changes in CO and CH_4, even if S_{OH} is constant.

In order to obtain the correct perturbation lifetime seen in Fig. 2.1A, we adjusted the OH source (S_{OH}) and additional loss term ($k_3[x]$). The values we obtained are in Table 2.1. This results in the 13.2 yr perturbation lifetime.

Direct measurements of OH are neither spatially dense enough, nor sufficiently precise to estimate global mean OH concentrations. This is because OH has a short lifetime (~1 seconds), exists in low concentrations (~ 10^6 molecules/cm^3), and has large variations in space and time, so variations in MCF are often used as a proxy for globally integrated OH concentrations (e.g., Bousquet et al., 2005; Montzka et al., 2011).

Table 2.1: The coupled chemical reactions in this table models our simplified chemistry for each hemisphere, denoted by the superscripts.

Chemical Equation	Reaction Constant
$\frac{d[\mathrm{CH_4}]^\mathrm{N}}{dt} = S^N_{\mathrm{CH_4}} - k^N_1[\mathrm{CH_4}]^\mathrm{N}[\mathrm{OH}]^\mathrm{N} + \frac{[\mathrm{CH_4}]^\mathrm{S} - [\mathrm{CH_4}]^\mathrm{N}}{\tau}$	$k_1 = 3.395 \times 10^{-15} \frac{\mathrm{cm}^3}{\mathrm{molec\ \ s}}$
$\frac{d[\mathrm{CH_4}]^\mathrm{S}}{dt} = S^S_{\mathrm{CH_4}} - k^N_1[\mathrm{CH_4}]^\mathrm{S}[\mathrm{OH}]^\mathrm{S} + \frac{[\mathrm{CH_4}]^\mathrm{N} - [\mathrm{CH_4}]^\mathrm{S}}{\tau}$	$k_1 = 3.395 \times 10^{-15} \frac{\mathrm{cm}^3}{\mathrm{molec\ \ s}}$
$\frac{d[\mathrm{CO}]^\mathrm{N}}{dt} = S^N_{\mathrm{CO}} + k_1[\mathrm{CH_4}]^\mathrm{N}[\mathrm{OH}]^\mathrm{N} - k_2[\mathrm{CO}]^\mathrm{N}[\mathrm{OH}]^\mathrm{N} + \frac{[\mathrm{CO}]^\mathrm{S} - [\mathrm{CO}]^\mathrm{N}}{\tau}$	$k_2 = 1.0133 \times 10^{-12} \frac{\mathrm{cm}^3}{\mathrm{molec\ \ s}}$
$\frac{d[\mathrm{CO}]^\mathrm{S}}{dt} = S^S_{\mathrm{CO}} + k_1[\mathrm{CH_4}]^\mathrm{S}[\mathrm{OH}]^\mathrm{S} - k_2[\mathrm{CO}]^\mathrm{S}[\mathrm{OH}]^\mathrm{S} + \frac{[\mathrm{CO}]^\mathrm{N} - [\mathrm{CO}]^\mathrm{S}}{\tau}$	$k_2 = 1.0133 \times 10^{-12} \frac{\mathrm{cm}^3}{\mathrm{molec\ \ s}}$
$\frac{d[\mathrm{OH}]^\mathrm{N}}{dt} = S^N_{\mathrm{OH}} - k_1[\mathrm{CH_4}]^\mathrm{N}[\mathrm{OH}]^\mathrm{N} - k_2[\mathrm{CO}]^\mathrm{N}[\mathrm{OH}]^\mathrm{N} - k_3[\mathrm{X}]^\mathrm{N}[\mathrm{OH}]^\mathrm{N}$	$k_3[X]^N = 0.99s^{-1}$
$\frac{d[\mathrm{OH}]^\mathrm{S}}{dt} = S^S_{\mathrm{OH}} - k_1[\mathrm{CH_4}]^\mathrm{S}[\mathrm{OH}]^\mathrm{S} - k_2[\mathrm{CO}]^\mathrm{S}[\mathrm{OH}]^\mathrm{S} - k_3[\mathrm{X}]^\mathrm{S}[\mathrm{OH}]^\mathrm{S}$	$k_3[X]^S = 1.23s^{-1}$
$\frac{d[\mathrm{MCF}]^\mathrm{N}}{dt} = S^N_{\mathrm{MCF}} - k_4[\mathrm{MCF}]^\mathrm{N}[\mathrm{OH}]^\mathrm{N} + \frac{[\mathrm{MCF}]^\mathrm{S} - [\mathrm{MCF}]^\mathrm{N}}{\tau}$	$6.05 \times 10^{-15} \frac{\mathrm{cm}^3}{\mathrm{molecs}}$
$\frac{d[\mathrm{MCF}]^\mathrm{S}}{dt} = S^S_{\mathrm{MCF}} - k_4[\mathrm{MCF}]^\mathrm{S}[\mathrm{OH}]^\mathrm{S} + \frac{[\mathrm{MCF}]^\mathrm{N} - [\mathrm{MCF}]^\mathrm{S}}{\tau}$	$6.05 \times 10^{-15} \frac{\mathrm{cm}^3}{\mathrm{molecs}}$

2.5 Chemical Feedbacks Result in Extended Methane Lifetime

Perturbations to methane do not decay with the methane budget lifetime, which is obtained by dividing the total atmospheric methane burden with the methane loss rate assuming steady-state. Instead, in order to account for the nonlinearities in the methane-CO-OH system, perturbation decay rates are calculated from eigenvalues of the Jacobian of the chemical system, (Prather, 1994; Prather, 1996; Christopher D. Holmes, 2018).

$$\mathbf{K}_{ij} = \frac{\partial(d[\mathrm{x_i}]/dt)}{\partial[\mathrm{x_j}]}. \tag{2.2}$$

Each element of the Jacobian, **K**, consists of the derivative of the rate equations in Table 2.1, $(d[\mathrm{x_i}]/dt)$, with respect to each species, $[\mathrm{x}_j]$. The complexity of the system is caused by the off-diagonal elements in the matrix, resulting in different perturbation modes with respective decay rates. This perturbation decay rate is also a function of the concentrations of the species in **K**, because the eigenvalues depend on the values in **K**. Substituting methane, CO, and OH concentrations of the modern atmosphere into Eq. 2.2 and inverting the minimum eigenvalue of **K** results in the methane perturbation lifetime that is ~40% longer than the budget lifetime.

We demonstrate this extended perturbation lifetime in Fig. 2.1A, running the model with prescribed emissions, adding a 10 Tg perturbation to methane emissions with interactive and non-interactive chemistry Fig. 2.1A. The perturbation lifetime of the non-interactive chemistry model decays with a ~9.4 yr e-folding lifetime, while the interactive chemistry decays with a ~13.2 yr lifetime. This is expected (Prather, 1994; Prather, 1996) and indicates that our forward box model is a realistic approximation of the chemical system. It should be noted that this perturbation lifetime

also holds for infinitesimally small perturbations to methane or CO, which drive correspondingly small perturbations to OH, a fact that is sometimes overlooked. The question is what impact these differences have on decadal-scale flux inversions, because most studies assume a fixed ~9 yr lifetime. As can be seen in Figure 2.1a, a methane perturbation decays much slower, so we expect an overestimation of methane flux inversions if this effect is ignored.

Chemical simulations of interactive chemistry, when compared to non-interactive chemistry, result in different equilibrium methane concentrations. We demonstrate this in Fig. 2.1b, where methane emissions are fixed to 275, 550, 1100, and 2200 Tg/yr with both interactive (solid lines) and non-interactive (dashed lines) chemistry. For emissions larger than the contemporary 550 Tg/yr case (Saunois et al., 2016), the interactive chemistry cases have much higher steady-state methane concentrations than their non-interactive counterparts, because methane concentrations affect OH. However, for the pre-industrial 275 Tg/yr case, the interactive steady state concentrations are substantially lower as OH would be about 25% higher. As our prescribed emissions become larger, the difference between methane steady state concentrations in the interactive and non-interactive cases further differ. In the 2200 Tg/yr case, the lifetime and steady-state lifetime differ by more than a factor of three, caused by OH depletion (Fig. 2.1c). Even after more than 150 years, the 2200 Tg/yr interactive chemistry case reaches concentrations of ~30 ppm, while OH decreases to 10% of contemporary concentrations, and both have not yet reached a steady state. It should be noted that this simulation ignores other methane sinks, e.g. stratospheric loss or soil uptake, both of which will dampen this effect in the actual atmosphere and avoid a runaway effect.

2.6 Effects of El Niño on Methane Concentrations

Here we use the coupled methane-CO-OH chemistry to examine the impact of strong biomass burning during El Niño events on both methane and CO, and consequently OH. Previous works have highlighted the importance of El Niño on methane (e.g., Saunois et al., 2016; J. Worden et al., 2013; Zhang et al., 2018), CO (e.g., Yin et al., 2016), emissions through wetlands and fires. El Niño can further impact OH recycling via changing emissions of lightning NO_x (e.g., Murray et al., 2014; Turner, Fung, et al., 2018) and through direct NO_x emissions from fires (e.g., Castellanos, Boersma, and Werf, 2014; Miyazaki et al., 2017), although NO_x effects are not explicitly represented here. However, NO_x emissions will have a more local to regional effect on OH, due to its shorter lifetime compared with CO and methane.

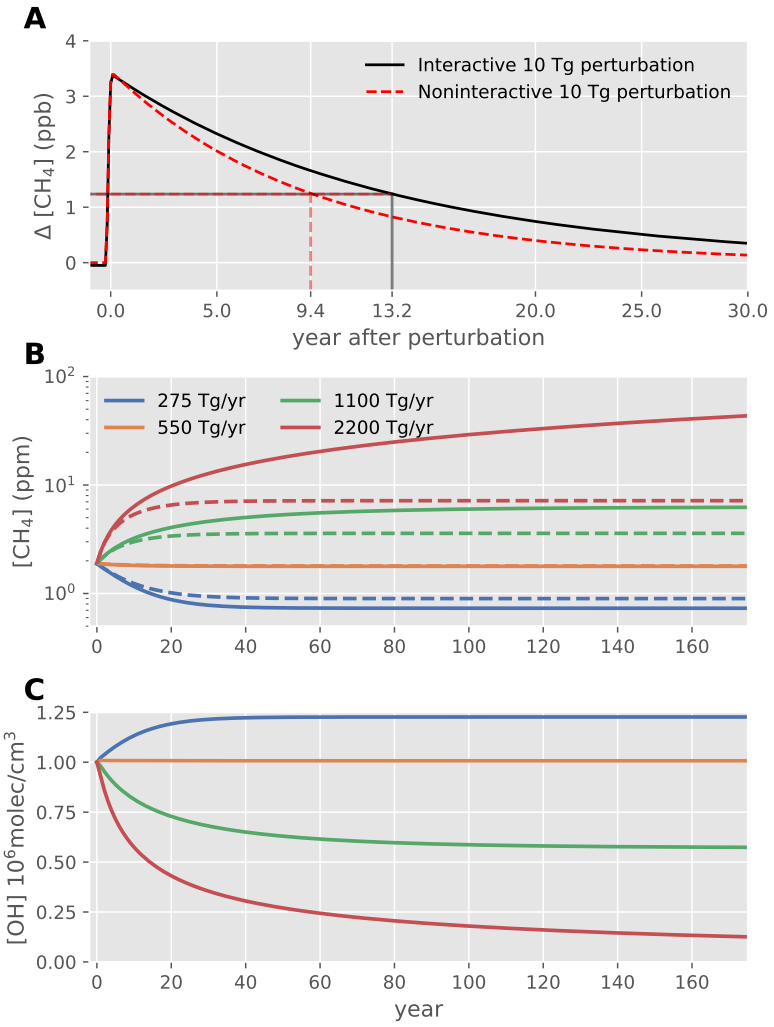

Figure 2.1: A 10 Tg perturbation of methane (Panel A) decays with a 13.2 yr lifetime for the interactive case (solid line), while the perturbation decays with a 9.4 year lifetime for the non-interactive case (dotted line). Methane concentrations (Panel B) and OH concentrations (Panel C) are shown for our steady-state test, where emissions are fixed to 275, 550, 1100, and 2200 Tg/yr for both interactive (solid lines) and non-interactive (dashed lines) chemistry.

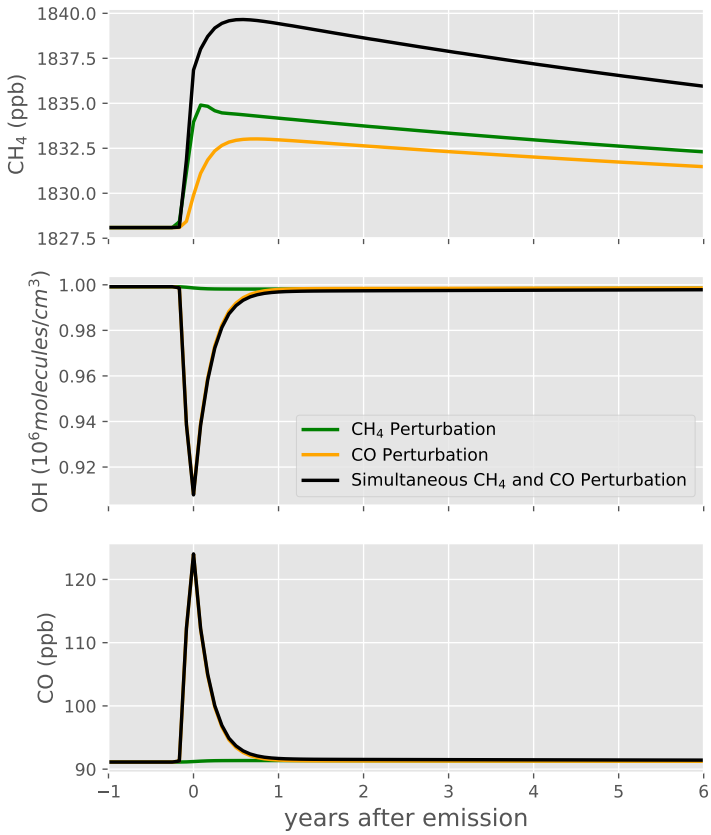

Figure 2.2: A 20 Tg pulse of methane (green) increases methane by 6.8 ppb. A 250 Tg perturbation of CO (orange) depletes OH by $\sim -8\%$, extending the methane lifetime, resulting in a 5 ppb increase in methane. The methane and CO joint response (blue) results in a 11.5 ppb increase.

Fig. 2.2 shows the results of three simulations with one-month-long perturbations: 1) a methane release of 20 Tg, 2) a CO release of 250 Tg, and 3) a simultaneous release of 20 Tg methane and 250 Tg CO, which is similar in magnitude to the 1997-1998 El Niño (Randerson et al., 2017). From this, we can observe the response of the system to individual perturbations as well as the joint response, testing our model with other El Niño results (e.g., Butler et al., 2005; Duncan et al., 2003; Rowlinson et al., 2019).

In Fig. 2.2, methane increases by ~6.8 ppb to a 20 Tg methane perturbation (the green line) and by ~5 ppb to the 250 Tg CO perturbation (the orange line). The latter is due to impact of CO on OH concentrations by $\sim -8\%$, not due to direct methane emissions. The decrease in the methane oxidation rate due to the decline in OH increases the methane lifetime in the atmosphere, acting as a pseudo-source of

methane that acts over several months even after the fires stopped. This OH response is within the range calculated by other studies using 3-D chemical transport models e.g., Butler et al. (2005) find a $\sim -2.2\%$ decline in [OH] between July 1997 and December 1998 ; Duncan et al. (2003) find -2.2% to -6.8% between September and December 1997 from the Indonesian fires; and most recently, Rowlinson et al. (2019) find $\sim -9\%$ between 1997 and 1998. This indicates that the magnitude of the OH response to CO perturbations in our model is realistic.

The indirect impact through CO emissions is comparable in magnitude to the direct methane emissions, resulting in a much stronger and delayed joint response of methane to perturbations typical for large-scale biomass burning events. The case of the combined methane and CO perturbation results in an 11.5 ppb increase in methane with almost half a year delay in its peak enhancement, demonstrating the coupling of the CH_4-CO-OH system. Hence, it is possible that increases in methane concentrations can be incorrectly attributed to increases in methane emissions, rather than CO emissions (or another species that can impact OH abundances). An El Niño scenario is thus an excellent test case for underlining the importance of interactive chemistry on not only the magnitude of response of methane and [OH] to perturbations, but also the timing of the response. In fact, the impact of biomass burning is highly complex. Locally, direct emissions of methane as well as strong perturbations in NO_x, radiation, CO and other trace gases can play a role, which we cannot quantify in our simplified model. The impact on hemispherically averaged CO concentrations, however, is well captured by our model and has a significant impact on methane concentrations (hence the term pseudo-source) but not in the area of biomass burning directly. Flux inversions using concentration gradients would thus not attribute these background changes in methane concentrations to the actual fires.

2.7 Inverting for methane Emissions

Our box model maps emissions to concentrations and thus, inverting our model maps concentrations to emissions. This enables us to quantify the effects of simplifying assumptions on methane flux inversions. Emissions are estimated using a non-linear Bayesian inversion method (Rodgers, 2000). We use observations of methane (NOAA), CO (NOAA), and MCF (NOAA, GAGE/AGAGE) concentrations, where hemispherically averaged observations were computed following the methods in Turner, Frankenberg, Wennberg, et al. (2017).

We used a non-linear bayesian inversion to obtain the methane fluxes seen in Fig. 2.3 and 2.4 (Rodgers, 2000). The elements of the state vector being fitted for are in Table 2.4 alongside the observations being used to constrain the inversion. The a priori assumptions and prior error for our inversion are shown in Table 2.1. For the MCF prior in the Northern Hemisphere, we set the error to 20% of the a priori with a minimum of 1.5 Gg. It should also be noted that the temporal correlation we employed was different for the case corresponding to (Rigby et al., 2017) and (Turner, Frankenberg, Wennberg, et al., 2017) (+I +[OH]) as compared to the other cases, which is the reason why the methane timeseries looks much smoother. We employed much shorter temporal correlations to the other cases in order to make the inter-annual variability more clear.

Table 2.2: Monitoring stations used for methane observations.

Station	Code	Latitude	Laboratory
Methane measurements			
Alert, Canada	ALT	82°N	NOAA/ESRL/INSTAAR
Ascension Island, UK	ASC	8°S	NOAA/ESRL/INSTAAR
Terceira Island, Azores	AZR	39°N	NOAA/ESRL/INSTAAR
Baring Head, NZ	BHD	41°S	NOAA/ESRL/INSTAAR
Barrow, USA	BRW	71°N	NOAA/ESRL/INSTAAR
Cold Bay, USA	CBA	55°N	NOAA/ESRL/INSTAAR
Cape Grim, Australia	CGO	41°S	NOAA/ESRL/INSTAAR
Cape Kumukahi, USA	KUM	20°N	NOAA/ESRL/INSTAAR
Lac La Biche, Canada	LLB	55°N	NOAA/ESRL/INSTAAR
High Altitude Global Climate Observation Center, Mexico	MEX	19°N	NOAA/ESRL/INSTAAR
Mace Head, Ireland	MHD	53°N	NOAA/ESRL/INSTAAR
Mauna Loa, USA	MLO	20°N	NOAA/ESRL/INSTAAR
Niwot Ridge, USA	NWR	40°N	NOAA/ESRL/INSTAAR
Cape Matatula, Samoa	SMO	14°S	NOAA/ESRL/INSTAAR
South Pole, Antarctica	SPO	90°S	NOAA/ESRL/INSTAAR
Summit, Greenland	SUM	73°N	NOAA/ESRL/INSTAAR
Tae-ahn Peninsula, Korea	TAP	37°N	NOAA/ESRL/INSTAAR
Mt. Waliguan, China	WLG	36°N	NOAA/ESRL/INSTAAR
Ny-Alesund, Norway	ZEP	80°N	NOAA/ESRL/INSTAAR
Alert, Canada	ALT	82°N	U. Heidelberg
Izana, Portugal	IZA	28°N	U. Heidelberg
Neumayer, Antarctica	NEU	71°S	U. Heidelberg
Niwot Ridge, USA	NWR	41°N	U.C. Irvine
Montana de Oro, USA	MDO	35°N	U.C. Irvine
Cape Grim, Australia	CGO	41°S	U. Washington
Olympic Peninsula, USA	OPW	48°N	U. Washington
Fraserdale, Canada	FSD	50°N	U. Washington
Majuro, Marshall Islands	MMI	7°N	U. Washington
Mauna Loa, USA	MLO	19°N	U. Washington
Baring Head, NZ	BHD	41°S	U. Washington
Barrow, USA	BRW	71°N	U. Washington
Tutuila, Samoa	SMO	14°S	U. Washington

Table 2.3: Methyl Chloroform and Carbon Monoxide observation stations

Station	Code	Latitude	Laboratory
Methyl Chloroform measurements			
Alert, Canada	ALT	82°N	NOAA/ESRL
Barrow, USA	BRW	71°N	NOAA/ESRL
Cape Grim, Australia	CGO	41°S	NOAA/ESRL
Cape Kumukahi, USA	KUM	20°N	NOAA/ESRL
Mace Head, Ireland	MHD	53°N	NOAA/ESRL
Mauna Loa, USA	MLO	20°N	NOAA/ESRL
Palmer Station, Antarctica	PSA	65°S	NOAA/ESRL
Niwot Ridge, USA	NWR	40°N	NOAA/ESRL
Cape Matatula, Samoa	SMO	14°S	NOAA/ESRL
South Pole, Antarctica	SPO	90°S	NOAA/ESRL
Summit, Greenland	SUM	73°N	NOAA/ESRL
Trinidad Head, USA	THD	41°N	NOAA/ESRL
Cape Grim, Australia	CGO	41°S	GAGE
Mace Head, Ireland	MHD	53°N	GAGE
Cape Meares, USA	ORG	45°N	GAGE
Ragged Point Barbados	RPB	13°N	GAGE
Cape Matatula, Samoa	SMO	14°S	GAGE
Cape Grim, Australia	CGO	41°S	AGAGE
Mace Head, Ireland	MHD	53°N	AGAGE
Ragged Point Barbados	RPB	13°N	AGAGE
Cape Matatula, Samoa	SMO	14°S	AGAGE
Trinidad Head, USA	THD	41°N	AGAGE
Station	Code	Latitude	Laboratory
Carbon Monoxide measurements			
Mauna Loa, USA	MLO	20°N	INSTAAR
Ragged Point Barbados	RPB	13°N	INSTAAR
Cape Matatula, Samoa	SMO	14°S	INSTAAR

2.8 Timescale for INcluding INteractive OH Chemistry

Here we estimate the impact of neglecting interactive OH chemistry in an idealized inversion test case. Methane emissions are prescribed in our forward model, assuming interactive chemistry with a constant 6300 Tg/yr-OH source, resulting in a synthetic methane concentrations time-series, shown in Fig. 2.3A. We use a scenario in which methane emissions abruptly and permanently increase from 550 to 570 Tg/yr, an increase similar to the one needed to explain the renewed growth rate after 2007. The resulting synthetic concentrations in Fig. 2.3A constitute synthetic observations used in two inversions, where we assume A) non interactive chemistry, and B) interactive chemistry. This test serves two purposes: 1) to test the perfor-

mance of our inversion, and 2) to calculate the error associated with neglecting interactive OH chemistry in an inversion, as was alluded to in (Prather and Christopher D. Holmes, 2017). This is equivalent to computing the forward model error of assuming fixed OH concentrations in atmospheric methane inversions (while the true atmosphere is interactive).

From our synthetic emissions test results (Fig. 2.3B and C), we find that the inversion is accurate with interactive chemistry. However, inverted methane emissions, in our non-interactive inversion, are consistently higher after our prescribed emissions increase, (Fig. 2.3b), reaching an overestimation of about 5 Tg/yr after only 10 years after the emissions change, which is 25% of the perturbation. This error increases to well over 8 Tg/yr after more than 20 years. This is because the increased methane emissions decrease OH concentrations, whereas the non-interactive concentrations inversion does not account for this OH response. This is non-negligible, because we only need a 20 Tg/yr source-sink imbalance to explain the 2007 renewed growth. Relative errors in these derived emission trends can thus be considerable if we assume fixed OH concentrations.

2.9 Emissions Estimates with Observed Concentrations

We performed inversions with increasing levels of complexity to obtain the biases associated with including (or neglecting) interactive OH chemistry and CO in emissions estimates constrained by methane, CO, and MCF observations. Table 2.4 describes the assumptions in each experiment. In the non-interactive case (-I), OH concentrations are fixed, and thus, inversions of methane emissions only respond to changes in methane concentrations, whereas in the interactive case (+I), methane emissions adjust to changes in both methane and OH concentrations. In particular, the ~210 ppb increase of methane between 1984 and 2017 would, assuming a constant OH source, decrease OH abundances by ~3.5%, extending the methane lifetime and result in an overestimation of methane emissions when compared to a scenario where [OH] is held constant (-I). The blue line in Fig 2.4a shows the difference between our methane inversion, which accounts for interactive chemistry (+I) and non-interactive chemistry (-I). Discounting interactive OH chemistry would lead to biased trends in the methane fluxes compared to the 1980 baseline, as increasing methane abundances will cause [OH] to decrease. When keeping CO constant, this could induce a 20 Tg bias in methane emissions changes between 1980 and 2015, as indicated by the green line's overall declining trend between 1980 and 2017.

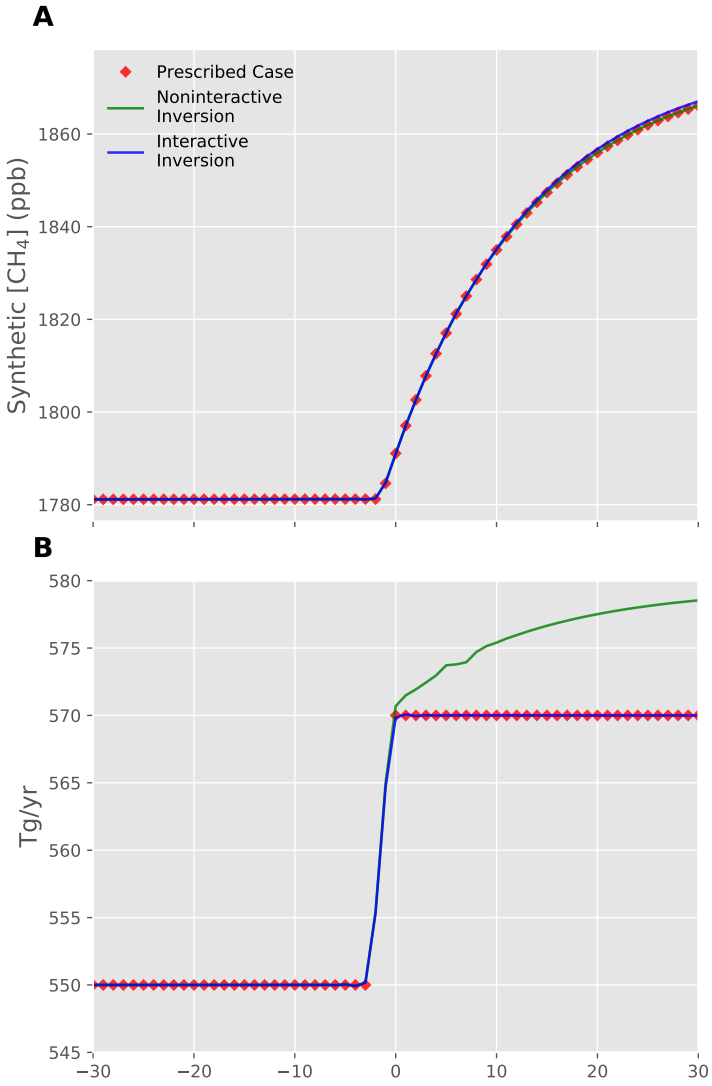

Figure 2.3: Inversion with prescribed emissions: Methane emissions were prescribed with an abrupt +20 Tg/yr step-change in emissions, resulting in a time-series of methane concentrations (shown in red in Panel A). These synthetic observations were used in two inversions shown in Panel B: Interactive OH Inversion (blue line) and Non-interactive OH Inversion (green line). Note that the prescribed emissions are shown as red diamonds in Panel B but are difficult to see, as they overlap with the Interactive OH Inversion.

Accounting for the decrease in CO emissions (Fig. 2.4d) would increase the availability of OH radicals to oxidize methane. We quantify this impact ($+I/+S_{CO}$) by allowing our inversion to adjust to the declining CO concentrations (Fig. 2.4d), fitting for CO sources, and comparing this to our non-interactive OH inversion (-I). CO sources exclude CO from methane oxidation and only considers direct emissions, which include biomass burning and combustion. The orange line's rising slope in Fig. 2.4a underlines that 1) decreasing CO abundances overcompensate the effect of increasing methane on OH, consistent with Gaubert et al. (2017), and 2) neglecting indirect effects of CO can result in an error of the inter-annual methane source variability of up to 10 Tg/yr. It should be noted here that our interactive chemistry results may differ from more sophisticated chemistry models, because our model only includes methane and CO effects. In reality, the OH source may have regionally increased due to rising NO_x emissions, which would buffer [OH] (C. D. Holmes et al., 2013; Naik et al., 2013; Nicely et al., 2018). We do not explicitly include this effect in our model.

Variations in stratospheric ozone and NO_x can result in OH recycling and production variability, and these OH sources have been thought to have increased in recent decades (e.g., C. D. Holmes et al., 2013; Naik et al., 2013; Nicely et al., 2018). To quantify this OH-source variability, ($+I + S_{OH}$) incorporates OH source variability, while ($+I + S_{CO} + S_{OH}$) also accounts for CO source variability. When we assume a variable OH source (+I +S_{OH}), the variability in methane emissions is dampened, because OH production and recycling are able to compensate for the variability in OH concentrations. As a result, methane emissions stabilize and decline between 2000 and 2010. This result also exhibits similar variability to the case corresponding to Turner, Frankenberg, Wennberg, et al. (2017) and Rigby et al. (2017), (-I+[OH]), where concentrations are fitted directly, without interactive chemistry. Also fitting for CO emissions (+I +S_{OH} + S_{CO}) further dampens the variability of methane emissions, because CO emissions are also allowed to compensate for variability in methane emissions. These cases are also similar to each other until about 2010, when MCF observation uncertainties reach instrument limitations (Naus et al., 2019).

The 1998 peak in methane emissions, due to El Niño, demonstrates the coupling of the methane-CO-OH system. We observe a local maximum in the CO concentrations in 1998 (Fig. 2.4D). All cases infer an increase in methane emissions with the 1998 El Niño, but the magnitude and duration are markedly different. Specifically, the ($-I$) case only accounts for methane emissions and infers ~48 Tg/yr "spike" in

Table 2.4: Varying complexity of simulations for flux inversions corresponding to experiments in Fig. 2.4.

Case Label	Interactive OH	Inverting [OH]	Inverting S_{CO}	Inverting S_{OH}	Constrained by
$-I$	no	no	n/a	n/a	$[CH_4]$
$-I + [OH]$	no	yes	n/a	n/a	$[CH_4]$
$+I$	yes	n/a	no	no	$[CH_4]$
$+I + S_{CO}$	yes	n/a	yes	no	$[CH_4]$[MCF][CO]
$+I + S_{OH}$	yes	n/a	no	yes	$[CH_4]$[MCF]
$+I + S_{CO} + S_{OH}$	yes	n/a	yes	yes	$[CH_4]$[MCF][CO]

1998 compared to 1997. This methane emissions spike is not observed in the cases with interactive chemistry. This is because they are able to accommodate the 1998 minimum in OH concentrations. As such, the interactive cases find a smaller magnitude emission increase and a different temporal signal. Specifically, 31 Tg/yr for ($+I + S_{OH}$) and 26 Tg/yr for ($+I + S_{OH} + S_{CO}$). When CO sources are also fitted in the latter case, the inversion is allowed to respond to higher CO concentrations (Fig. 2.4d), and we see even less methane emissions, due to a release of CO from increased biomass burning (Sec. 2.6).

2.10 Summary and Recommendations

Studies calculating global methane emissions have conclusions that are dependent on the assumptions on chemical reaction rates within their inversions. This is because the methane lifetime depends on the concentration of the OH radical which, in turn, depends on the concentration of CO and methane as well as sources of OH. There are no perfect methods to constrain global OH concentrations, and more work should be done to constrain trends in the concentration and production of hydroxyl radicals (e.g., Li et al., 2018; Miyazaki et al., 2017; Wolfe et al., 2019). In decadal methane emissions estimates with fixed OH concentrations, we find a systematic and non-negligible negative bias in inversions that do not consider this chemical feedback. When accounting for CO concentration variations, we find decreased CO emissions beginning in the 2000's increased the availability of OH, increasing methane emissions estimates. However, accounting for OH source variability results in methane emissions estimates with similar trend and variability to Rigby et al. (2017) and Turner, Frankenberg, Wennberg, et al. (2017), where OH concentrations are fitted directly without interactive chemistry. This is due to compensating OH production accounting for variabilities in OH concentrations. It should be noted that

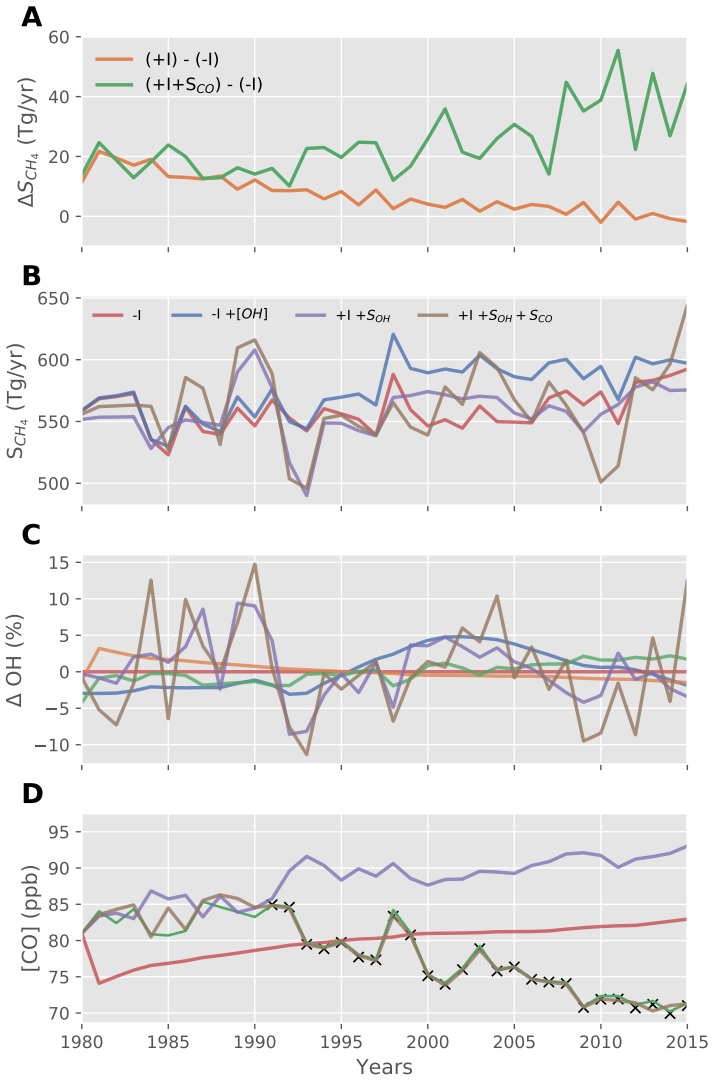

Figure 2.4: Methane Inversions Constrained by Methane, CO, and MCF Observations: The green line in Panel A shows the difference between our interactive chemistry case (+I) and non-interactive chemistry case (-I), while the orange line shows the difference between our interactive chemistry case with fitted CO sources ($+I + S_{CO}$) and non-interactive chemistry case (-I). Methane emissions calculations (Panel B) differ when the inversion is allowed to respond to variations in OH concentrations (shown in Panel C). Panel D shows observed CO concentrations (black Xes) and our CO fits. The assumptions and constraints for each experiment are listed in Table 2.4.

other chemical effects that may have a large impact on OH abundances, such as NO_x, Ozone, and water vapor effects (C. D. Holmes et al., 2013; Naik et al., 2013; Nicely et al., 2018) are not explicitly represented in our model, so the question *"how does OH production and recycling vary over time?"* remains and should be a priority research objective.

Moving towards a more robust methane trend analysis, global methane emissions inversions at decadal timescales should account for the chemistry affecting methane lifetime in the atmosphere. Inversions with chemical transport models may provide transport effects, however, they neglect the non-negligible impacts of OH chemistry on methane lifetime, as their OH fields are usually assumed to be static. This may also have implications for paleoclimate studies (e.g., Dickens et al., 1995; Frieling et al., 2016). Future inversions should include this methane chemical feedback, informed by climate variables relevant for OH production and concentrations. For example, ~90% of variations in OH production can be parameterized by temperature, water vapor, column ozone, biomass burning emissions, and lightning NO_x emissions (C. D. Holmes et al., 2013), so OH production and recycling (S_{OH}) can have real-world constraints (Castellanos, Boersma, and Werf, 2014; C. D. Holmes et al., 2013; Miyazaki et al., 2017). Simplified parameterizations can capture primary drivers of OH production and recycling, while joint inversions of species that modulate OH concentrations, informed by bottom-up inventories, will more accurately represent methane lifetimes, bringing decadal-scale methane inversions closer to the real world.

ACKNOWLEDGMENTS

This work was supported by a NSF Graduate Research Fellowship (to N. H. Nguyen) and a grant from the Grantham Foundation (to Y. Yin and N. H. Nguyen). A. J. Turner is supported as a Miller Fellow with the Miller Institute for Basic Research in Science at UC Berkeley. The authors declare no conflic of interest.

The 2-hemispheres box model can be accessed via Github at:

`https://github.com/Newton-Climate/Methane_OH_box`;

Surface observations were accessed from the following sources:
CH_4 NOAA: `ftp://aftp.cmdl.noaa.gov/data/trace_gases/ch4/flask/`;
MCF NOAA: `ftp://aftp.cmdl.noaa.gov/data/hats/solvents/CH3CCl3/`;
MCF GAGE/AGAGE: `http://agage.mit.edu/`;
CO NOAA: `ftp://aftp.cmdl.noaa.gov/data/trace_gases/co/flask/surface/`

BIBLIOGRAPHY

Bousquet, P et al. (2005). "Two decades of OH variability as inferred by an inversion of atmospheric transport and chemistry of methyl chloroform". In: *Atmos. Chem. Phys.*, p. 22.

Butler, T. M. et al. (2005). "Simultaneous mass balance inverse modeling of methane and carbon monoxide". In: *Journal of Geophysical Research: Atmospheres* 110 (D21). ISSN: 2156-2202. DOI: 10.1029/2005JD006071. URL: https://agupubs.onlinelibrary.wiley.com/doi/abs/10.1029/2005JD006071 (visited on 11/19/2019).

Castellanos, P., K. F. Boersma, and G. R. van der Werf (Apr. 17, 2014). "Satellite observations indicate substantial spatiotemporal variability in biomass burning NO_x emission factors for South America". In: *Atmospheric Chemistry and Physics* 14.8, pp. 3929–3943. ISSN: 1680-7316. DOI: https://doi.org/10.5194/acp-14-3929-2014. URL: https://www.atmos-chem-phys.net/14/3929/2014/ (visited on 11/19/2019).

Dickens, Gerald R. et al. (1995). "Dissociation of oceanic methane hydrate as a cause of the carbon isotope excursion at the end of the Paleocene". In: *Paleoceanography* 10.6, pp. 965–971. ISSN: 1944-9186. DOI: 10.1029/95PA02087. URL: https://agupubs.onlinelibrary.wiley.com/doi/abs/10.1029/95PA02087 (visited on 09/25/2019).

Duncan, B. N. et al. (2003). "Indonesian wildfires of 1997: Impact on tropospheric chemistry". In: *Journal of Geophysical Research: Atmospheres* 108 (D15). ISSN: 2156-2202. DOI: 10.1029/2002JD003195. URL: https://agupubs.onlinelibrary.wiley.com/doi/abs/10.1029/2002JD003195 (visited on 11/25/2019).

Frieling, Joost et al. (Oct. 25, 2016). "Thermogenic methane release as a cause for the long duration of the PETM". In: *Proceedings of the National Academy of Sciences* 113.43, pp. 12059–12064. ISSN: 0027-8424, 1091-6490. DOI: 10.1073/pnas.1603348113. URL: https://www.pnas.org/content/113/43/12059 (visited on 09/25/2019).

Gaubert, B. et al. (2017). "Chemical Feedback From Decreasing Carbon Monoxide Emissions". In: *Geophysical Research Letters* 44.19, pp. 9985–9995. ISSN: 1944-8007. DOI: 10.1002/2017GL074987. URL: https://agupubs.onlinelibrary.wiley.com/doi/abs/10.1002/2017GL074987 (visited on 01/18/2019).

Holmes, C. D. et al. (Jan. 11, 2013). "Future methane, hydroxyl, and their uncertainties: key climate and emission parameters for future predictions". In: *Atmospheric Chemistry and Physics* 13.1, pp. 285–302. ISSN: 1680-7324. DOI: 10.5194/acp-13-285-2013. URL: https://www.atmos-chem-phys.net/13/285/2013/ (visited on 08/19/2019).

Holmes, Christopher D. (2018). "Methane Feedback on Atmospheric Chemistry: Methods, Models, and Mechanisms". In: *Journal of Advances in Modeling Earth Systems* 10.4, pp. 1087–1099. ISSN: 1942-2466. DOI: 10.1002/2017MS001196. URL: https://agupubs.onlinelibrary.wiley.com/doi/abs/10.1002/2017MS001196 (visited on 11/19/2019).

IPCC (2013). *Climate Change 2013: The Physical Science Basis. Contribution of Working Group I to the Fifth Assessment Report of the Intergovernmental Panel on Climate Change*. Cambridge, United Kingdom and New York, NY, USA: Cambridge University Press. 1535 pp. ISBN: ISBN 978-1-107-66182-0. DOI: 10.1017/CBO9781107415324. URL: www.climatechange2013.org.

Lawrence, M G and P Jockel (2001). "What does the global mean OH concentration tell us?" In: *Atmos. Chem. Phys.*, p. 13.

Lelieveld, J. et al. (2002). "Stability of tropospheric hydroxyl chemistry". In: *Journal of Geophysical Research: Atmospheres* 107 (D23), ACH 17–1–ACH 17–11. ISSN: 2156-2202. DOI: 10.1029/2002JD002272. URL: https://agupubs.onlinelibrary.wiley.com/doi/abs/10.1029/2002JD002272 (visited on 12/31/2019).

Lelieveld, Jos et al. (Oct. 5, 2016). "Global tropospheric hydroxyl distribution, budget and reactivity". In: *Atmospheric Chemistry and Physics* 16.19, pp. 12477–12493. ISSN: 1680-7324. DOI: 10.5194/acp-16-12477-2016. URL: https://www.atmos-chem-phys.net/16/12477/2016/ (visited on 03/20/2019).

Li, Mengze et al. (Sept. 11, 2018). "Tropospheric OH and stratospheric OH and Cl concentrations determined from CH 4 , CH 3 Cl, and SF 6 measurements". In: *npj Climate and Atmospheric Science* 1.1, p. 29. ISSN: 2397-3722. DOI: 10.1038/s41612-018-0041-9. URL: https://www.nature.com/articles/s41612-018-0041-9 (visited on 03/20/2019).

McNorton, Joe et al. (June 30, 2016). "Role of OH variability in the stalling of the global atmospheric CH_4 growth rate from 1999 to 2006". In: *Atmospheric Chemistry and Physics* 16.12, pp. 7943–7956. ISSN: 1680-7316. DOI: https://doi.org/10.5194/acp-16-7943-2016. URL: https://www.atmos-chem-phys.net/16/7943/2016/ (visited on 11/25/2019).

Miyazaki, Kazuyuki et al. (Jan. 27, 2017). "Decadal changes in global surface NO $_x$ emissions from multi-constituent satellite data assimilation". In: *Atmospheric Chemistry and Physics* 17.2, pp. 807–837. ISSN: 1680-7324. DOI: 10.5194/acp-17-807-2017. URL: https://www.atmos-chem-phys.net/17/807/2017/ (visited on 11/19/2019).

Montzka, S. A. et al. (Jan. 7, 2011). "Small Interannual Variability of Global Atmospheric Hydroxyl". In: *Science* 331.6013, pp. 67–69. ISSN: 0036-8075, 1095-9203. DOI: 10.1126/science.1197640. URL: https://science.sciencemag.org/content/331/6013/67 (visited on 06/19/2019).

Murray, L. T. et al. (Apr. 9, 2014). "Factors controlling variability in the oxidative capacity of the troposphere since the Last Glacial Maximum". In: *Atmospheric Chemistry and Physics* 14.7, pp. 3589–3622. ISSN: 1680-7316. DOI: https://doi.org/10.5194/acp-14-3589-2014. URL: https://www.atmos-chem-phys.net/14/3589/2014/acp-14-3589-2014.html (visited on 07/03/2019).

Naik, V. et al. (May 27, 2013). "Preindustrial to present-day changes in tropospheric hydroxyl radical and methane lifetime from the Atmospheric Chemistry and Climate Model Intercomparison Project (ACCMIP)". In: *Atmospheric Chemistry and Physics* 13.10, pp. 5277–5298. ISSN: 1680-7324. DOI: 10.5194/acp-13-5277-2013. URL: https://www.atmos-chem-phys.net/13/5277/2013/ (visited on 11/26/2019).

Naus, Stijn et al. (Jan. 11, 2019). "Constraints and biases in a tropospheric two-box model of OH". In: *Atmospheric Chemistry and Physics* 19.1, pp. 407–424. ISSN: 1680-7324. DOI: 10.5194/acp-19-407-2019. URL: https://www.atmos-chem-phys.net/19/407/2019/ (visited on 06/07/2019).

Nicely, Julie M. et al. (2018). "Changes in Global Tropospheric OH Expected as a Result of Climate Change Over the Last Several Decades". In: *Journal of Geophysical Research: Atmospheres* 123.18, pp. 10, 774–10, 795. ISSN: 2169-8996. DOI: 10.1029/2018JD028388. URL: https://agupubs.onlinelibrary.wiley.com/doi/abs/10.1029/2018JD028388 (visited on 06/19/2019).

Nisbet, E. G. et al. (Sept. 1, 2016). "Rising atmospheric methane: 2007–2014 growth and isotopic shift". In: *Global Biogeochemical Cycles* 30.9, pp. 1356–1370. ISSN: 1944-9224. DOI: 10.1002/2016GB005406. URL: https://agupubs.onlinelibrary.wiley.com/doi/10.1002/2016GB005406 (visited on 11/27/2019).

Prather, Michael J. (May 1994). "Lifetimes and eigenstates in atmospheric chemistry". In: *Geophysical Research Letters* 21.9, pp. 801–804. ISSN: 1944-8007. DOI: 10.1029/94GL00840. URL: https://agupubs.onlinelibrary.wiley.com/doi/abs/10.1029/94GL00840 (visited on 11/27/2019).

– (Sept. 1996). "Time scales in atmospheric chemistry: Theory, GWPs for CH4 and CO, and runaway growth". In: *Geophysical Research Letters* 23.19, pp. 2597–2600. ISSN: 1944-8007. DOI: 10.1029/96GL02371. URL: https://agupubs.onlinelibrary.wiley.com/doi/abs/10.1029/96GL02371 (visited on 06/12/2018).

Prather, Michael J. and Christopher D. Holmes (May 23, 2017). "Overexplaining or underexplaining methane's role in climate change". In: *Proceedings of the National Academy of Sciences* 114.21, pp. 5324–5326. ISSN: 0027-8424, 1091-6490. DOI: 10.1073/pnas.1704884114. URL: http://www.pnas.org/content/114/21/5324 (visited on 06/12/2018).

Randerson, J.T. et al. (2017). *Global Fire Emissions Database, Version 4.1 (GFEDv4)*. ORNL Distributed Active Archive Center. DOI: 10.3334/ORNLDAAC/1293. URL: https://daac.ornl.gov/cgi-bin/dsviewer.pl?ds_id=1293.

Rigby, Matthew et al. (May 23, 2017). "Role of atmospheric oxidation in recent methane growth". In: *Proceedings of the National Academy of Sciences* 114.21, pp. 5373–5377. ISSN: 0027-8424, 1091-6490. DOI: 10.1073/pnas.1616426114. URL: http://www.pnas.org/content/114/21/5373 (visited on 06/12/2018).

Rodgers, Clive D (2000). *Inverse methods for atmospheric sounding: theory and practice*. Vol. 2. World scientific.

Rowlinson, Matthew J. et al. (July 9, 2019). "Impact of El Niño–Southern Oscillation on the interannual variability of methane and tropospheric ozone". In: *Atmospheric Chemistry and Physics* 19.13, pp. 8669–8686. ISSN: 1680-7316. DOI: https://doi.org/10.5194/acp-19-8669-2019. URL: https://www.atmos-chem-phys.net/19/8669/2019/ (visited on 11/22/2019).

Saunois, Marielle et al. (Dec. 12, 2016). "The global methane budget 2000–2012". In: *Earth System Science Data* 8.2. Publisher: Copernicus GmbH, pp. 697–751. ISSN: 1866-3508. DOI: 10.5194/essd-8-697-2016. URL: https://essd.copernicus.org/articles/8/697/2016/ (visited on 10/15/2022).

Schaefer, Hinrich et al. (Mar. 10, 2016). "A 21st century shift from fossil-fuel to biogenic methane emissions indicated by 13CH4". In: *Science*, aad2705. ISSN: 0036-8075, 1095-9203. DOI: 10.1126/science.aad2705. URL: http://science.sciencemag.org/content/early/2016/03/09/science.aad2705 (visited on 09/11/2018).

Schwietzke, Stefan et al. (Oct. 2016). "Upward revision of global fossil fuel methane emissions based on isotope database". In: *Nature* 538.7623, pp. 88–91. ISSN: 1476-4687. DOI: 10.1038/nature19797. URL: https://www.nature.com/articles/nature19797 (visited on 08/19/2019).

Shindell, Drew T. et al. (2005). "An emissions-based view of climate forcing by methane and tropospheric ozone". In: *Geophysical Research Letters* 32.4. ISSN: 1944-8007. DOI: 10.1029/2004GL021900. URL: https://agupubs.onlinelibrary.wiley.com/doi/abs/10.1029/2004GL021900 (visited on 11/27/2019).

Thompson, R. L. et al. (2018). "Variability in Atmospheric Methane From Fossil Fuel and Microbial Sources Over the Last Three Decades". In: *Geophysical Research Letters* 45.20, pp. 11, 499–11, 508. ISSN: 1944-8007. DOI: 10.1029/2018GL078127. URL: https://agupubs.onlinelibrary.wiley.com/doi/abs/10.1029/2018GL078127 (visited on 12/24/2019).

Turner, Alexander J., Christian Frankenberg, and Eric A. Kort (Feb. 19, 2019). "Interpreting contemporary trends in atmospheric methane". In: *Proceedings of the National Academy of Sciences* 116.8, pp. 2805–2813. ISSN: 0027-8424, 1091-

6490. DOI: 10.1073/pnas.1814297116. URL: https://www.pnas.org/content/116/8/2805 (visited on 06/19/2019).

Turner, Alexander J., Christian Frankenberg, Paul O. Wennberg, et al. (Apr. 12, 2017). "Ambiguity in the causes for decadal trends in atmospheric methane and hydroxyl". In: *Proceedings of the National Academy of Sciences*, p. 201616020. ISSN: 0027-8424, 1091-6490. DOI: 10.1073/pnas.1616020114. URL: http://www.pnas.org/content/early/2017/04/11/1616020114 (visited on 08/14/2018).

Turner, Alexander J., Inez Fung, et al. (Sept. 4, 2018). "Modulation of hydroxyl variability by ENSO in the absence of external forcing". In: *Proceedings of the National Academy of Sciences* 115.36, pp. 8931–8936. ISSN: 0027-8424, 1091-6490. DOI: 10.1073/pnas.1807532115. URL: https://www.pnas.org/content/115/36/8931 (visited on 03/20/2019).

Wolfe, Glenn M. et al. (June 4, 2019). "Mapping hydroxyl variability throughout the global remote troposphere via synthesis of airborne and satellite formaldehyde observations". In: *Proceedings of the National Academy of Sciences* 116.23, pp. 11171–11180. ISSN: 0027-8424, 1091-6490. DOI: 10.1073/pnas.1821661116. URL: https://www.pnas.org/content/116/23/11171 (visited on 11/19/2019).

Worden, H. M. et al. (Jan. 22, 2013). "Decadal record of satellite carbon monoxide observations". In: *Atmospheric Chemistry and Physics* 13.2, pp. 837–850. ISSN: 1680-7324. DOI: 10.5194/acp-13-837-2013. URL: https://www.atmos-chem-phys.net/13/837/2013/ (visited on 11/20/2019).

Worden, John et al. (Sept. 28, 2013). "El Niño, the 2006 Indonesian peat fires, and the distribution of atmospheric methane: METHANE FROM 2006 INDONESIAN PEAT FIRES". In: *Geophysical Research Letters* 40.18, pp. 4938–4943. ISSN: 00948276. DOI: 10.1002/grl.50937. URL: http://doi.wiley.com/10.1002/grl.50937 (visited on 07/02/2019).

Worden, John R. et al. (Dec. 20, 2017). "Reduced biomass burning emissions reconcile conflicting estimates of the post-2006 atmospheric methane budget". In: *Nature Communications* 8.1, p. 2227. ISSN: 2041-1723. DOI: 10.1038/s41467-017-02246-0. URL: https://www.nature.com/articles/s41467-017-02246-0 (visited on 01/18/2018).

Yin, Yi et al. (2016). "Variability of fire carbon emissions in equatorial Asia and its nonlinear sensitivity to El Niño". In: *Geophysical Research Letters* 43.19, pp. 10, 472–10, 479. ISSN: 1944-8007. DOI: 10.1002/2016GL070971. URL: https://agupubs.onlinelibrary.wiley.com/doi/abs/10.1002/2016GL070971 (visited on 11/26/2019).

Zhang, Zhen et al. (June 2018). "Enhanced response of global wetland methane emissions to the 2015–2016 El Niño-Southern Oscillation event". In: *Environmental Research Letters* 13.7, p. 074009. ISSN: 1748-9326. DOI: 10.1088/1748-

9326/aac939. URL: https://doi.org/10.1088%2F1748-9326%2Faac939 (visited on 07/02/2019).

Chapter 3

STRATOSPHERIC AND ENSO IMPACTS ON TROPOSPHERIC METHANE EMISSIONS AND HYDROXYL VARIABILITY

3.1 Background and Motivation

Transport to the stratosphere is a significant sink for methane, accounting for approximately 3-16% of total methane loss (Saunois, Bousquet, et al., 2016; Saunois, Stavert, et al., 2020; IPCC, 2013). Methane that reaches the stratosphere undergoes oxidation, resulting in the production of water vapor, which acts as a radiative forcer and amplifies methane's contribution to climate change (Shindell et al., 2005). However, there are large uncertainties in the impact of strat-trop exchange on methane emissions inversions. Patra et al. (2011) demonstrated that the representation of tropospheric to stratospheric transport in chemical transport models has a significant influence on top-down methane emissions calculations. To address this, we utilize observed lower stratospheric water vapor observations to gauge strat-trop exchange and evaluate its impact on the methane sink through stratospheric escape and oxidation by the Hydroxyl Radical (OH).

Neglecting variations in the stratosphere-troposphere exchange time can not only introduce errors in the estimation of methane loss to the stratosphere, but also in inferring OH concentrations using MCF constraints. Methane oxidation by OH is the primary methane destruction mechanism. MCF, a compound phased out under the Montreal Protocol, serves as an indicator for global OH concentrations. Once MCF emissions ceased, its loss rate became directly proportional to OH concentrations, given that its oxidation by OH is its sole tropospheric destruction mechanism (Montzka et al., 2011; McNorton et al., 2016; Lelieveld et al., 2016; Turner, Frankenberg, et al., 2017; Rigby et al., 2017). Consequently, inaccuracies in the stratosphere-troposphere exchange time can therefore influence calculated MCF loss rates, leading to potential misestimations of global OH concentrations (Prather and Holmes, 2017). This, in turn, can have a notable effect on methane emission assessments. Therefore, it's essential to accurately determine the stratosphere-troposphere exchange time to fully quantify methane's secondary sink—its transport to the stratosphere—as well as its primary sink through OH oxidation. Accurately understanding and quantifying methane emissions variations and trends thus depend

on accurately representing the effects of stratospheric-tropospheric exchange on methane loss.

Water vapor in the lower stratosphere originates from upwelling from the troposphere and photo-chemical oxidation of methane in the stratosphere. H_2O concentrations in the lower stratosphere have been linked to the variability of stratosphere-troposphere exchange (Fu et al., 2015; Lu et al., 2020; Randel and Jensen, 2013). Although increased Lower stratospheric water vapor concentrations would intuitively indicate stronger tropical upwelling and stratospheric circulation, the majority of the effects of stratospheric-tropospheric exchange actually decrease H_2O concentrations in the lower stratosphere, due to increased upwelling of dry air entering the lower stratosphere (Fu et al., 2015; Lu et al., 2020).

The Brewer-Dobson Circulation is primarily responsible for this transport, with the ascending branch driving the transport from the troposphere to the stratosphere in the tropics and the descending branch responsible for the transport from the stratosphere to the troposphere in the high latitudes. It is worth noting that stratospheric-tropospheric exchange has been shown to modify the chemical composition of the lower stratosphere, and its strengthening (+1.3-3.9% per decade) is expected due to climate change forcing (Fu et al., 2015).

3.2 ENSO and Its Impact on Methane Emissions

ENSO, together with the Arctic Oscillation, influences the variability of the Brewer-Dobson Circulation through enhanced deep convection (Minganti et al., 2020; Diallo et al., 2019). Moreover, ENSO has an impact on the availability of OH in the atmosphere through multiple pathways. El Niño years are associated with elevated wildfire activity, leading to increased methane and CO emissions. This, in turn, reduces OH concentrations, as surges in methane and CO consume OH Radicals (Nguyen et al., 2020). Additionally, in the absence of external forcing, ENSO can increase OH concentrations by promoting deep convection and subsequent lightning NO_x production (Turner, Fung, et al., 2018). Lastly, the intensified deep convection associated with El Niño events enhances the stratospheric-tropospheric exchange, thereby increasing the stratospheric methane sink. As a result, ENSO affects methane emissions calculations through multiple pathways.

The objective of this study is to calculate the stratosphere-troposphere exchange time, quantify its variability, and evaluate its impact on methane's stratospheric sink and OH oxidation (proxied by MCF). The ultimate goal is to assess how the derived

exchange time can improve the accuracy of global methane emission estimates and trends.

3.3 Observational Constraints

We utilize observations of methane (NOAA), CO (NOAA), and MCF (NOAA, GAGE/AGAGE) concentrations, with hemispheric averaging following Turner, Frankenberg, et al. (2017). Hemispheric averaging is performed by bootstrapping from deseasonalized surface observations. We sample from the observational record in each hemisphere with replacement, considering the number of available observational records for that species in that hemisphere. Sites with less than 5 years of data are rejected, and older observations have higher uncertainties than more recent observations, with a minimum uncertainty of 2 ppb. The randomly drawn observations are then blocked-averaged into 1-year windows. This process is repeated 50 times to compute the mean and variance from these 50 time series.

For stratospheric water vapor, we use the NOAA SWOOSH data product (Davis et al., 2016), which provides a harmonized, gridded, and continuous H_2O stratospheric dataset derived from a combination of limb-sounding satellites and reanalysis. We focus on variations in lower stratospheric water vapor averaged between 100 and 200 hPa and 60° South to 60° North on an annual basis. The resulting lower stratospheric water vapor time-series, seen in Fig. 3.4, is used to map variations in the stratosphere-troposphere exchange time.

3.4 Tracer Growth-rate Correlations

Chemical tracers have been used to track and quantify larger scale circulation, such as strat-trop exchange. Seasonal cycles of tracers such as ozone (Ruiz and Prather, 2022) and N_2O (Prather, Froidevaux, and Livesey, 2023; Ruiz, Prather, et al., 2021; Ruiz and Prather, 2022; Simmonds et al., 2013) near the surface have been observed at northern high latitudes during summer, coinciding with mixing from the stratosphere. Specifically, tropospheric N_2O concentrations decrease at downwelling latitudes during spring (Simmonds et al., 2013; Assonov et al., 2013).

N_2O, the third most important anthropogenic greenhouse gas, primarily results from agricultural activities. N_2O and methane emissions sources, which can also come from agriculture, are often collocated. In the troposphere, N_2O has negligible sinks and is relatively inert. However, in the stratospheric chemical environment, N_2O is oxidized and photolyzed. As a result, stratospheric air entering the troposphere, due to the Brewer-Dobson Circulation, contains less N_2O than tropospheric air, and this

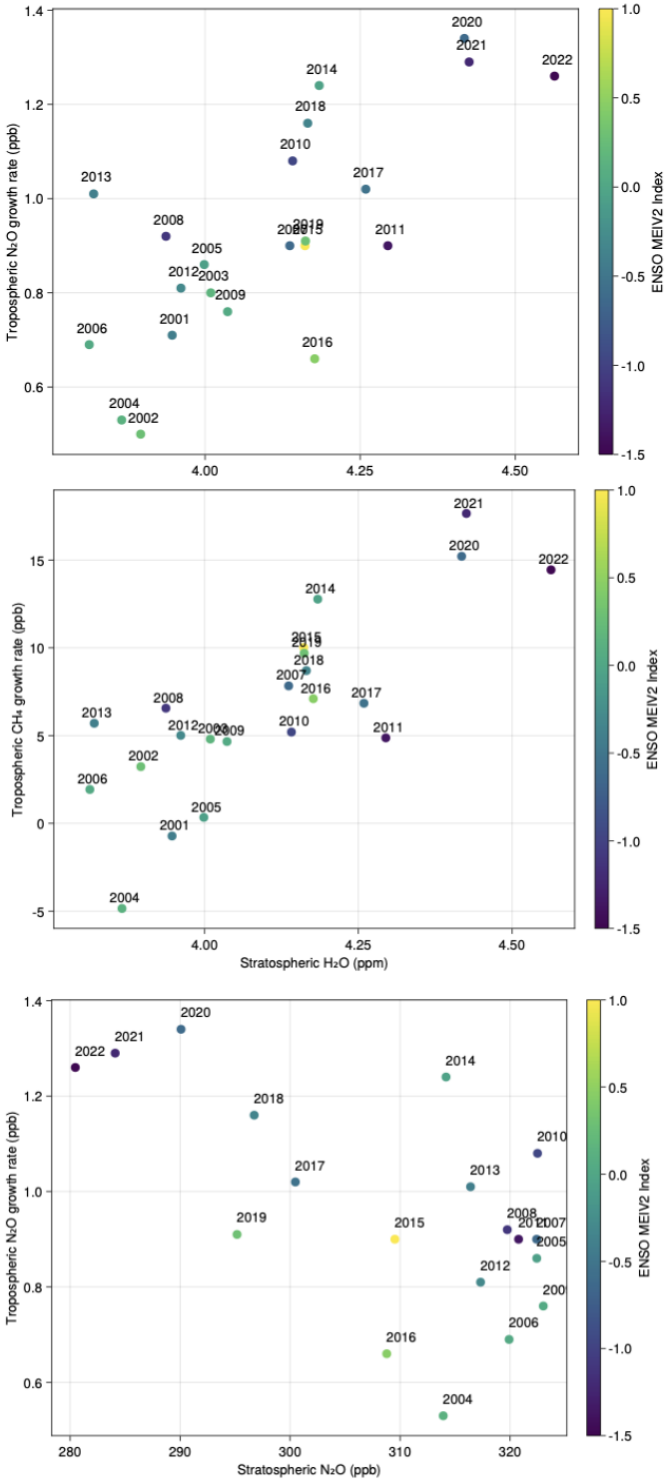

Figure 3.1: Tracer Correlations: All three panels show a scatter plot of stratospheric vs tropospheric tracers colored by the ENSO MEIV2 Index (Kobayashi et al., 2015) with points labeled by year. Top panel shows a positive correlation between stratospheric [H_2O] concentrations and the tropospheric N_2O growth rate. Middle panel shows a positive correlation between the stratospheric [H_2O] and tropospheric CH_4 growth rate. Bottom panel shows negative correlation between stratospheric N_2O concentration and the tropospheric N_2O growth rate.

minimum has been observed at high latitudes. Therefore, N_2O has been proposed as a proxy for distinguishing between tropospheric and stratospheric air, and the N_2O growth-rate have been shown to be modulated by inter-annual variations in strat-trop exchange (Ruiz, Prather, et al., 2021; Simmonds et al., 2013).

Figure 3.4 shows the average lower stratospheric water vapor concentrations between 60°S and 60°N. A significant negative anomaly is observed in 2001, indicating a substantial change in stratospheric-tropospheric exchange. This anomaly coincides with a drop in methane and N_2O growth rates, as shown in the top and bottom panels of Figure 3.4, suggesting a correlation between surface N_2O and methane growth rates and stratospheric-tropospheric exchange. Lower stratospheric water vapor concentrations therefore seem to proxy strat-trop exchange.

Based on the presented evidence, we aim to use information from tracer correlations to constrain stratospheric-tropospheric exchange times using a box model. We will then utilize this tracer-constrained exchange time to reevaluate methane emissions over recent decades.

3.5 Lower Stratospheric Water Vapor Observations Proxy Stratosphere-Troposphere Exchange

Lower stratospheric water vapor concentrations can serve as a proxy for stratosphere-troposphere (strat-trop) exchange as they are directly influenced by this exchange process. It has been observed that enhanced stratosphere-troposphere exchange often leads to decreased water vapor concentrations in the lower stratosphere. This seemingly counterintuitive result arises because as ascending air, which may have high water vapor content, ascends to the tropopause, it encounters the temperature minimum. At this cold point, a significant portion of its water vapor condenses out. Consequently, the air that subsequently enters the lower stratosphere is drier. This drier air acts to dilute the existing water vapor concentrations in the lower stratosphere, leading to reduced H_2O concentrations. Therefore, increased exchange between the troposphere and stratosphere typically results in diminished water vapor concentrations in the lower stratosphere (Fu et al., 2015; Lu et al., 2020).

Our study documents notable fluctuations in these concentrations from 1990 to 2021, as seen in the middle panel of Fig. 3.4. From 1990 to 1999, lower stratospheric water vapor concentrations decreased from 4.49 ppm to 4.22 ppm, representing a change of -6.0%. This decrease in water vapor concentrations suggests an increase in stratosphere-troposphere exchange during this period.

In the stabilization period (2000-2007), the concentrations remained relatively lower than the previous decade. This implies continuous enhanced stratosphere-troposphere exchange during this period, which likely contributed to the observed decline in methane emissions and OH variability.

During the subsequent years (2007-2019), there was a slight further decrease in water vapor concentration by -2.1%, indicating a continuous increase in stratosphere-troposphere exchange. However, in the most recent years (2019-2021), water vapor concentrations increased significantly by +6.4%. This increase suggests a dramatic decrease of stratosphere-troposphere exchange, aligning with the observed surge in methane emissions, indicating that the stratospheric sink of methane decreased, leading to even more methane growth.

3.6 Chemical Box Model

We developed a 4-box model that maps emissions to concentrations by simulating methane chemistry and inter-hemispheric transport. The four boxes represent the Northern Hemisphere, Southern Hemisphere, Northern Stratosphere, and Southern Stratosphere. The simplicity of the 4-box model is ideal for this study since inter-hemispheric transport timescales are more relevant than intra-hemispheric transport for the examined decadal timescales.

Each tropospheric box models the interactions between methane, CO, and the Hydroxyl radical (OH). Since CO is the largest OH sink, we follow Prather (1994) and Nguyen et al. (2020) in modeling the CH_4-CO-OH system while accounting for the variability in the methane perturbation lifetime. Variations in OH abundances result in a perturbation lifetime of 13.5 years, which is 40% longer than the perturbation lifetime assuming fixed OH concentrations.

Chemical abundances in the stratospheric boxes follow a first-order reaction, with the decay rate of each species determined by the stratospheric lifetime of that species. Transport to the stratospheric boxes is proportional to the tropospheric-stratospheric gradient and inversely proportional to the stratospheric-tropospheric exchange time, set as a baseline of 3 years with variability proportional to variations in lower stratospheric water vapor concentrations.

We employ a Bayesian non-linear inversion algorithm to infer methane emissions and OH abundances. MCF is used to calculate variations in OH concentrations, while lower stratospheric water vapor is directly mapped onto the stratospheric-tropospheric exchange time. For example, a +2% increase in lower stratospheric

water vapor corresponds to a -2% decrease in the stratosphere-troposphere exchange time.

To assess the impact of stratospheric exchange time variations on methane emissions and OH abundances, we simulate two cases: 1) with the stratosphere turned off and 2) with the stratosphere and variability in the exchange time turned on. This allows us to quantify the effect of stratosphere-troposphere exchange time variations on methane emissions inversions and OH concentrations.

3.7 Results and Discussion

Methane Emissions Trends

In the previous section, we established a causal link between methane and stratospheric H_2O concentrations. Here, we will qualitatively discuss initial results of our methane flux inversions. For more detailed results and figures, we refer the reader to a subsiquent paper.

Methane emissions have exhibited noticeable variations from 1990 to 2021. The methane emissions inferred by the model that includes the stratosphere consistently show higher emissions than the model without the stratosphere. Interestingly, incorporating stratospheric-tropospheric exchange has made the emissions time-series much smoother than the emissions derived without considering the stratosphere. It is an interesting result that including the stratosphere decreases the inter-annual variation in derived methane emissions. Including the stratosphere also improves the fitting between the model and observations compared to excluding the stratosphere, indicating that the model with stratospheric effects provides a more accurate representation of reality.

OH Variability Trends

OH variability, which refers to the percent change in OH concentrations relative to the mean of the time-series, exhibits a trend that somewhat mirrors methane emissions. In initial results, we observe a very good fit of MCF, which proxies OH variability, between both model outputs and the observations, consistently below 1% relative error. Including the stratosphere also makes the OH time-series smoother than the model without the stratosphere, and a downward trend in OH concentrations over recent decades is observed, which is an interesting result.

Relationships to El Niño

El Niño years were associated with significant alterations in methane emissions, OH variability, and lower stratospheric water vapor concentrations. For the years 1991, 1997, 1998, 2002, 2009, 2015, and 2020, considered strong El Niño years, we observed specific shifts in these parameters. The stratosphere-inclusive model depicted an average increase of 4.9% (approximately 29.9 Tg/yr) in methane emissions during El Niño years, while the model excluding stratospheric effects showed a lesser average increase of 3.7% (around 21.4 Tg/yr). Similarly, the stratosphere-inclusive model noted a decrease in OH concentrations of about 3.1%, whereas the non-stratosphere model recorded a larger decrease of about 4.5% during El Niño years.

These results reinforce the suggestion that El Niño events correspond to amplified sea surface temperatures and increased atmospheric instability. El Niño also appears to accelerate stratosphere-troposphere exchange, as indicated by the lower stratospheric water vapor concentrations.

3.8 Conclusions and Recommendations

In this study, we quantified the impact of variations in stratospheric-tropospheric exchange on methane emissions. By utilizing variations in lower stratospheric water vapor observations to map exchange time variability, we found that stratospheric loss affects not only stratospheric methane loss but also inferred OH concentrations through error aliasing onto MCF.

We observed that incorporating variability in stratospheric-tropospheric exchange significantly improved the fits of our methane emissions inversions and resulted in smoother inter-annual variability in both derived methane emissions and OH concentrations. The inclusion of strat-trop exchange played a role in the stabilization of methane concentrations during the period from 2000 to 2007, leading to a slight increase in the flux from the troposphere to the stratosphere. Additionally, we found a consistent association between higher stratospheric water vapor concentrations and El Niño events. Incorporating this information into our inversions had a more pronounced effect on methane emissions and OH concentrations compared to inversions that did not consider the stratosphere. These findings have important implications for understanding the linkage between ENSO and methane emissions and loss (Nguyen et al., 2020; Worden et al., 2013; Zhang et al., 2018; Rowlinson et al., 2019).

Looking ahead, expanding vertical profile measurements will improve our understanding of stratospheric methane loss (Roche et al., 2021; Kuai et al., 2012). Measurement campaigns such as the NOAA Air Core measurements (Karion et al., 2010), should be expanded to more regions, especially the tropics, where methane variability, exchange, and chemistry are most dynamic. Additionally, ground-based vertical profile measurements, such as those obtained from laser heterodyne radiometers, should be developed to directly infer methane gradients on-site. These measurements would provide constraints for process-based chemical transport models.

Furthermore, it is crucial to prioritize the incorporation of processes affecting stratosphere-troposphere exchange in chemical transport models. Currently, there are significant differences in vertical gradients among chemical transport models used to infer methane emissions (Patra et al., 2011). Therefore, errors in modeling stratosphere-troposphere exchange time introduce errors into inferred methane emissions. Advancements in both modeling stratospheric-tropospheric variability and measuring vertical methane gradients will bring methane emissions inversions closer to real-world accuracy.

BIBLIOGRAPHY

Assonov, S. S. et al. (Nov. 1, 2013). "N2O as a tracer of mixing stratospheric and tropospheric air based on CARIBIC data with applications for CO2". In: *Atmospheric Environment* 79, pp. 769–779. ISSN: 1352-2310. DOI: 10.1016/j.atmosenv.2013.07.035. URL: https://www.sciencedirect.com/science/article/pii/S1352231013005566 (visited on 02/18/2021).

Davis, Sean M et al. (2016). "The Stratospheric Water and Ozone Satellite Homogenized (SWOOSH) database: a long-term database for climate studies". In.

Diallo, Mohamadou et al. (Jan. 11, 2019). "Structural changes in the shallow and transition branch of the Brewer–Dobson circulation induced by El Niño". In: *Atmospheric Chemistry and Physics* 19.1. Publisher: Copernicus GmbH, pp. 425–446. ISSN: 1680-7316. DOI: https://doi.org/10.5194/acp-19-425-2019. URL: https://acp.copernicus.org/articles/19/425/2019/ (visited on 02/18/2021).

Fu, Q. et al. (2015). "Observational evidence of strengthening of the Brewer-Dobson circulation since 1980". In: *Journal of Geophysical Research: Atmospheres* 120.19. _eprint: https://onlinelibrary.wiley.com/doi/pdf/10.1002/2015JD023657, pp. 10, 214–10, 228. ISSN: 2169-8996. DOI: 10.1002/2015JD023657. URL: https://onlinelibrary.wiley.com/doi/abs/10.1002/2015JD023657 (visited on 05/23/2023).

IPCC (2013). *Climate Change 2013: The Physical Science Basis. Contribution of Working Group I to the Fifth Assessment Report of the Intergovernmental Panel on Climate Change*. Cambridge, United Kingdom and New York, NY, USA: Cambridge University Press. 1535 pp. ISBN: ISBN 978-1-107-66182-0. DOI: 10.1017/CBO9781107415324. URL: www.climatechange2013.org.

Karion, Anna et al. (Nov. 1, 2010). "AirCore: An Innovative Atmospheric Sampling System". In: *Journal of Atmospheric and Oceanic Technology* 27.11. Publisher: American Meteorological Society Section: Journal of Atmospheric and Oceanic Technology, pp. 1839–1853. ISSN: 0739-0572, 1520-0426. DOI: 10.1175/2010JTECHA1448.1. URL: https://journals.ametsoc.org/view/journals/atot/27/11/2010jtecha1448_1.xml (visited on 01/06/2023).

Kobayashi, Shinya et al. (2015). "The JRA-55 Reanalysis: General Specifications and Basic Characteristics". In: *Journal of the Meteorological Society of Japan. Ser. II* 93.1, pp. 5–48. ISSN: 0026-1165, 2186-9057. DOI: 10.2151/jmsj.2015-001. URL: https://www.jstage.jst.go.jp/article/jmsj/93/1/93_2015-001/_article (visited on 07/21/2023).

Kuai, Le et al. (Sept. 1, 2012). "Vertically constrained CO2 retrievals from TCCON measurements". In: *Journal of Quantitative Spectroscopy and Radiative Transfer* 113.14, pp. 1753–1761. ISSN: 0022-4073. DOI: 10.1016/j.jqsrt.2012.04.

024. URL: https://www.sciencedirect.com/science/article/pii/S0022407312002397 (visited on 02/18/2021).

Lelieveld, Jos et al. (Oct. 5, 2016). "Global tropospheric hydroxyl distribution, budget and reactivity". In: *Atmospheric Chemistry and Physics* 16.19, pp. 12477–12493. ISSN: 1680-7324. DOI: 10.5194/acp-16-12477-2016. URL: https://www.atmos-chem-phys.net/16/12477/2016/ (visited on 03/20/2019).

Lu, Jinpeng et al. (Sept. 3, 2020). "Analysis of factors influencing tropical lower stratospheric water vapor during 1980–2017". In: *npj Climate and Atmospheric Science* 3.1. Number: 1 Publisher: Nature Publishing Group, pp. 1–11. ISSN: 2397-3722. DOI: 10.1038/s41612-020-00138-7. URL: https://www.nature.com/articles/s41612-020-00138-7 (visited on 02/18/2021).

McNorton, Joe et al. (June 30, 2016). "Role of OH variability in the stalling of the global atmospheric CH_4 growth rate from 1999 to 2006". In: *Atmospheric Chemistry and Physics* 16.12, pp. 7943–7956. ISSN: 1680-7316. DOI: https://doi.org/10.5194/acp-16-7943-2016. URL: https://www.atmos-chem-phys.net/16/7943/2016/ (visited on 11/25/2019).

Minganti, Daniele et al. (Nov. 3, 2020). "Climatological impact of the Brewer–Dobson circulation on the N_2O budget in WACCM, a chemical reanalysis and a CTM driven by four dynamical reanalyses". In: *Atmospheric Chemistry and Physics* 20.21. Publisher: Copernicus GmbH, pp. 12609–12631. ISSN: 1680-7316. DOI: 10.5194/acp-20-12609-2020. URL: https://acp.copernicus.org/articles/20/12609/2020/ (visited on 05/30/2023).

Montzka, S. A. et al. (Jan. 7, 2011). "Small Interannual Variability of Global Atmospheric Hydroxyl". In: *Science* 331.6013, pp. 67–69. ISSN: 0036-8075, 1095-9203. DOI: 10.1126/science.1197640. URL: https://science.sciencemag.org/content/331/6013/67 (visited on 06/19/2019).

Nguyen, Newton H. et al. (2020). "Effects of Chemical Feedbacks on Decadal Methane Emissions Estimates". In: *Geophysical Research Letters* 47.3, e2019GL085706. ISSN: 1944-8007. DOI: 10.1029/2019GL085706. URL: https://agupubs.onlinelibrary.wiley.com/doi/abs/10.1029/2019GL085706 (visited on 02/10/2020).

Patra Prabir K., P. K. et al. (Dec. 19, 2011). "TransCom model simulations of CH₄ and related species: linking transport, surface flux and chemical loss with CH₄ variability in the troposphere and lower stratosphere". In: *Atmospheric Chemistry and Physics* 11.24, pp. 12813–12837. ISSN: 1680-7324. DOI: 10.5194/acp-11-12813-2011. URL: https://acp.copernicus.org/articles/11/12813/2011/ (visited on 02/18/2021).

Prather, Michael J. (May 1994). "Lifetimes and eigenstates in atmospheric chemistry". In: *Geophysical Research Letters* 21.9, pp. 801–804. ISSN: 1944-8007. DOI:

10.1029/94GL00840. URL: https://agupubs.onlinelibrary.wiley.com/doi/abs/10.1029/94GL00840 (visited on 11/27/2019).

Prather, Michael J., Lucien Froidevaux, and Nathaniel J. Livesey (Jan. 18, 2023). "Observed changes in stratospheric circulation: decreasing lifetime of N 2 O, 2005–2021". In: *Atmospheric Chemistry and Physics* 23.2, pp. 843–849. ISSN: 1680-7324. DOI: 10.5194/acp-23-843-2023. URL: https://acp.copernicus.org/articles/23/843/2023/ (visited on 03/20/2023).

Prather, Michael J. and Christopher D. Holmes (May 23, 2017). "Overexplaining or underexplaining methane's role in climate change". In: *Proceedings of the National Academy of Sciences* 114.21, pp. 5324–5326. ISSN: 0027-8424, 1091-6490. DOI: 10.1073/pnas.1704884114. URL: http://www.pnas.org/content/114/21/5324 (visited on 06/12/2018).

Randel, William J. and Eric J. Jensen (Mar. 2013). "Physical processes in the tropical tropopause layer and their roles in a changing climate". In: *Nature Geoscience* 6.3. Number: 3 Publisher: Nature Publishing Group, pp. 169–176. ISSN: 1752-0908. DOI: 10.1038/ngeo1733. URL: https://www.nature.com/articles/ngeo1733 (visited on 02/18/2021).

Rigby, Matthew et al. (May 23, 2017). "Role of atmospheric oxidation in recent methane growth". In: *Proceedings of the National Academy of Sciences* 114.21, pp. 5373–5377. ISSN: 0027-8424, 1091-6490. DOI: 10.1073/pnas.1616426114. URL: http://www.pnas.org/content/114/21/5373 (visited on 06/12/2018).

Roche, Sébastien et al. (Apr. 28, 2021). "Retrieval of atmospheric CO₂ vertical profiles from ground-based near-infrared spectra". In: *Atmospheric Measurement Techniques* 14.4, pp. 3087–3118. ISSN: 1867-8548. DOI: 10.5194/amt-14-3087-2021. URL: https://amt.copernicus.org/articles/14/3087/2021/ (visited on 08/11/2022).

Rowlinson, Matthew J. et al. (July 9, 2019). "Impact of El Niño–Southern Oscillation on the interannual variability of methane and tropospheric ozone". In: *Atmospheric Chemistry and Physics* 19.13, pp. 8669–8686. ISSN: 1680-7316. DOI: https://doi.org/10.5194/acp-19-8669-2019. URL: https://www.atmos-chem-phys.net/19/8669/2019/ (visited on 11/22/2019).

Ruiz, Daniel J. and Michael J. Prather (Feb. 15, 2022). "From the middle stratosphere to the surface, using nitrous oxide to constrain the stratosphere–troposphere exchange of ozone". In: *Atmospheric Chemistry and Physics* 22.3. Publisher: Copernicus GmbH, pp. 2079–2093. ISSN: 1680-7316. DOI: 10.5194/acp-22-2079-2022. URL: https://acp.copernicus.org/articles/22/2079/2022/ (visited on 01/29/2023).

Ruiz, Daniel J., Michael J. Prather, et al. (2021). "How Atmospheric Chemistry and Transport Drive Surface Variability of N2O and CFC-11". In: *Journal of Geophysical Research: Atmospheres* 126.8. _eprint: https://onlinelibrary.wiley.com/doi/pdf/10.1029/2020JD033979, e2020JD033979. ISSN: 2169-8996. DOI: 10.1029/2020JD033979. URL: https:

//onlinelibrary.wiley.com/doi/abs/10.1029/2020JD033979 (visited on 01/30/2023).

Saunois, Marielle, Philippe Bousquet, et al. (Dec. 12, 2016). "The global methane budget 2000–2012". In: *Earth System Science Data* 8.2. Publisher: Copernicus GmbH, pp. 697–751. ISSN: 1866-3508. DOI: 10.5194/essd-8-697-2016. URL: https://essd.copernicus.org/articles/8/697/2016/ (visited on 10/15/2022).

Saunois, Marielle, Ann R. Stavert, et al. (July 15, 2020). "The Global Methane Budget 2000–2017". In: *Earth System Science Data* 12.3. Publisher: Copernicus GmbH, pp. 1561–1623. ISSN: 1866-3508. DOI: 10.5194/essd-12-1561-2020. URL: https://essd.copernicus.org/articles/12/1561/2020/ (visited on 10/15/2022).

Shindell, Drew T. et al. (2005). "An emissions-based view of climate forcing by methane and tropospheric ozone". In: *Geophysical Research Letters* 32.4. ISSN: 1944-8007. DOI: 10.1029/2004GL021900. URL: https://agupubs.onlinelibrary.wiley.com/doi/abs/10.1029/2004GL021900 (visited on 11/27/2019).

Simmonds, P. G. et al. (2013). "Interannual fluctuations in the seasonal cycle of nitrous oxide and chlorofluorocarbons due to the Brewer-Dobson circulation". In: *Journal of Geophysical Research: Atmospheres* 118.19. _eprint: https://agupubs.onlinelibrary.wiley.com/ pp. 10, 694–10, 706. ISSN: 2169-8996. DOI: https://doi.org/10.1002/jgrd.50832. URL: https://agupubs.onlinelibrary.wiley.com/doi/abs/10.1002/jgrd.50832 (visited on 02/18/2021).

Turner, Alexander J., Christian Frankenberg, et al. (Apr. 12, 2017). "Ambiguity in the causes for decadal trends in atmospheric methane and hydroxyl". In: *Proceedings of the National Academy of Sciences*, p. 201616020. ISSN: 0027-8424, 1091-6490. DOI: 10.1073/pnas.1616020114. URL: http://www.pnas.org/content/early/2017/04/11/1616020114 (visited on 08/14/2018).

Turner, Alexander J., Inez Fung, et al. (Sept. 4, 2018). "Modulation of hydroxyl variability by ENSO in the absence of external forcing". In: *Proceedings of the National Academy of Sciences* 115.36, pp. 8931–8936. ISSN: 0027-8424, 1091-6490. DOI: 10.1073/pnas.1807532115. URL: https://www.pnas.org/content/115/36/8931 (visited on 03/20/2019).

Worden, John et al. (Sept. 28, 2013). "El Niño, the 2006 Indonesian peat fires, and the distribution of atmospheric methane: METHANE FROM 2006 INDONESIAN PEAT FIRES". In: *Geophysical Research Letters* 40.18, pp. 4938–4943. ISSN: 00948276. DOI: 10.1002/grl.50937. URL: http://doi.wiley.com/10.1002/grl.50937 (visited on 07/02/2019).

Zhang, Zhen et al. (June 2018). "Enhanced response of global wetland methane emissions to the 2015–2016 El Niño-Southern Oscillation event". In: *Environmental Research Letters* 13.7, p. 074009. ISSN: 1748-9326. DOI: 10.1088/1748-

9326/aac939. URL: https://doi.org/10.1088%2F1748-9326%2Faac939 (visited on 07/02/2019).

Chapter 4

TOWARDS LABORATORY-LEVEL ACCURACY IN THE FIELD: ENVIRONMENTAL IMPACTS ON GREENHOUSE GAS SENSING MEASURED BY FREQUENCY COMBS

4.1 Abstract

Accurate measurements of greenhouse gas (GHG) gradients and long-term trends are crucial for informing climate policy. However, achieving such accuracy requires a comprehensive understanding and quantification of environmental biases, which affect GHG trends and gradients. This study leverages the capabilities of Dual-Comb Spectroscopy (DCS) to systematically quantify these biases in both synthetic and real-world scenarios. The findings are pertinent to future DCS applications and other remote sensing instruments.

For methane, we found that the Hitran 2008 and TCCON line-lists exhibited less systematic bias compared to other line-lists. However, synthetic retrievals revealed an 8% variable error in retrieved methane concentrations across different line-lists, primarily due to pressure broadening errors. In the case of CO_2, the OCO ABSCO lookup table performed best, which account for additional non-Voigt effects. Comparing to other line-lists, there was a 0.8% variable error in CO_2 concentration retrievals, mainly attributed to pressure broadening errors.

During a multi-week field deployment of DCS, we found discrepancies of up to 2% in methane concentrations and 0.5% in CO_2 concentrations when using different spectroscopic databases. These disparities fluctuated with environmental conditions, underscoring the imperative of accurately modeling these effects.

Beyond the effects of pressure and temperature, we highlight the significant role of water vapor broadening, particularly for CO_2 retrievals. Neglecting to account for water vapor broadening can lead to a 1% error in retrieved CO_2 concentrations and a 0.1% error in the CO_2 column, posing substantial variable bias given the variability and high concentrations of water vapor in many remote sensing settings.

We emphasize the necessity to improve the accuracy of modeling environmental effects on GHG spectroscopy. The promising capabilities of DCS allow for laboratory-level accurate measurements to be conducted directly in the field, which

would expand the GHG observation network for verification of climate change mitigation strategies.

4.2 Background

Understanding sources and sinks of greenhouse gases (GHGs) is crucial for accurate GHG emission assessments, which depend on capturing spatial gradients in concentrations. Our knowledge of fluxes from a top-down perspective typically comes from atmospheric inversions, relying on spatial and temporal gradients in observed GHG concentrations. As the primary anthropogenic greenhouse gases are long-lived, their relative concentrations changes are low, requiring high accuracy and precision, well below the 1% level. The most accurate measurements can be obtained from in-situ measurements. For example, the National Oceanic and Atmospheric Administration (NOAA) maintains a global network of flask-sampling sites for GHG monitoring, but air samples must be collected in flasks and shipped for analysis, a costly and logistically challenging process (Conway et al., 1994; Keeling, 1960; Pales and Keeling, 1965; Sweeney et al., 2015). These difficulties restrict highly accurate GHG measurements to a limited number of locations. While satellite observations offer broader spatial coverage, their accuracy and spatial resolution are often limited compared to ground-based measurements (Miller et al., 2007; Jacob et al., 2016). In this study, we employ Dual Comb Spectroscopy to explore a novel remote sensing technique that could be used continuously on the ground over longer pathlengths. We systematically assess the errors in retrieved CO_2 and methane concentrations under different environmental conditions, aiming to expand the current measurement network and bridge the gap between ground-based and satellite observations.

Dual-Comb Spectroscopy (DCS) has emerged as a promising solution to supplement the NOAA network, delivering remote, high-accuracy GHG concentration measurements (Rieker et al., 2014). With its broad-band, high signal-to-noise ratio (SNR), and high spectral resolution capabilities, DCS is well-suited for GHG remote sensing. Field deployments have demonstrated its potential and usefulness in remote sensing applications (e.g., Coburn et al., 2018; Cossel et al., 2017; Waxman, Cossel, Truong, et al., 2017; Waxman, Cossel, Giorgetta, et al., 2019).

Nonetheless, accurately measuring and monitoring atmospheric GHG concentrations presents challenges due to limitations of our knowledge of spectroscopic parameters (Collins et al., 2022). Spectroscopic databases lack the 0.1% accuracy

needed for background monitoring (e.g., Delahaye, Maxwell, et al., 2016; Hartmann, Tran, and Toon, 2009; Hobbs et al., 2020) and the presence of other gases, particularly water vapor, can interfere with measurements and retrievals (e.g., Christian Frankenberg et al., 2008; Hammer et al., 2013). Variable biases based on environmental factors cannot be easily subtracted or averaged out, necessitating sub-percent accuracy in spectroscopic parameters necessary for modeling GHG spectra.

Here, our objective is to leverage the promising remote sensing capabilities of the DCS to systematically quantify spectroscopic biases in greenhouse gas spectroscopy. DCS capabilities and field setup are outlined in Section 4.3. We focus on variable bias from pressure, temperature, and humidity, because errors in modeling the impact of these environmental conditions propagate into GHG retrieval errors. This is explained further in Section 4.4. To do this, in Section 4.5, we use the DCS to assess the accuracy and systematic biases of multiple spectroscopic line-lists. In Section 4.6, we then quantify the impact of environmental variable bias, with respect to pressure and temperature errors, on retrieving GHGs through idealized synthetic retrievals. Section 4.7 applies these principles by assessing the impact of environmental variable biases from DCS observations measured during a multi-week feild campaign. We focus on water vapor impacts on GHG retrievals in Section 4.8. Finally, we summarize and discuss our findings in Section 4.9 and conclude by discussing the implications of our findings on GHG remote sensing in Section 4.10.

4.3 Dual-Comb Spectroscopy Technique

Dual-Comb Spectroscopy

Dual-Comb Spectroscopy (DCS) utilizes laser frequency combs, originally designed for pico-second timekeeping (see Fortier and Baumann (2019) for a review). Frequency combs emit laser light at around 100,000 distinct, evenly spaced frequencies, resembling the teeth of a comb (Telle et al., 1999; Udem, Holzwarth, and Hänsch, 2002). DCS uses two frequency combs, mapping infrared (THz) to radio frequencies (kHz) through destructive interference. The resulting radio-frequency comb can be read by commercial radio-frequency detectors, reducing instrument cost (Coddington, Newbury, and Swann, 2016; Rieker et al., 2014).

For laboratory-level accuracy, the frequency combs need long-term frequency stability and comb coherence. This is achieved by phase-locking each tooth of the combs to a Continuous Wave (CW) Laser and referencing the destructed comb teeth to a common quartz microwave oscillator (Truong et al., 2016). This self-referencing

protocol offers laboratory-level accuracy and stability in a field setting for GHG remote sensing.

Field Setup

Our DCS generates light between 6,000 and 6,400 cm^{-1} (1560 - 1660 nm) at 80,000 stable frequencies, resulting in an equidistant spectral sampling of 0.0067 cm^{-1}. The DCS has an instrument-lineshape full-width at half max of 4×10^{-4} cm^{-1}, making the instrument line-shape negligible. This is ideal for long-term monitoring, because temporal drifts in the instrument line-shape require instruments to be recalibrated. Given that the DCS instrument line-shape is negligible, DCS would be an ideal instrument for an automated measurement network.

The DCS design follows Sinclair et al. (2015). Both frequency combs are powered by a 10 mW femto-second, mode-locked laser centered at 1550 nm, with light amplified to 300 mW through an erbium-doped non-linear fiber.

The DCS was deployed at the NIST facility in Boulder, CO, for 15 days from 21 September to 5 October, 2016. It was mounted atop a building and aimed at a retro-reflector 1 km away on a nearby hill. The 2 km round-trip signal was read by an InGaAs photodetector and saved on the FPGA. Post-processing further aggregated the data into 30-second intervals, and Fourier Transforms produced transmission spectra for GHG concentration retrievals. An example measurement is shown in Fig. 4.1

A commercial cavity ring-down spectrometer (Picarro Model 3012) was deployed alongside a pressure and temperature sensor to act as a reference for our measurements. It was calibrated to the WMO error standard with a reference mixed gas, resulting in an instrument uncertainty of 0.7 ppm for CO_2 and 1.5 ppb for CH_4. The instrument was mounted on a radio tower 30 m above the ground along the DCS beam path. Further details about the field configuration can be found in Waxman, Cossel, Truong, et al. (2017).

Spatial Representation of Measurements

Though the point sensor serves as a reference, the point sensor and open-path DCS will not perfectly match due to the different spatial footprints (Bai et al., 2019). The point sensor is more sensitive to small-scale enhancements and turbulence-induced fluctuations. However, the Picarro instrument remains a useful benchmark for DCS retrievals.

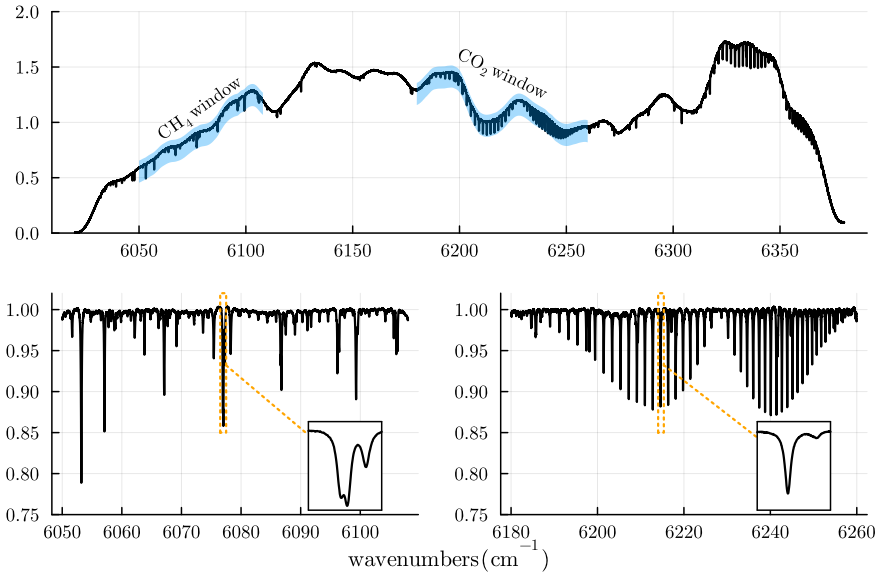

Figure 4.1: Top row: Example original DCS spectrum covering the entire spectral range with an envelope determined by the DCS setup. Bottom row shows a focus on transmissions in the CH_4 window (bottom left), between 6050 to 6108 cm^{-1}, and the CO_2 retrieval window (bottom right), between 6180-6260 cm^{-1}. An inset into individual transitions shows the high spectral resolution of the DCS system.

To minimize spatial representation error, we retrieve pressure and temperature from DCS spectra over the path instead of relying on nearby point-scale sensors. Accurate retrieval of pressure and temperature over the path is crucial for calculating the dry air column density, which is required to convert retrieved total column estimates of GHG into dry mixing ratios. Other instruments use ancillary measurements of O_2 to infer the dry-air column (e.g., Mendonca et al., 2019). DCS can also measure O_2 concentrations (Malarich et al., 2023). However, due to its high spectral sampling, we can calculate the dry air column by directly retrieving pressure, temperature, and water vapor over the light-path.

4.4 Retrieval Approach

Problem Statement

The retrieval problem for an open-path system involves determining the greenhouse gas column density (in molecules/cm^2) from the shape and depth of the measured absorption lines and then converting it to a volume mixing ratio. The GHG column density is divided by the dry air column density to achieve this conversion:

$$[GHG_{vmr}] = \frac{GHG_{cd}}{air_{cd} - H_2O_{cd}} \tag{4.1}$$

In Eq. 4.1, air_{cd} represents the column density of air, GHG_{cd} the GHG column density, and H_2O_{cd} the column density of water vapor. The dry air column density dry_{cd}, defined as the air density without considering water, i.e. $air_{cd} - H_2O_{cd}$, is calculated using a modification of the Ideal Gas Law:

$$\rho_{dry} = \frac{p_{dry}}{RT} = \frac{p(1 - [H_2O_{vmr}])}{RT} \tag{4.2}$$

$$dry_{cd} = \rho_{dry}\Delta x \tag{4.3}$$

Eq. 4.2 relates the number density of dry air (ρ_{dry}) to the atmospheric state, determined by pressure (p), temperature (T), and the water vapor mixing ratio ($[H_2O_{vmr}]$). The dry air column density (dry_{cd}) is calculated by multiplying the dry air number density (ρ_{dry}) by the round-trip path-length (Δx). Fractional errors in obtained p and T propagate directly into errors in $[GHG_{vmr}]$, even if GHG_{cd} is bias free. Thus, it is important to minimize errors in modeling pressure and temperature-dependent absorption cross-sections that could propagate into variable biases in the dry air column and consequently GHG concentration. An alternative approach is to measure a proxy gas for dry air, such as O_2, which can alleviate this source of bias.

This paper examines biases in retrieving GHG concentrations, both for GHG column density retrievals and its conversion to a column-averaged mixing ratio using the derived dry air column.

Retrieval Algorithm

To retrieve GHG concentrations from measured spectra, we employ a non-linear inversion using the Lambert-Beer Law:

$$\tau(\lambda) = \sum_{i}^{n} [GHG_{vmr}] \cdot dry_{cd} \cdot \sigma(\lambda, p, T) \tag{4.4}$$

$$T(\lambda) = \exp^{-\tau(\lambda)} \tag{4.5}$$

The optical depth (τ) depends on the GHG column density and the absorption cross-section (σ). Here, the cross-section is calculated using the Voigt line-shape from the vSmartMOM.jl tool based on the Hitran database or, alternatively, more complex line-shapes using lookup tables, such as the OCO-2 mission ABSCO table linelist Version 5.1, which include collisional narrowing effects as well as full line-mixing. Eq. 4.5 relates the transmission (T) to the optical depth.

Evaluations of the forward model map the chemical and environmental state (e.g., concentrations, pressure, and temperature) to simulated spectra observed by the instrument. To find the optimal state, the misfit between the simulated spectra and the observed spectra is minimized by iteratively selecting state parameters and evaluating the forward model. Exploration and selection of the state is done by non-linear least squares fitting (Rodgers, 2000). The algorithm is as follows:

$$x_{i+1} = x_i + \left(\mathbf{K^T S_\epsilon^{-1} K}\right)^{-1} \mathbf{K^T S_\epsilon^{-1}} \left(y - f(x)\right) \tag{4.6}$$

Here, y is the observed spectrum, $f(x)$ is the modelled spectrum, $\mathbf{S}_\epsilon$ is the error covariance matrix (purely diagonal), and $\mathbf{K}$ is the Jacobian matrix. The Jacobian is calculated using automated differentiation techniques in *Julia* using the ForwardDiff.jl package. Finally, x_i is our state vector at the ith iteration, and it includes the vertical column density (vcd) of each of the gases being retrieved, pressure, temperature, and a polynomial term to account for baseline variations of the transmission (see top row in Figure 1). Here, we use Legendre polynomials of degree 100 to account for the low-frequency variability in the DCS baseline.

A crucial aspect of our retrieval is using the column density in the state vector rather than the volume-mixing ratio. This approach separates spectroscopic errors from pressure and temperature errors. Pressure and temperature errors will affect the dry air column amount, propagating into the derived GHG concentration. Fitting for the column amount individually enables error contributions to be calculated independently.

4.5 Greenhouse Gas Spectroscopy

Spectroscopic Line-Lists

Accurate modeling of pressure, temperature, and wavelength-dependent absorption lines is essential for retrieving pressure and temperature from the absorption line shapes. The Voigt line-shape model accounts for both pressure and temperature effects by convolving the temperature-dependent Lorentzian line-shape and the

Species	Line-lists	Retrieval Window
CH_4	TCCON, Hitran 2008, Hitran 2016, Hitran 2020	6050-6108 cm^{-1}
CO_2	OCO ABSCO, TCCON, Hitran 2016, Hitran 2020	6180-6260 cm^{-1}
H_2O	TCCON	6050-6108, 6180-6260 cm^{-1}

Table 4.1: Spectroscopic line-lists and retrieval windows used to retrieve greenhouse gas amounts in our experiment. For H_2O, we used TCCON exclusively, as it provided the best fits and enables us to isolate fitting errors just due to differences on GHG absorption cross sections.

pressure-dependent Gaussian line-shape. More complex profiles than the standard Voigt Profile have recently been used to account for additional physical effects, such as the molecular velocity changes that occur with molecular collisions (known as velocity changes), the speed-dependence on collisional broadening and shifting coefficients (speed dependence), and the interaction of neighboring transitions (line-mixing) (e.g., Delahaye, Maxwell, et al., 2016; Hartmann, Tran, and Toon, 2009; D. A. Long et al., 2022; Payne et al., 2020).

Table 4.1 displays the line-lists being used in our study. We use the HITRAN 2008 (Rothman et al., 2009), Hitran 2016 (Gordon, Rothman, Hill, et al., 2017), and Hitran 2020 (Gordon, Rothman, Hargreaves, et al., 2022) line-lists as well as a line-list optimized for retrievals within the Total Carbon Column Observing network TCCON (Tune, n.d.; Wunch et al., 2011), which updates some Hitran parameters, also for H_2O, to optimize spectral fits in TCCON retrieval windows. For these line-lists, we generate cross-sections using the Voigt line-shape. In addition, we use tabulated cross section data from the ACOS/OCO-2 absorption coefficients Version 5.1 (ABSCO) developed for the Orbiting Carbon Observatory missions (labeled as OCO here) (Payne et al., 2020). The ABSCO tables account for velocity changes, speed-dependence, and line-mixing. Using multiple line-lists enables us to quantify how biases vary with pressure and temperature in the most commonly used spectroscopic databases.

Using DCS Capabilities to Examine Systematic Errors in GHG Spectroscopy

We can examine the accuracy of the CO_2 and methane spectroscopy by looking at the spectral residuals of our retrieval's and comparing them to the measured DCS spectrum. The data shown in Figs 4.2 and 4.3 are obtained from averaging the spectra over a 24 hour period on Day 0 and dividing by the instrument baseline. Spectra were averaged in order to minimize random noise so that systematic offsets

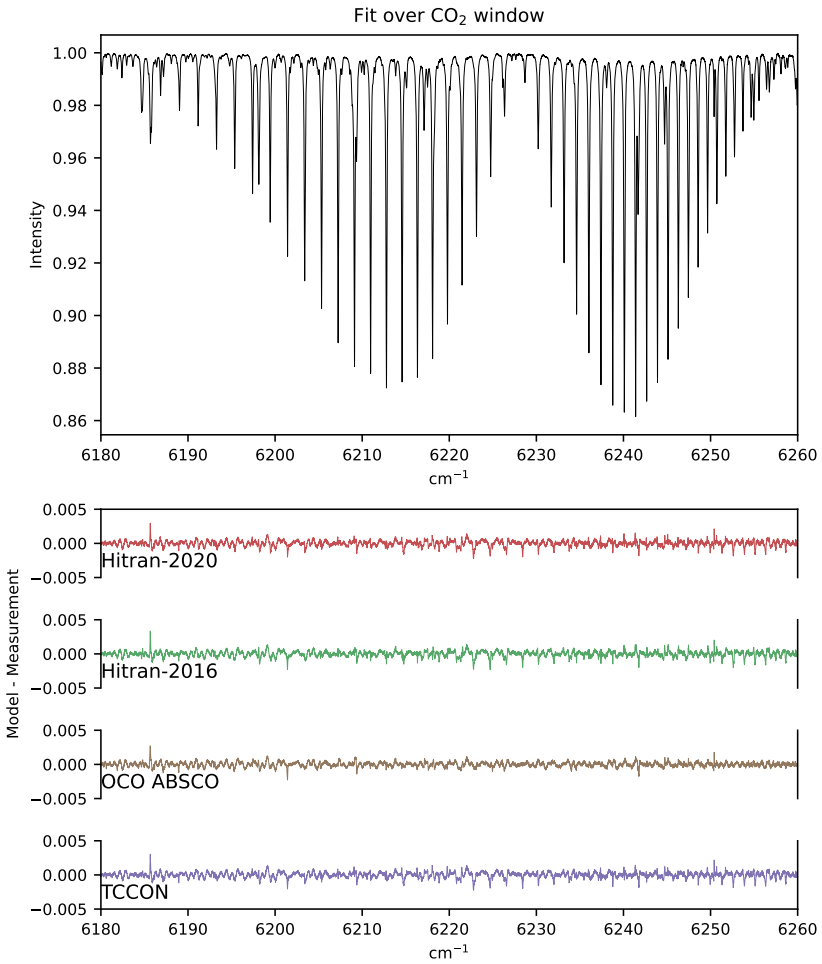

Figure 4.2: DCS Absorption spectrum (top) over the CO_2 retrieval window (6180-6260 cm^{-1}). The bottom panel shows modelled residuals from the OCO, Hitran 2016, Hitran 2020, and TCCON line-lists, as outlined in Table 4.1.

and individual absorption features can be closely inspected. Transmission spectra measured by the DCS are plotted in Panel A of Figs 4.2 and 4.3. The ideal instrument line-shape of the DCS enables time-averaging without instrument drift, increasing the signal-to noise ratio, and is another advantage of the DCS instrument.

Systematic Errors in CO_2 Spectroscopy

CO_2 was retrieved from the window between 6180-6260 cm^{-1}. Fig. 4.2 shows prominent absorption features at 6215 and 6240 cm^{-1}. Examining the residuals in Panel B, we see that in general, all of the line-lists tested here have minimal systematic residuals. However, we do see spikes in the residuals throughout the spectrum, with the largest at 6185 cm^{-1}. This indicates that there are some missing

lines in those regions which may be due to missing water lines. Although the differences between the Line-lists are small, we do see that OCO does perform most well.

Although there is not a significant difference between each of these spectral residuals, OCO does perform best. This is due to the additional physical processes accounted for in the OCO spectroscopy, which includes line-mixing and other processes beyond just pressure and temperature broadening. Incorporating additional physical processes makes calculations of the dry air column amount more accurate (Hartmann, Tran, and Toon, 2009; D. A. Long et al., 2022; Malina et al., 2022; Thompson et al., 2012).

Systematic Errors in CH_4 Spectroscopy

Fig 4.3A shows the measured transmission spectrum of the DCS over our methane retrieval window between 6050-6108 cm^{-1}. We see that this region is highly populated with methane and water absorption lines. Examining the residuals in Fig. 4.3B, we see that there are more systematic offsets with spikes atmore places, indicating missing absorption lines. Hitran 2008 and TCCON perform most well, with only one main offset at 6078 cm^{-1}, while Hitran 2016 performs least well. Hitran 2020 and 2016 have similar number of systematic offsets, with 8 main spikes seen in the residuals at 6056, 6067, 6078, 6088, 6096, 6099, and 6105 cm^{-1}.

The next-generation methane observation satellite, Merlin, will be launched in 2028. Merlin will employ differential absorption LIDAR to measure the R6 methane transition at 6076 cm^{-1} (1645 nm) to achieve better than 1% accuracy in methane concentrations (Delahaye, Maxwell, et al., 2016). Fig. 4.4 shows a zoom into the methane R6 transition between 6076 to 6079 cm^{-1}. We find that here, there are systematic residuals in all the line-lists. This indicates that there are both parameter and model errors in this spectral region. We see that Hitran 2016 and 2020 has a sine-shaped residual between 6076.75-6077 cm^{-1}. However, this is not seen in Hitran 2008 and TCCON. All line-lists also have a dip at 6078.25 cm^{-1}, which may come from inaccuracies in modeling the absorption line-shape in this specific transition.

Delahaye, Maxwell, et al. (2016) and Delahaye, Ghysels, et al. (2019) more closely examined this specific transition. They find that accounting for additional processes, such as line-mixing and collision induced absorption, through the Hartman Tran Profile improves the fits to 0.1%. Since the DCS has a broader spectral range,

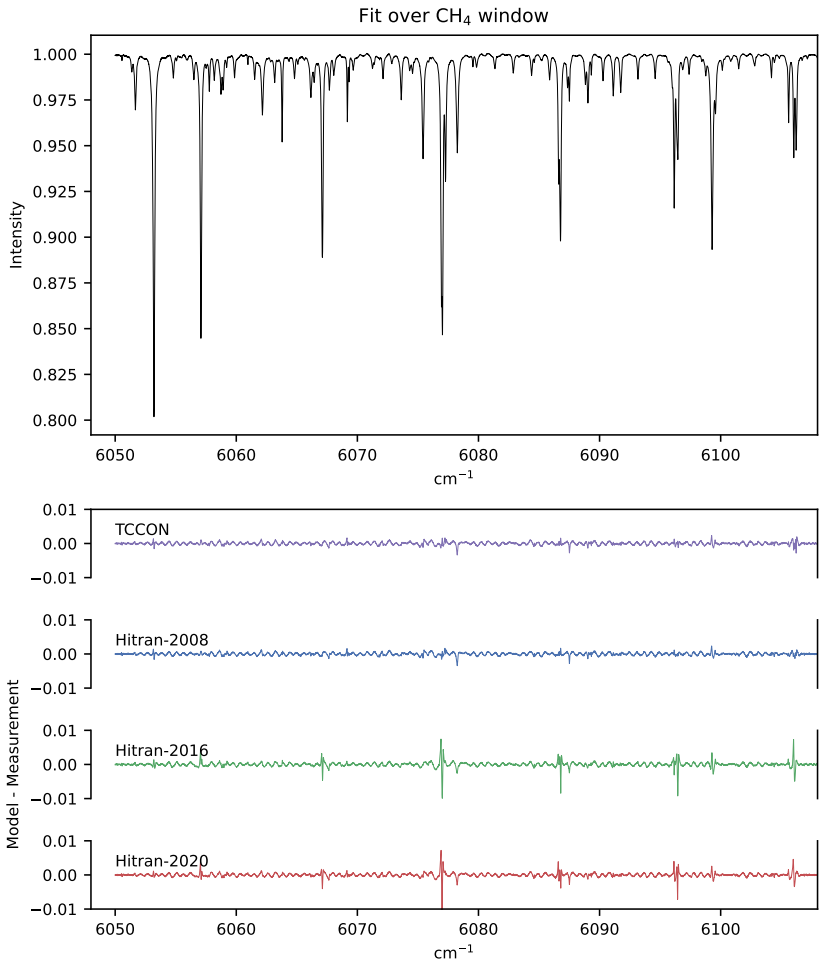

Figure 4.3: DCS absorption spectrum over the CH_4 fitting window (6050-6108 cm^{-1}), on top. The bottom panel shows the residuals with modelled spectra using the Hitran TCCON, 2008, Hitran 2016, and Hitran 2020 line-lists.

similar analyses and parameter optimizations should be performed over additional transitions in the DCS ranges to obtain the most accurate modeled absorptions of methane.

Methane's spectroscopy is continuously evolving (Devi et al., 2015; Delahaye, Maxwell, et al., 2016; C. Frankenberg et al., 2008; Zolot et al., 2013). This is because Methane spectroscopy is particularly challenging, due to the manifolds in vibrational and rotational transitions, which creates a blend of overlapping absorption lines, resulting in line-shape asymmetries and additional difficulty in modeling the line-shape (Boudon, Rey, and Loëte, 2006). The Voigt Profile does not account for these more complex processes. However, Rieker et al. (2014) found that errors in the Voigt parameters are larger than errors from not employing more complex line-

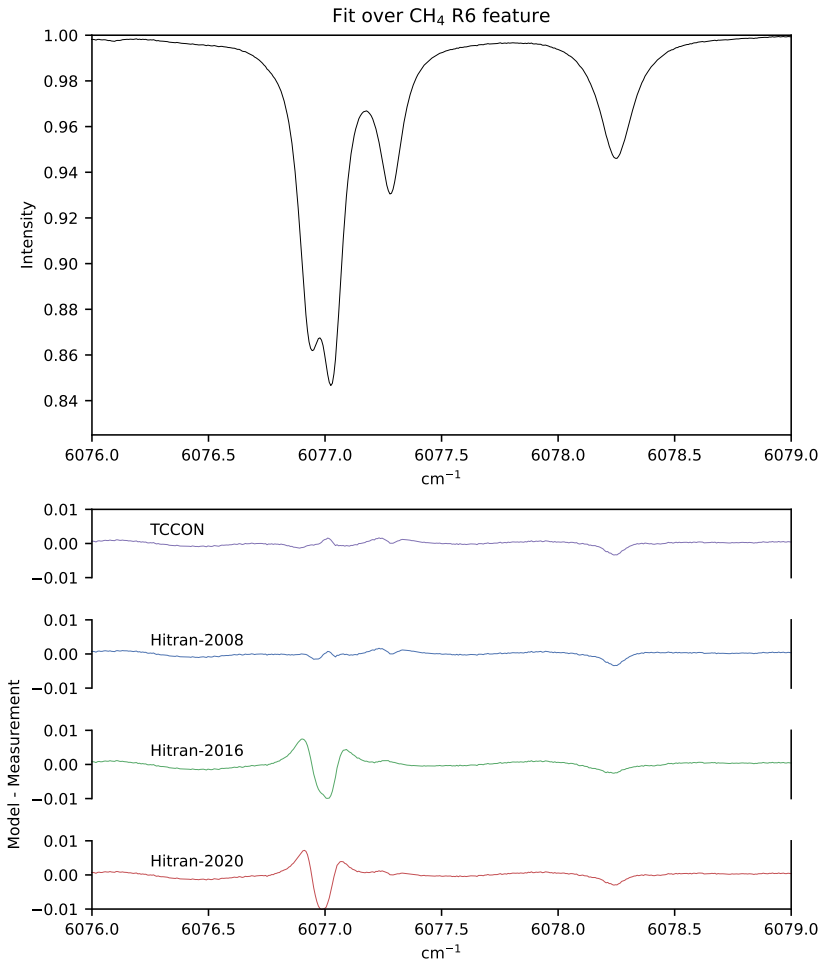

Figure 4.4: Zoom into the CH_4 R6 transition, which will be observed by the Merlin Mission. The bottom panel shows spectral residuals between modelled and measured spectra for TCCON, Hitran 2008, Hitran 2016, and Hitran 2020 line-lists.

shapes. This should be explored further. Quantifying the effects of using Voight versus more advanced line-shapes on methane retrievals would be also important for the methane remote sensing community. Calculating more accurate spectroscopic parameters for methane is an on-going effort, and we find that it is necessary in order to achieve highly accurate methane measurements with the DCS.

4.6 Synthetic Retrieval Experiments

Systematically Decomposing GHG column, pressure, and temperature errors

In the previous section, we examined systematic biases in GHG spectroscopy. Now, we will perform synthetic retrievals to systematically quantify environmental variable biases, specifically pressure and temperature, in our line-lists for greenhouse

gases. We generated synthetic spectra using the most accurate line-lists for each species over a range of pressures and temperatures, and we assumed the synthetic spectra to be free from water vapor effects (i.e., dry air). We then performed retrievals using different line-lists to calculate the retrieval error while fitting for GHG column, pressure, and temperature. This allowed us to systematically decompose the contributions of GHG column density, pressure, and temperature errors on retrieved GHG concentrations and quantify their pressure and temperature dependence.

We can separate spectroscopic biases from environmental variable biases by analyzing the retrieved GHG column density from our synthetic retrievals. This is the numerator in Eq. 4.2. The GHG column density is less affected by errors in pressure, temperature, and humidity than the GHG concentrations. Systematically quantifying how biases in the GHG column density vary with environmental conditions is applicable not only to DCS retrievals, but also to retrievals from other instruments.

Errors in pressure, temperature, and humidity affect GHG concentrations through the calculation of the dry air column density (Eq. 4.2 and denominator in Eq. 4.1). Therefore, errors in retrieving these environmental variables will propagate into the GHG concentrations.

These experiments enable us to quantify the size of the variable biases, observed through the dynamic range of each color map. We can also see how these biases vary with pressure and temperature. Results are displayed in Figs 4.5 and 4.6. These plots, from the top to bottom row, show the retrieval error for the GHG concentrations, GHG column density, pressure, and temperature with respect to pressure and temperature for all line-lists examined here.

Methane Biases

Our synthetic methane spectra were generated using Hitran 2008, our most accurate line-list. Retrievals were performed using Hitran 2016, 2020, and TCCON line-lists. Fig. 4.5 shows our results.

These synthetic experiments show that errors in retrieving methane concentrations have high variable bias, which can be seen in the top row of Fig. 4.5. These effects are more prominent in Hitran 2016 and 2020 line-lists, with errors ranging between 7-15% and 0-8%, respectively. The dynamic range for both is similar at 8%, with 45-degree error contours. This indicates that errors in retrieving methane concentrations depend on both pressure and temperature. The highest errors for Hitran 2016 and

2020 are located at higher pressures and temperatures, maximizing at the top right, while errors are smaller at lower pressures and temperatures. TCCON has a different pattern, with horizontal error contours, indicating temperature dependence.

The second row of Fig. 4.5 shows errors in the methane column density are much smaller than methane concentrations errors. The range for Hitran 2016 and 2020 is between 0-1.5%, and TCCON is between -0.35% to 0.1%. This 1.5% dynamic range in retrieving methane column densities is much larger than the 8% dynamic range in the retrieval error for methane concentrations.

The pressure error exhibits very similar error patterns to the methane concentrations error. This indicates that pressure errors dominate the overall concentrations retrieval error through the calculation of the dry air column density. Hitran 2016 and 2020 have similar dynamic ranges of 6%, with errors ranging from -5% to -11% and -6% to 0%, respectively. The pressure error for Hitran 2016 and 2020 depends on both pressure and temperature. On the other hand, the pressure bias from TCCON ranges from 0% to 2% and mainly depends on temperature.

Although errors in temperature are much smaller than pressure, the temperature errors are still substantial. Hitran 2016 and 2020 have dynamic ranges of 0.95% and 0.6%, while TCCON has a dynamic range of 0.28%. Hitran temperature errors depend on both pressure and temperature, while TCCON only depend on temperature. Although these temperature errors are smaller than the methane pressure errors, the errors among these line-lists indicate that temperature effects on methane spectroscopy need to be improved for highly accurate methane retrievals.

Our synthetic methane retrievals indicate that the main error and disagreement in accurately calculating methane concentrations stem from the dry air column density. The largest error arises from errors in modeling pressure broadening, which propagate into errors in the dry air column density. Hitran 2016 and 2020 exhibit similar pressure and temperature biases with similar dynamic ranges, but the errors seem to be shifted from each other. On the other hand, TCCON has very similar results to Hitran 2008.

Overall, our findings highlight the need for further improvement in methane spectroscopy. Accurate spectroscopic parameters for modeling both pressure and temperature effects on methane absorption are necessary, but more emphasis should be put on accurate pressure broadening parameters.

CO_2 Biases

CO_2 in the 1.6-micron region has been extensively studied due to the accuracy requirements of the OCO missions (Thompson et al., 2012; Hartmann, Tran, and Toon, 2009; Payne et al., 2020). Nonetheless, uncertainties persist. Fig. 4.6 presents the retrieval errors for synthetic spectra created using the OCO line-list, while the retrievals were performed with the Hitran 2016, 2020, and TCCON line-lists. In comparison to methane, the errors for CO_2 are generally smaller, and it is more difficult to attribute error sources.

The first row of Fig. 4.6 displays the error in retrieved concentrations. TCCON exhibits the lowest overall dynamic range, around 0.25%, ranging from 2.0-2.25% and primarily depends on pressure. Hitran 2020 ranges from 0 to 1.2% and is temperature-dependent with horizontal isolines. Hitran 2016 is fairly similar to Hitran 2020, with a dynamic range of 0.7%, from 1.8-2.5%. These variable biases of less then 0.8%, although smaller than methane, are still important to address.

The second row in Fig. 4.6 shows the CO_2 column density error. Hitran 2016 and 2020 have errors ranging from -0.2% to 0.15% and -0.1% to 0.2%, respectively. They both have a similar dynamic range of less than 0.1%. TCCON errors exhibit a dynamic range of about 0.45%, ranging from 0.35 - 0.8%, with horizontally aligned isolines, indicating temperature dependence. Variable biases in the CO_2 column density are relatively small.

Generally, errors depend on temperature for all line-lists. Pressure errors seem to be the largest, but they are much lower than methane. The third row of Fig. 4.6 displays pressure errors. Hitran 2016 ranges from -2.8 to -2%, a 0.8% difference. Hitran 2020 ranges from -1.25% to +0.25%, a 1.5% difference. TCCON ranges from -1.8% to -1.1%, a 0.7% difference. They are primarily temperature-dependent but have some pressure dependence as well. Generally, the errors appear to have similar temperature and pressure dependence across all the line-lists. These variable biases in pressure broadening are substantial.

The fourth row of Fig. 4.6 shows temperature errors. Hitran 2016 ranges from -0.35% to -0.2%, a 0.15% dynamic range. Hitran 2020 ranges from 0.01% to 0.11%, a 0.1% difference. TCCON ranges from 0.04% to 0.3%, a 0.26% difference. All errors are very small. Hitran 2016 and 2020 exhibit the same behavior, with the lowest errors in the lower right corner and increasing towards the top-left corner. TCCON looks different, with the highest values at the lowest pressure and temperature, and opposite at the high pressure and temperature. Temperature effects on CO_2

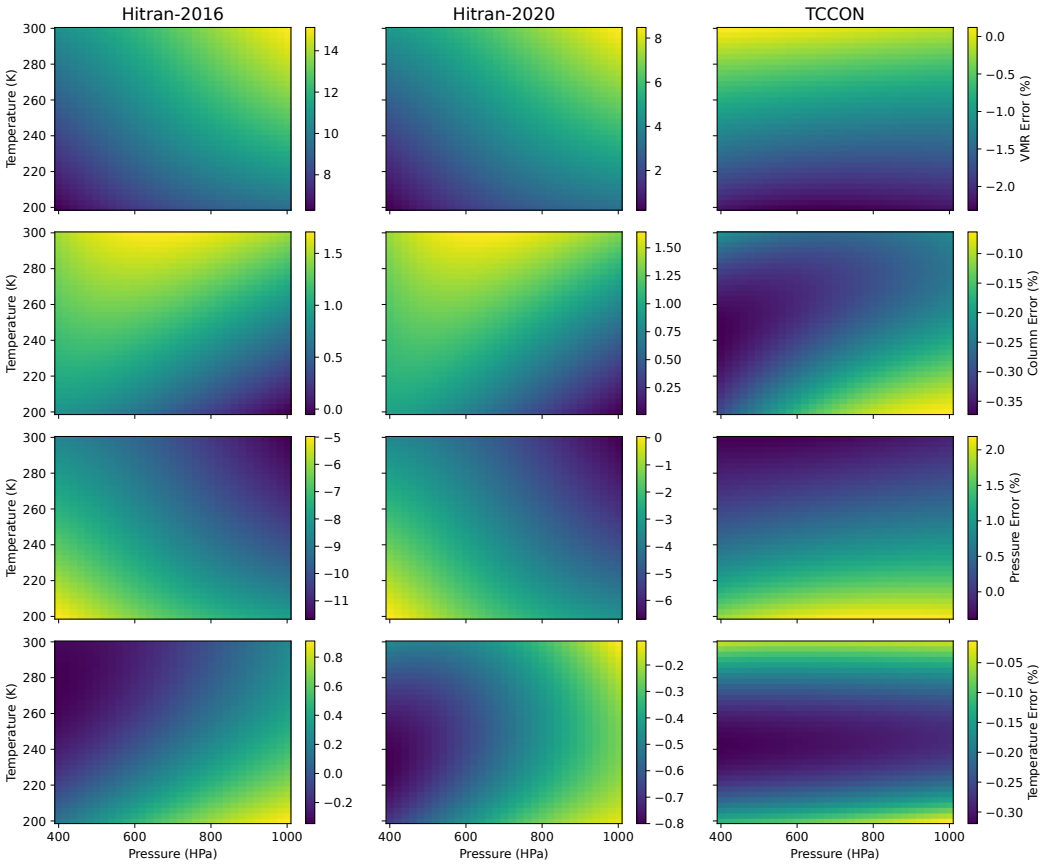

Figure 4.5: Retrieval error for CH_4 synthetic retrievals. The 'true spectra' were generated with Hitran 2008. From top to bottom row, errors in concentrations (denoted as VMR), methane column density, retrieved pressure, and retrieved temperature are plotted as a function of pressure and temperature. Retrievals were performed with Hitran 2016, Hitran 2020, and TCCON line-lists.

spectroscopy seem to be well constrained.

In summary, CO_2 line-lists show greater agreement than methane line-lists. CO_2 column density errors are found to be small. The majority of errors in retrieving CO_2 concentrations stem from pressure errors, with minor contributions from temperature errors. To enhance the accuracy of CO_2 spectroscopy, efforts should focus on obtaining more precise pressure broadening parameters and improving the temperature dependence of these parameters.

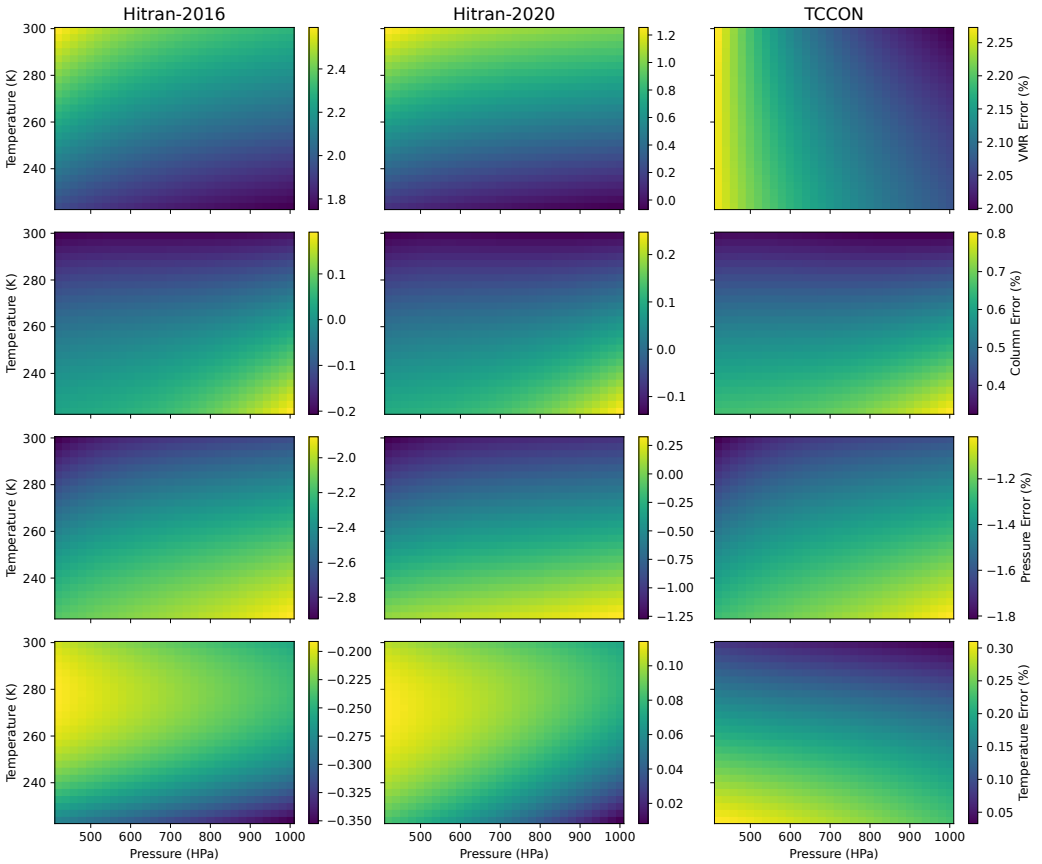

Figure 4.6: Retrieval errors from our CO_2 synthetic retrieval experiments. The 'true spectra' were generated wie OCO ABSCO line-list. From top to bottom row, errors in concentrations (denoted as VMR), CO_2 column density, retrieved pressure, and retrieved temperature are plotted as a function of pressure and temperature. Retrievals were performed with Hitran 2016, Hitran 2020, and TCCON line-lists.

4.7 DCS Field Retrieval Results

Analyzing Field Retrievals

In the previous section, we quantified the biases that corresponded to errors in retrieving pressure and temperature in idealized synthetic retrievals. Here, we will see how these variable biases affect the accuracy of Ghg retrievals in a field setting, which was described in Section 2. We used different line-lists to retrieved CO_2, methane, and water vapor concentrations from the DCS and had the Picarro instrument as a reference.

Here, our objective is to quantify the effects of environmental variable biases on both the GhG column density and GHG concentrations in a real-world setting. To do this, we separated the GHG column density and GhG concentrations for multiple

line-lists. Table 4.1 shows the line-lists and retrieval setup.

CO_2 Retrievals

Regional-scale gradients of column-averaged CO_2 concentrations in the atmosphere are about 2% (8 ppm) (Thompson et al., 2012). Inferring CO_2 sources at this scale requires sub-ppm accuracy. A global network should be capable of this laboratory-level accuracy, which the DCS can theoretically provide directly in the field.

Fig 4.7A shows the retrieved time series for a two-week period in our study. We can see some diurnal patterns, with ~40 ppm (~10%) CO_2 spikes in the time-series, which likely correspond to rush-hour traffic. CO_2 emissions exhibit a more pronounced diurnal cycle, because the sources of CO_2, such as vehicle traffic and electricity production, are diurnally varying (Waxman, Cossel, Giorgetta, et al., 2019).

Our algorithm retrieves CO_2 over the window between 6180-6260 cm^{-1}, and we employed the Hitran 2016, Hitran 2020, TCCON, and OCO ABSCO line-lists. All the line-lists used here track very closely with the in-situ reference observations, denoted as black dots. Differences among the different line-lists used are small and difficult to discern, indicating that the CO_2 spectroscopy is in agreement.

The relative GhG column differences between different spectroscopic databases and the OCO database are displayed in Fig. 4.7B. It should be emphasized that the mean bias has been subtracted out, because the main objective here is to analyze the variable bias. We compare against the OCO database, because it is the best performing, as seen in Fig. 4.2. Differences in the CO2 spectroscopy are relatively small, with column percent differences ranging from -0.1% to 0.1%, with differences very close to zero for a majority of the time-series. These small errors indicate that the CO_2 spectroscopy is sufficiently accurate to be within the 0.1% accuracy threshold required for long-term GhG monitoring.

Accounting for environmental variable biases, which is introduced when calculating the CO_2 concentrations, introduces larger errors. Fig. 4.7C displays the relative error between retrieved CO_2 concentrations from the DCS in comparison to the best performing line-list, the OCO spectroscopy. The mean bias was subtracted out to highlight the variable bias. Concentrations were calculated using retrieved p and T seen in Fig. 4.7D and E, with H_2O seen in Fig. 4.9. We can see that the error ranges between -0.5% and 0.5% with a majority of the datapoints around 0.2%. These errors are larger than the 0.1% accuracy threshold required for long-term

monitoring. Temperature retrievals generally agree, while pressure retrievals have slight offsets among different line-lists. This indicates that improved parameters on modeling the effect of environmental variables, mainly pressure broadening, on CO_2 are necessary.

Methane Retrievals

Fig. 4.8A displays the retrieved time-series for methane. We observe that methane exhibits a less pronounced diurnal cycle than CO_2. Methane's peak is approximately 200 ppb above background concentrations, with a particularly abrupt increase for about a day at the beginning of the time-series. This largest increase also coincides with the most pronounced CO_2 peak. Interestingly, the temperature fits for both retrieval windows during this period are systematically different from the in-situ measurements, which usually align almost perfectly with local temperature measurements. These differences are too large to be caused by a retrieval bias and are likely due to strong temperature gradients, potentially along gradients towards the hill. Methane still exhibits a diurnal cycle, albeit less than the CO_2 diurnal cycle, which is driven by boundary layer height and urban emissions in Boulder.

We used the Hitran 2008, 2016, and 2020 line-lists, along with the TCCON line-list, to retrieve methane concentrations. In contrast to CO_2, we observe that the retrieved concentrations among different spectroscopic databases are more spread out for methane than for CO_2 (see panel A). Hitran 2016 consistently has higher values than the other line-lists. Methane concentrations can vary by up to 300 ppb, which is attributed to spectroscopic errors. Hitran 2008 is closest to the in-situ observations, denoted as black dots, suggesting that Hitran 2008 may be the most accurate line-list. Errors in pressure and temperature-dependent spectroscopic parameters can induce errors in not only the methane column amount, but also the dry air column density, affecting overall methane concentrations.

Fig. 4.8B displays the offset between the methane column density. The mean bias has been subtracted so that variable biases can be examined. The relative differences are with respect to the best performing spectroscopy, Hitran 2008.

In comparison to CO_2, there is a much larger disagreement for the methane column density. The variable bias ranges from -2% to 2%, which is significantly larger than the 0.1% seen for the CO_2 relative column error. Hitran 2016 (the orange line) exhibits the largest variable bias, reaching a -2% error during the last two days, while Hitran 2020, although showing biases up to 1%, is in closer agreement

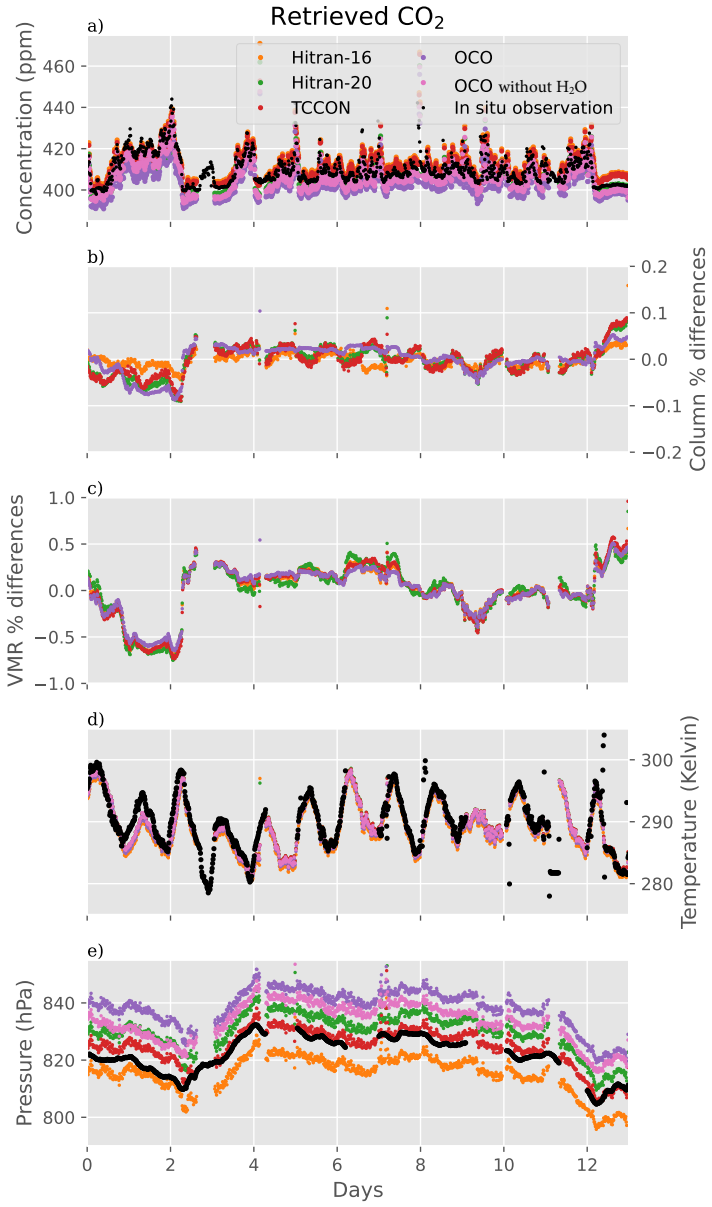

Figure 4.7: Retrieved CO_2 concentrations with line-lists outlined in Table 4.1 from our DCS field deployment in Boulder, Colorado, USA over a two week period. From top to bottom, the panels show CO_2 concentrations, relative errors in column densities with respect to the OCO spectroscopy, relative concentration errors with respect to the OCO spectroscopy, retrieved temperature, and retrieved pressure. In-situ observations from the Picarro instrument are plotted in black dots.

with Hitran 2008. These results indicate that methane spectroscopy requires further improvement for long-term background monitoring.

Methane concentrations exhibit larger errors than CO_2. Fig. 4.8B shows the variable error for retrieved methane concentrations in comparison with the best performing line-list, Hitran 2008. Hitran 2016 reaches -2%, while other line-lists regularly range from -0.5% to 0.5%. Comparing Panels B and C, it appears that errors in the methane column density are larger than errors in the methane concentrations. This suggests that errors in the methane column density are being compensated by errors in retrieved environmental variables. Panel D shows agreement in retrieved temperature among different line-lists, while Panel E displays a large disagreement between different line-lists in retrieved pressure. This points to pressure broadening errors as the source of this compensating error. Our results indicate that the effects of pressure on modeling methane spectra need improvement to enable more accurate methane concentration retrievals.

Water Vapor Retrievals

Fig. 4.9 presents the retrieved H_2O concentrations. H_2O concentrations were retrieved over the CO_2 window between 6180 and 6260,cm^{-1} using the TCCON line-list. We opted for a single line-list to enable a more consistent comparison of methane and CO_2 spectroscopy, avoiding the added complexity of multiple H_2O line-lists.

As seen in Fig. 4.9B, H_2O exhibits greater variability than methane or CO_2, with concentrations ranging from 0.7% to 1.75%. The highest H_2O concentrations occur during days 0-2, appearing to correspond with lower measured pressure. It is worth noting that the in-situ observations align well with the retrieved H_2O concentrations from the DCS. The relatively high H_2O concentrations at the beginning of the time-series represent an important feature, which will be further discussed in the subsequent section.

4.8 H_2O Broadening

Effect of H_2O broadening can be substantial

In the previous section, we found that retrieval errors correspond strongly to water vapor concentrations. Water vapor complicates ghg retrievals by spectral cross-interference and broadens spectral lines more efficiently than dry air (Hobbs et al., 2020). Fig. 4.7 and 4.8 show the impact of water vapor broadening on our ghg retrievals. We can see that there is a larger disagreement between the retrieved DCS

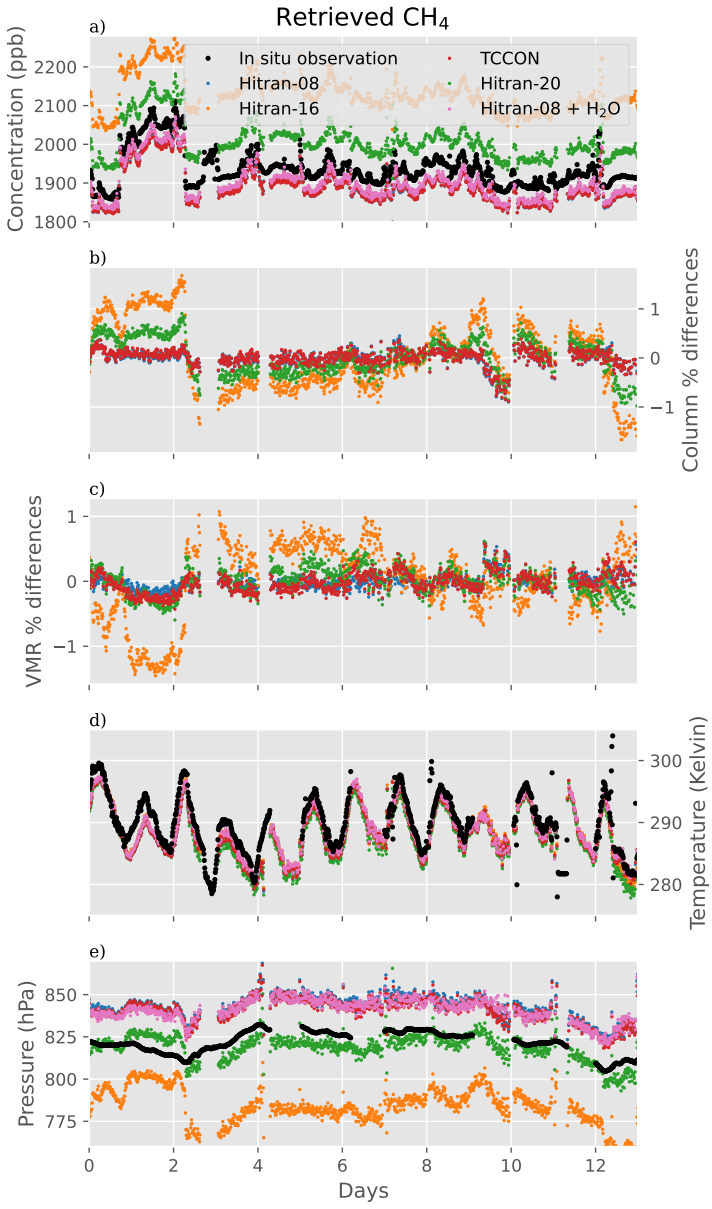

Figure 4.8: Retrieved CH_4 from our DCS field-deployment. The figure is arranged as in Fig. 4.7. Panels B and C display the relative concentrations error and relative CH_4 column error with respect to the Hitran 2008 spectroscopy with water broadening.

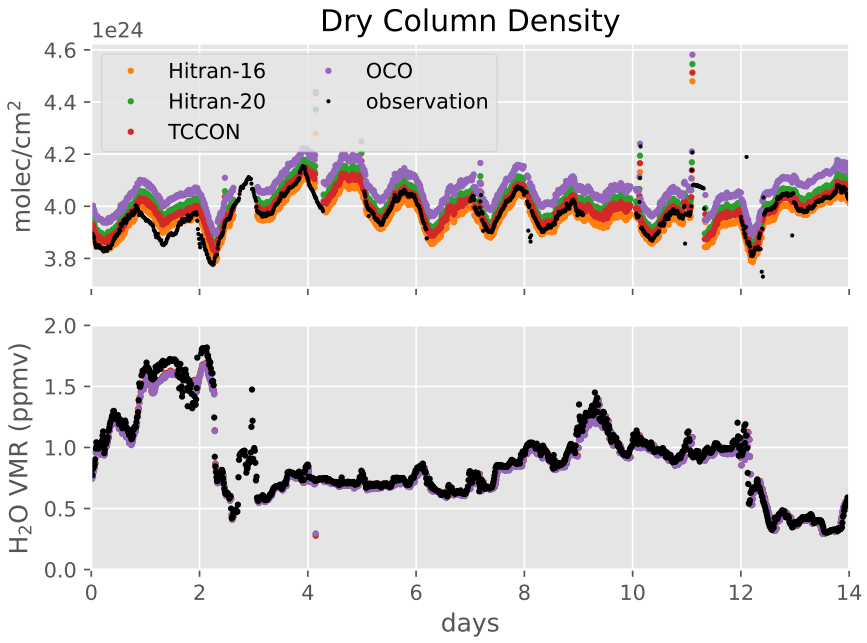

Figure 4.9: The top panel displays the calculated dry air column, while the bottom panel displays retrieved water vapor concentrations. The dry air column density was calculated using the retrieved pressure and temperature in Eq. 4.2.

concentrations in comparison to the Picarro on days 0-2, which are days with higher water vapor concentrations, as seen in Fig. 4.9.

Water Broadening on Methane

Water vapor broadening is 1.34 times more efficient in broadening methane lineshapes than dry air (Delahaye, Landsheere, et al., 2016; Tan et al., 2019). Given that laboratory-derived H_2O broadening parameters for methane are limitted, we accounted for this effect by instead calculating an effective pressure when computing the absorption cross-sections. H_2O broadening can increase pressure broadening, so we instead calculated an effective pressure ($p_{effective}$) to account for additional pressure broadening due to water vapor concentrations.

$$p_{effective} = p(1 + 0.34[H_2O]) \tag{4.7}$$

The blue line in Fig. 4.8B and C shows the impact of water vapor broadening on our methane retrievals. We see that water vapor can have up to a 10 pbb (0.05%) impact on methane retrievals on days with higher water vapor concentrations. Although the impact of water on methane retrievals is relatively small, it should be taken into

account for background methane monitoring, where accuracy requirements are at the sub-percent level.

Water Broadening on CO_2

H_2O broadening on CO_2 can be up to 2 times more efficient than dry air (Adkins, David A. Long, and Hodges, 2021; Sung et al., 2009; Tan et al., 2019). While the OCO spectroscopy accounts for this effect, the values of this parameter were obtained from another spectral window located at 2325 cm^{-1} (4.3 microns) (Oyafuso et al., 2017; Sung et al., 2009; Tan et al., 2019). In order to test the effect of H_2O broadening on CO_2 retrievals, we developed and OCO ABSCO line-list without water vapor effects by using the full OCO lookup table and set the water vapor concentrations to zero%. We call this OCO V2 here and compare retrieval results with the OCO table with H_2O broadening.

The pink lines in Fig 4.7 show the difference between accounting for and neglecting H_2O broadening on the DCS CO_2 retrievals. There is a 4.5,ppm difference in CO_2 concentrations, corresponding to more than 1%. H_2O broadening not only affects the CO_2 retrievals through the dry air column, but also the CO_2 column density itself. H_2O broadening varies with the rotational state of CO_2. We can see that this enhanced pressure broadening resulting from H_2O adds a 0.1% error. This error affects not only DCS retrievals, but also the CO_2 retrievals of other instruments, because variable errors in the CO_2 column density cannot be reduced by ancillary measurements of the dry column. Given these results, we recommend obtaining accurate H_2O broadening parameters and their temperature dependence for future work.

Neglecting H_2O broadening on methane and CO_2 retrievals over these windows can induce a 0.05% and 1% error on CH_4 and CO_2 retrievals respectively. Given that neglecting H_2O broadening already has a sizable effect at 1.5% H_2O concentrations, this effect can only be larger in tropical atmospheres, where concentrations can be up to 5%. Obtaining accurate CO_2 water vapor broadening parameters and their temperature dependence should therefore be a key objective for highly accurate ghg measurements by both ground-based and space-based sensors.

4.9 Summary and Discussion

This study aimed to systematically quantify the impact of environmental variable errors on greenhouse gas (GHG) retrievals using Dual-Comb Spectroscopy's remote sensing capabilities. Unlike random or systematic errors, environmental variable

errors cannot simply be averaged or subtracted out. Instead, accurately modeling environmental effects on GHG spectroscopy is required to mitigate these errors.

We developed a retrieval algorithm that isolates the effects of pressure and temperature from the retrieved GHG amounts, utilizing the DCS's high spectral resolution. The high spectral sampling of the DCS also allows direct retrieval of pressure and temperature solely from the shape of the measured absorption cross-sections. Our findings highlight the significance of accurately modeling pressure-broadening effects on GHGs.

In the case of methane, the Hitran 2008 and TCCON line-lists exhibited fewer systematic biases compared to other line-lists. Discrepancies among line-lists can lead to substantial differences in retrieved concentrations, with an 8% dynamic range relating to pressure and temperature variations. However, the variable error in retrieving pressure, with a dynamic range of 6%, dominates. In real-world applications, different spectroscopic databases can yield methane concentrations that differ by up to 2%, with pressure retrieval errors contributing the majority of this discrepancy. Thus, while both temperature and pressure broadening parameters require improvements for highly accurate methane measurements, pressure broadening effects demand more attention.

For CO_2, the OCO ABSCO lookup table yielded the best performance because it accounts for additional non-Voigt effects. Synthetic retrievals revealed less than 0.8% variable error in retrieving CO_2 concentrations, mainly attributed to errors in modeling pressure broadening. Field retrievals of CO_2 using different line-lists revealed a 0.5% disagreement in concentrations, which, despite being smaller than methane, exceeds the 0.1% accuracy required for background monitoring. Like methane, the majority of the disagreement among different line-lists arises from errors in retrieving pressure.

In addition to pressure and temperature errors, we found that accounting for H_2O broadening is important for CO_2. Neglecting H_2O broadening can induce a 1% error in retrieved CO_2 concentrations. This is because H_2O can be two times more efficient than dry air broadening, affecting the retrieved pressure. H2O broadening can also affect the CO_2 column density by 0.1%, which is on par with spectroscopic disagreements among different line-lists. This is important not only for DCS retrievals, but also the retrievals for other instruments. Given the size of this effect at only 1.7% H_2O concentrations, this effect can only be more substantial in tropical atmospheres, where H_2O concentrations can be up to 5%. Current H_2O broadening

parameters used in CO_2 spectroscopy are borrowed from another spectral region. Therefore, calculating accurate H_2O broadening parameters should be a priority for accurate CO_2 remote sensing.

4.10 Implications and Recommendations

Environmental biases are crucial to address as they significantly impact measurements of greenhouse gas gradients and long-term trend analysis. These biases cannot be simply averaged or subtracted out; rather, they require an accurate modeling of environmental impacts on GHG absorption. Our study leveraged the high-resolution capabilities of Dual-Comb Spectroscopy (DCS) to systematically quantify these environmental biases.

Our findings have broad implications not only for DCS but also for other remote sensing instruments. The variable errors in retrieving the greenhouse gas column density can affect the accuracy of retrievals from these instruments. Therefore, understanding and mitigating these errors is essential for ensuring accurate greenhouse gas measurements across different sensing instruments.

While additional measurements of the dry air column can be useful, our results indicate that errors in the greenhouse gas column density can exceed the 0.1% accuracy threshold required for background monitoring, especially in the case of methane. Therefore, such additional measurements alone may not be sufficient to meet the required accuracy threshold.

To achieve the high-precision measurements necessary for effective greenhouse gas monitoring, our study suggests that accurately modeling the effects of pressure, temperature, and humidity on GHG spectroscopy should be a priority. Enhancements to both temperature and pressure broadening parameters are crucial, with a particular emphasis on accurately modeling pressure broadening effects. This is especially true for methane. Additionally, given the impact of water vapor broadening on GHG retrievals, accurate parameters for this effect should be a key objective, especially for CO_2.

Our study underscores the immense potential of DCS in bringing laboratory-level accuracy in remote sensing of GHGs directly to field settings. The superior spectral resolution, stability, and range of DCS, when combined with accurate modeling of environmental effects on GHG spectroscopy, holds significant promise in advancing our understanding of GHG dynamics and informing GHG flux inversions. Therefore, sustained efforts in refining and applying this technology, along with a focus on

improving GHG spectroscopy, will contribute substantially to expanding the GHG observation network and facilitating the verification of climate change mitigation policies.

BIBLIOGRAPHY

Adkins, Erin M., David A. Long, and Joseph T. Hodges (Aug. 1, 2021). "Air-broadening in near-infrared carbon dioxide line shapes: Quantifying contributions from O2, N2, and Ar". In: *Journal of Quantitative Spectroscopy and Radiative Transfer* 270, p. 107669. ISSN: 0022-4073. DOI: 10.1016/j.jqsrt.2021.107669. URL: https://www.sciencedirect.com/science/article/pii/S002240732100162X (visited on 03/01/2023).

Bai, Mei et al. (Feb. 18, 2019). "Comparison of slant open-path flux gradient and static closed chamber techniques to measure soil N₂O emissions". In: *Atmospheric Measurement Techniques* 12.2, pp. 1095–1102. ISSN: 1867-8548. DOI: 10.5194/amt-12-1095-2019. URL: https://amt.copernicus.org/articles/12/1095/2019/ (visited on 01/13/2023).

Boudon Vincent, V., M. Rey, and M. Loëte (Apr. 1, 2006). "The vibrational levels of methane obtained from analyses of high-resolution spectra". In: *Journal of Quantitative Spectroscopy and Radiative Transfer* 98.3, pp. 394–404. ISSN: 0022-4073. DOI: 10.1016/j.jqsrt.2005.06.003. URL: https://www.sciencedirect.com/science/article/pii/S0022407305002608 (visited on 05/05/2023).

Coburn, Sean et al. (Apr. 20, 2018). "Regional trace-gas source attribution using a field-deployed dual frequency comb spectrometer". In: *Optica* 5.4. Publisher: Optical Society of America, pp. 320–327. ISSN: 2334-2536. DOI: 10.1364/OPTICA.5.000320. URL: https://www.osapublishing.org/optica/abstract.cfm?uri=optica-5-4-320 (visited on 02/18/2021).

Coddington, Ian, Nathan Newbury, and William Swann (Apr. 20, 2016). "Dual-comb spectroscopy". In: *Optica* 3.4. Publisher: Optical Society of America, pp. 414–426. ISSN: 2334-2536. DOI: 10.1364/OPTICA.3.000414. URL: https://www.osapublishing.org/optica/abstract.cfm?uri=optica-3-4-414 (visited on 02/18/2021).

Collins, W. et al. (July 4, 2022). "Monitoring methane emissions from oil and gas operations‡". In: *Optics Express* 30.14. Publisher: Optica Publishing Group, pp. 24326–24351. ISSN: 1094-4087. DOI: 10.1364/OE.464421. URL: https://opg.optica.org/oe/abstract.cfm?uri=oe-30-14-24326 (visited on 05/14/2023).

Conway E. K., Thomas J. et al. (1994). "Evidence for interannual variability of the carbon cycle from the National Oceanic and Atmospheric Administration/Climate Monitoring and Diagnostics Laboratory Global Air Sampling Network". In: *Journal of Geophysical Research: Atmospheres* 99 (D11). _eprint: https://onlinelibrary.wiley.com/doi/pdf/10.1029/94JD01951, pp. 22831–22855. ISSN: 2156-2202. DOI: 10.1029/94JD01951. URL: https://onlinelibrary.wiley.com/doi/abs/10.1029/94JD01951 (visited on 05/03/2023).

Cossel, Kevin C. et al. (July 20, 2017). "Open-path dual-comb spectroscopy to an airborne retroreflector". In: *Optica* 4.7. Publisher: Optical Society of America, pp. 724–728. ISSN: 2334-2536. DOI: 10.1364/OPTICA.4.000724. URL: https://www.osapublishing.org/optica/abstract.cfm?uri=optica-4-7-724 (visited on 02/18/2021).

Delahaye, T., M. Ghysels, et al. (2019). "Measurement and Modeling of Air-Broadened Methane Absorption in the MERLIN Spectral Region at Low Temperatures". In: *Journal of Geophysical Research: Atmospheres* 124.6. _eprint: https://onlinelibrary.wiley.com/doi/pdf/10.1029/2018JD028917, pp. 3556–3564. ISSN: 2169-8996. DOI: 10.1029/2018JD028917. URL: https://onlinelibrary.wiley.com/doi/abs/10.1029/2018JD028917 (visited on 03/01/2023).

Delahaye, T., X. Landsheere, et al. (Apr. 1, 2016). "Measurements of H2O broadening coefficients of infrared methane lines". In: *Journal of Quantitative Spectroscopy and Radiative Transfer* 173, pp. 40–48. ISSN: 0022-4073. DOI: 10.1016/j.jqsrt.2015.12.015. (Visited on 03/01/2023).

Delahaye, T., S. E. Maxwell, et al. (2016). "Precise methane absorption measurements in the 1.64 m spectral region for the MERLIN mission". In: *Journal of Geophysical Research: Atmospheres* 121.12, pp. 7360–7370. ISSN: 2169-8996. DOI: 10.1002/2016JD025024. (Visited on 01/06/2022).

Devi, V. Malathy et al. (Sept. 1, 2015). "Self- and air-broadened line shapes in the 23 P and R branches of 12CH4". In: *Journal of Molecular Spectroscopy*. Spectroscopy with Synchrotron Radiation 315, pp. 114–136. ISSN: 0022-2852. DOI: 10.1016/j.jms.2015.05.003. URL: https://www.sciencedirect.com/science/article/pii/S0022285215000934 (visited on 02/13/2022).

Fortier, Tara and Esther Baumann (Dec. 6, 2019). "20 years of developments in optical frequency comb technology and applications". In: *Communications Physics* 2.1. Number: 1 Publisher: Nature Publishing Group, pp. 1–16. ISSN: 2399-3650. DOI: 10.1038/s42005-019-0249-y. URL: https://www.nature.com/articles/s42005-019-0249-y (visited on 02/18/2021).

Frankenberg, C. et al. (Sept. 1, 2008). "Pressure broadening in the 2ν$_3$ band of methane and its implication on atmospheric retrievals". In: *Atmospheric Chemistry and Physics* 8.17. Publisher: Copernicus GmbH, pp. 5061–5075. ISSN: 1680-7316. DOI: 10.5194/acp-8-5061-2008. URL: https://acp.copernicus.org/articles/8/5061/2008/ (visited on 01/31/2022).

Frankenberg, Christian et al. (2008). "Tropical methane emissions: A revised view from SCIAMACHY onboard ENVISAT". In: *Geophysical Research Letters* 35.15. _eprint: https://onlinelibrary.wiley.com/doi/pdf/10.1029/2008GL034300. ISSN: 1944-8007. DOI: 10.1029/2008GL034300. URL: https://onlinelibrary.wiley.com/doi/abs/10.1029/2008GL034300 (visited on 05/09/2023).

Gordon, I. E., L. S. Rothman, R. J. Hargreaves, et al. (Jan. 1, 2022). "The HITRAN2020 molecular spectroscopic database". In: *Journal of Quantitative Spectroscopy and Radiative Transfer* 277, p. 107949. ISSN: 0022-4073. DOI: 10.1016/j.jqsrt.2021.107949. URL: https://www.sciencedirect.com/science/article/pii/S0022407321004416 (visited on 03/24/2022).

Gordon, I. E., L. S. Rothman, C. Hill, et al. (Dec. 1, 2017). "The HITRAN2016 molecular spectroscopic database". In: *Journal of Quantitative Spectroscopy and Radiative Transfer*. HITRAN2016 Special Issue 203, pp. 3–69. ISSN: 0022-4073. DOI: 10.1016/j.jqsrt.2017.06.038. URL: https://www.sciencedirect.com/science/article/pii/S0022407317301073 (visited on 12/12/2021).

Hammer, S. et al. (May 7, 2013). "Assessment of a multi-species in situ FTIR for precise atmospheric greenhouse gas observations". In: *Atmospheric Measurement Techniques* 6.5, pp. 1153–1170. ISSN: 1867-8548. DOI: 10.5194/amt-6-1153-2013. URL: https://amt.copernicus.org/articles/6/1153/2013/ (visited on 10/17/2022).

Hartmann, J.-M., H. Tran, and G. C. Toon (Oct. 1, 2009). "Influence of line mixing on the retrievals of atmospheric CO_2 from spectra in the 1.6 and 2.1 μm regions". In: *Atmospheric Chemistry and Physics* 9.19. Publisher: Copernicus GmbH, pp. 7303–7312. ISSN: 1680-7316. DOI: 10.5194/acp-9-7303-2009. URL: https://acp.copernicus.org/articles/9/7303/2009/ (visited on 05/09/2023).

Hobbs, Jonathan M. et al. (Dec. 1, 2020). "Spectroscopic uncertainty impacts on OCO-2/3 retrievals of XCO2". In: *Journal of Quantitative Spectroscopy and Radiative Transfer* 257, p. 107360. ISSN: 0022-4073. DOI: 10.1016/j.jqsrt.2020.107360. URL: https://www.sciencedirect.com/science/article/pii/S0022407320305586 (visited on 05/09/2023).

Jacob, Daniel J. et al. (Nov. 18, 2016). "Satellite observations of atmospheric methane and their value for quantifying methane emissions". In: *Atmospheric Chemistry and Physics* 16.22, pp. 14371–14396. ISSN: 1680-7324. DOI: 10.5194/acp-16-14371-2016. URL: https://www.atmos-chem-phys.net/16/14371/2016/ (visited on 04/03/2020).

Keeling, Charles D. (1960). "The Concentration and Isotopic Abundances of Carbon Dioxide in the Atmosphere". In: *Tellus* 12.2, pp. 200–203. ISSN: 2153-3490. DOI: 10.1111/j.2153-3490.1960.tb01300.x. (Visited on 05/03/2023).

Long, D. A. et al. (Nov. 1, 2022). "The effects of advanced spectral line shapes on atmospheric carbon dioxide retrievals". In: *Journal of Quantitative Spectroscopy and Radiative Transfer* 291, p. 108324. ISSN: 0022-4073. DOI: 10.1016/j.jqsrt.2022.108324. URL: https://www.sciencedirect.com/science/article/pii/S002240732200259X (visited on 03/01/2023).

Malarich, Nathan A. et al. (Jan. 30, 2023). "Validation of open-path dual-comb spectroscopy against an O_2 background". In: *Optics Express* 31.3. Publisher: Optica Publishing Group, pp. 5042–5055. ISSN: 1094-4087. DOI: 10.1364/OE.480301. URL: https://opg.optica.org/oe/abstract.cfm?uri=oe-31-3-5042 (visited on 02/13/2023).

Malina, Edward et al. (Apr. 20, 2022). "On the consistency of methane retrievals using the Total Carbon Column Observing Network (TCCON) and multiple spectroscopic databases". In: *Atmospheric Measurement Techniques* 15.8. Publisher: Copernicus GmbH, pp. 2377–2406. ISSN: 1867-1381. DOI: 10.5194/amt-15-2377-2022. URL: https://amt.copernicus.org/articles/15/2377/2022/ (visited on 01/31/2023).

Mendonca, Joseph et al. (Jan. 3, 2019). "Using a speed-dependent Voigt line shape to retrieve O_2 from Total Carbon Column Observing Network solar spectra to improve measurements of XCO_2". In: *Atmospheric Measurement Techniques* 12.1. Publisher: Copernicus GmbH, pp. 35–50. ISSN: 1867-1381. DOI: 10.5194/amt-12-35-2019. URL: https://amt.copernicus.org/articles/12/35/2019/ (visited on 04/01/2022).

Miller, C. E. et al. (2007). "Precision requirements for space-based data". In: *Journal of Geophysical Research: Atmospheres* 112 (D10). ISSN: 2156-2202. DOI: 10.1029/2006JD007659. (Visited on 05/03/2023).

Oyafuso, Fabiano et al. (June 1, 2017). "High accuracy absorption coefficients for the Orbiting Carbon Observatory-2 (OCO-2) mission: Validation of updated carbon dioxide cross-sections using atmospheric spectra". In: *Journal of Quantitative Spectroscopy and Radiative Transfer* 203. DOI: 10.1016/j.jqsrt.2017.06.012.

Pales, Jack C. and Charles D. Keeling (1965). "The concentration of atmospheric carbon dioxide in Hawaii". In: *Journal of Geophysical Research (1896-1977)* 70.24. _eprint: https://onlinelibrary.wiley.com/doi/pdf/10.1029/JZ070i024p06053, pp. 6053–6076. ISSN: 2156-2202. DOI: 10.1029/JZ070i024p06053. URL: https://onlinelibrary.wiley.com/doi/abs/10.1029/JZ070i024p06053 (visited on 05/03/2023).

Payne, Vivienne H. et al. (Nov. 1, 2020). "Absorption coefficient (ABSCO) tables for the Orbiting Carbon Observatories: Version 5.1". In: *Journal of Quantitative Spectroscopy and Radiative Transfer* 255, p. 107217. ISSN: 0022-4073. DOI: 10.1016/j.jqsrt.2020.107217. URL: https://www.sciencedirect.com/science/article/pii/S0022407320302016 (visited on 12/12/2021).

Rieker, G. B. et al. (Nov. 20, 2014). "Frequency-comb-based remote sensing of greenhouse gases over kilometer air paths". In: *Optica* 1.5, p. 290. ISSN: 2334-2536. DOI: 10.1364/OPTICA.1.000290. URL: https://www.osapublishing.org/abstract.cfm?URI=optica-1-5-290 (visited on 04/29/2020).

Rodgers, Clive D (2000). *Inverse methods for atmospheric sounding: theory and practice*. Vol. 2. World scientific.

Rothman, L. S. et al. (June 1, 2009). "The HITRAN 2008 molecular spectroscopic database". In: *Journal of Quantitative Spectroscopy and Radiative Transfer*. HITRAN 110.9, pp. 533–572. ISSN: 0022-4073. DOI: 10.1016/j.jqsrt.2009.02.013. URL: https://www.sciencedirect.com/science/article/pii/S0022407309000727 (visited on 12/12/2021).

Sinclair, L. C. et al. (Aug. 1, 2015). "Invited Article: A compact optically coherent fiber frequency comb". In: *Review of Scientific Instruments* 86.8. Publisher: American Institute of Physics, p. 081301. ISSN: 0034-6748. DOI: 10.1063/1.4928163. URL: https://aip-scitation-org.caltech.idm.oclc.org/doi/10.1063/1.4928163 (visited on 01/03/2022).

Sung, Keeyoon et al. (May 2009). "Fourier transform infrared spectroscopy measurements of H2O-broadened half-widths of CO2 at 4.3 mThis article is part of a Special Issue on Spectroscopy at the University of New Brunswick in honour of Colan Linton and Ron Lees." In: *Canadian Journal of Physics* 87.5. Publisher: NRC Research Press, pp. 469–484. ISSN: 0008-4204. DOI: 10.1139/P08-130. URL: https://cdnsciencepub.com/doi/full/10.1139/P08-130 (visited on 03/08/2023).

Sweeney, Colm et al. (2015). "Seasonal climatology of CO2 across North America from aircraft measurements in the NOAA/ESRL Global Greenhouse Gas Reference Network". In: *Journal of Geophysical Research: Atmospheres* 120.10, pp. 5155–5190. DOI: 10.1002/2014JD022591.

Tan, Y. et al. (2019). "Introduction of Water-Vapor Broadening Parameters and Their Temperature-Dependent Exponents Into the HITRAN Database: Part I—CO2, N2O, CO, CH4, O2, NH3, and H2S". In: *Journal of Geophysical Research: Atmospheres* 124.21, pp. 11580–11594. DOI: 10.1029/2019JD030929. (Visited on 04/01/2022).

Telle, H.R. et al. (Oct. 1, 1999). "Carrier-envelope offset phase control: A novel concept for absolute optical frequency measurement and ultrashort pulse generation". In: *Applied Physics B* 69.4, pp. 327–332. ISSN: 1432-0649. DOI: 10.1007/s003400050813. URL: https://doi.org/10.1007/s003400050813 (visited on 05/09/2023).

Thompson, David R. et al. (Nov. 1, 2012). "Atmospheric validation of high accuracy CO2 absorption coefficients for the OCO-2 mission". In: *Journal of Quantitative Spectroscopy and Radiative Transfer* 113.17, pp. 2265–2276. ISSN: 0022-4073. DOI: 10.1016/j.jqsrt.2012.05.021. URL: https://www.sciencedirect.com/science/article/pii/S0022407312002804 (visited on 04/01/2022).

Truong, Gar-Wing et al. (Dec. 26, 2016). "Accurate frequency referencing for fieldable dual-comb spectroscopy". In: *Optics Express* 24.26. Publisher: Optical Society of America, pp. 30495–30504. ISSN: 1094-4087. DOI: 10.1364/OE.24.

030495. URL: https://www.osapublishing.org/oe/abstract.cfm?uri=oe-24-26-30495 (visited on 02/18/2021).

Tune, Geoffrey C. (n.d.). *Atmospheric Line List for the 2014 TCCON Data Release (GGG2014.R0) [Data set]*. Toon, G. C. (2015). Atmospheric Line List for the 2014 TCCON Data Release (GGG2014.R0) [Data set]. CaltechDATA. https://doi.org/10.14291/TCCON.GGG2014.ATM.R0/1221656. DOI: 10.14291/TCCON.GGG2014.ATM.R0/1221656.

Udem, Th, R. Holzwarth, and T. W. Hänsch (Mar. 2002). "Optical frequency metrology". In: *Nature* 416.6877. Number: 6877 Publisher: Nature Publishing Group, pp. 233–237. ISSN: 1476-4687. DOI: 10.1038/416233a. URL: https://www.nature.com/articles/416233a (visited on 05/09/2023).

Waxman, Eleanor M., Kevin C. Cossel, Fabrizio Giorgetta, et al. (Apr. 3, 2019). "Estimating vehicle carbon dioxide emissions from Boulder, Colorado, using horizontal path-integrated column measurements". In: *Atmospheric Chemistry and Physics* 19.7. Publisher: Copernicus GmbH, pp. 4177–4192. ISSN: 1680-7316. DOI: https://doi.org/10.5194/acp-19-4177-2019. URL: https://acp.copernicus.org/articles/19/4177/2019/ (visited on 02/18/2021).

Waxman, Eleanor M., Kevin C. Cossel, Gar-Wing Truong, et al. (Sept. 11, 2017). "Intercomparison of open-path trace gas measurements with two dual-frequency-comb spectrometers". In: *Atmospheric Measurement Techniques* 10.9. Publisher: Copernicus GmbH, pp. 3295–3311. ISSN: 1867-1381. DOI: https://doi.org/10.5194/amt-10-3295-2017. URL: https://amt.copernicus.org/articles/10/3295/2017/ (visited on 02/18/2021).

Wunch, Debra et al. (May 28, 2011). "The Total Carbon Column Observing Network". In: *Philosophical Transactions of the Royal Society A: Mathematical, Physical and Engineering Sciences* 369.1943. Publisher: Royal Society, pp. 2087–2112. DOI: 10.1098/rsta.2010.0240.

Zolot, A. M. et al. (Mar. 1, 2013). "Broad-band frequency references in the near-infrared: Accurate dual comb spectroscopy of methane and acetylene". In: *Journal of Quantitative Spectroscopy and Radiative Transfer* 118, pp. 26–39. ISSN: 0022-4073. DOI: 10.1016/j.jqsrt.2012.11.024. URL: https://www.sciencedirect.com/science/article/pii/S0022407312005304 (visited on 02/13/2022).

Chapter 5

MAIN FINDINGS, SUMMARY, AND RECOMMENDATIONS

5.1 Overview

Mitigating methane emissions is the most viable and crucial strategy to mitigate anthropogenic climate change in the coming decades. As the second most significant contributor to greenhouse gas-induced warming after carbon dioxide, methane plays a critical role in accelerating climate change. Therefore, it is of paramount importance that we accurately quantify, attribute, and trace methane emissions and trends to their respective sources. The findings presented in my dissertation significantly contribute to these goals by advancing our understanding of the two primary methane destruction mechanisms: oxidation by the OH radical and escape to the stratosphere. Furthermore, I contributed novel methodologies for accurate, traceable, and automated greenhouse gas measurements directly in the field, which has enabled me to quantify the errors associated with biases in greenhouse gas spectroscopy, using laser frequency combs. Through these advancements, my PhD dissertation has enhanced our understanding of methane destruction processes and moves the field of greenhouse gas remote sensing towards more precise and reliable measurements.

5.2 Main Findings in this Dissertation

In Chapter 2, I quantified the effect that variations in the hydroxyl radical can have on methane emissions estimates. OH variations affect methane emissions by changing the methane perturbation lifetime from 9 to 13.5 years. This 40% increase in the methane perturbation lifetime can significantly affect methane emissions. This is because trends of carbon monoxide concentrations (CO) also affect the methane lifetime via OH abundances. I showed that CO emissions can increase methane concentrations indirectly by increasing the methane lifetime. This significantly enhances the climate impact of wildfires. Ignoring both OH changes and CO changes can bias methane emissions assessments by 20 Tg/yr, which is twice that of the US fossil fuel industry. Incorporating the variable lifetime of methane is therefore necessary for accurate methane trend analyses.

I also quantified the effect of methane loss through stratospheric tropospheric exchange in Chapter 3. Lower stratospheric water vapor observations can be used to

proxy strat-trop exchange. I found that accounting for stratospheric loss not only impacts methane loss directly but also affects our calculations of methane destruction by altering the inferred variations of OH concentrations. This is because Methyl Chloroform oxidation is used to proxy OH concentrations, and previous studies have assumed MCF loss to the stratosphere to be either negligible or constant in time. After incorporating lower stratospheric H_2O concentrations to proxy strat-trop exchange time, methane emissions from my model became much smoother. A large portion of this change in methane emissions trends and variability is due to changes in MCF loss frequencies.

In addition, I found that El Nino corresponded to higher strat-trop exchange, as seen by increased lower stratospheric H_2O concentrations. El Nino years coincided with higher methane emissions, lower OH concentrations, and increased strat-trop exchange, an important result that links larger-scale atmospheric dynamics with atmospheric chemistry.

To enhance future global observational capabilities, in Chapter 4, I used laser frequency combs to examine the interaction of light with methane and CO_2 molecules under different environmental conditions. Laser frequency combs, originally designed for picosecond time-keeping, enable automated, accurate, and stable greenhouse gas measurements with ranges of over a kilometer.

I used the accuracy and stability of frequency combs to quantify environmental biases on greenhouse gas spectroscopy. Environmental conditions affect the absorption of radiation by greenhouse gases, which affects the accuracy of greenhouse gas retrievals. This is due to inaccuracies in modeling pressure and temperature broadening effects. I found that errors in modeling pressure broadening effects dominate both methane and CO_2 retrieval errors. Differences in the parameters used to model pressure and temperature broadening can lead to up to an 8% difference in concentrations for methane. In the field deployments of our frequency comb, we found more than a 2% variable error for methane retrievals. In addition, water vapor broadening, which arises during times of higher humidity, can contribute substantial errors to CO_2 retrievals. I found a more than 1% error in CO_2 retrievals when discounting the effects of water vapor broadening. This was in an atmosphere with only 1.7% humidity. This effect can only be larger in areas like the tropics, which can have up to 5% humidity. This underlines the importance of accurately modeling environmental effects on molecular absorption for accurate greenhouse gas measurements and monitoring.

5.3 Recommendations and Concluding Remarks

Overall, this thesis has made substantial contributions to our understanding of methane sink processes and remote sensing techniques. It has underscored the urgent need for observational, theoretical, and laboratory advancements in order to fully comprehend and quantify the complex methane cycle. Accurate modeling and measurement of methane sources and sinks are imperative for effective mitigation of anthropogenic climate change. To this end, it is crucial to expand our global observational capabilities by increasing the measurement of methane emissions and understanding the underlying destruction processes. Addressing the remaining uncertainties in variations of the OH radical and obtaining precise OH reaction rates, concentrations, and distributions will significantly enhance our ability to attribute methane trends to specific sectors and develop targeted mitigation strategies. Additionally, a comprehensive understanding of methane transport, particularly within the troposphere and towards the stratosphere, requires advancements in both modeling and measurement techniques. Ground-based vertical profile retrievals, if proven accurate, offer an affordable and automated means to measure vertical gradients of methane and CO_2, thereby enabling precise constraints on methane transport and chemical processes. Furthermore, the utilization of laser frequency combs to expand the global observation network, particularly in under-sampled regions such as the tropics, will provide crucial insights into the major sources, oxidation, and transport of methane. However, to fully capitalize on the potential of laser frequency combs, theoretical advancements in greenhouse gas spectroscopy are needed, particularly in accurately modeling pressure and water vapor broadening effects. By advancing our knowledge and capabilities in methane emissions attribution, monitoring, and mitigation, we can enable effective policies in our collective efforts to combat climate change.